TOPICAL REVIEW • OPEN ACCESS

Inorganic–organic interfaces in hybrid solar cells

To cite this article: Jens Niederhausen *et al* 2021 *Electron. Struct.* **3** 033002

View the article online for updates and enhancements.

You may also like

- Recent advances in mechanical strain engineering of low-dimensional semiconductors and their applications in high-performance quantum emitters
  Lue Tao, Weiwen Ou, Yang Li et al.

- Spectroscopy and control of near-surface defects in conductive thin film ZnO
  Leah L Kelly, David A Racke, Philip Schulz et al.

- Bias-induced reconstruction of hybrid interface states in magnetic molecular junctions
  Lingmei Zhang, Yuanyuan Miao, Zhipeng Cao et al.

Electronic Structure

TOPICAL REVIEW

Inorganic–organic interfaces in hybrid solar cells

Jens Niederhausen[1],[*] , Katherine A Mazzio[2],[3] and Rowan W MacQueen[4]

[1] Institute for Nanospectroscopy, Helmholtz-Zentrum Berlin für Materialien und Energie GmbH, 14109 Berlin, Germany
[2] Joint Research Group Operando Battery Analysis, Helmholtz-Zentrum Berlin für Materialien und Energie GmbH, 12489 Berlin, Germany
[3] Department of Chemistry, Humboldt-Universität zu Berlin, 12489 Berlin, Germany
[4] Department Spins in Energy Conversion and Quantum Information Science (ASPIN), Helmholtz-Zentrum Berlin für Materialien und Energie GmbH, 14109 Berlin, Germany
[*] Author to whom any correspondence should be addressed.

E-mail: jens.niederhausen@helmholtz-berlin.de

Abstract

In this review, we present important concepts to describe inorganic–organic interfaces in hybrid solar cells. We discuss the formation of hybrid interfaces, provide an introduction to the ground-state electronic structure of the individual components, and detail the overall electronic landscape after combining into a hybrid material for different relevant cases. We then explore the impact of hybrid interfaces on photophysical processes that are crucial for the photovoltaic performance of hybrid solar cells. Within this framework, we discuss methods for hybrid interface modification toward the optimization of hybrid solar cells, such as doping, the application of interlayers, and morphological control.

1. Motivation: why go hybrid?

A hybrid solar cell utilizes organic and inorganic semiconductors (OSCs/ISCs) to convert sunlight into electricity using the photovoltaic effect. The interfaces that are formed between the inorganic and organic material domains of these devices, which control many of their key attributes, are naturally called hybrid interfaces.

Hybrid interfaces are often implemented to improve certain interface properties or facilitate functions that would be impossible in a non-hybrid configuration. Two important examples are shown in figure 1. But hybrid interfaces may also come into being through pure necessity, for example, the need to collect charges from an organic bulk heterojunction at an (inorganic) metal oxide electrode. This review covers both these varieties of hybrid interface, though it is the promise of the former that is our main motivation.

What could be the appeal of hybrid solar cells in today's photovoltaics landscape? For decades now, multiple junction cells featuring III–V semiconductors have been the champions of ultimate solar cell power conversion efficiency, while the more economical cells based on silicon, CdTe, CIGS(e), and more recently lead halide perovskites continue to gain efficiency [1]. With these technologies standing dominant, and indium tin oxide (ITO) and other effective inorganic transparent conductors in place, what are the properties through which OSCs can complement or even out-perform ISCs?

1.1. Chemical composition and compositional tuning

The virtually infinite flexibility in adjusting the chemical structures of organic materials allows the fine-tuning of their chemical, electronic, and mechanical properties. This allows combining controlled surface bonding, efficient passivation, and selective charge transport in a single molecule. It also permits alteration of the solubility characteristics, which opens up a large variety of processing routes.

Solar cells are slated to eventually supply a large fraction of the world's electricity demand [2]. To provide the required terawatts of electrical power, the sheer scale of solar cell production necessitates replacement of solar cell components employing scarce resources, like indium and gallium, with more earth-abundant
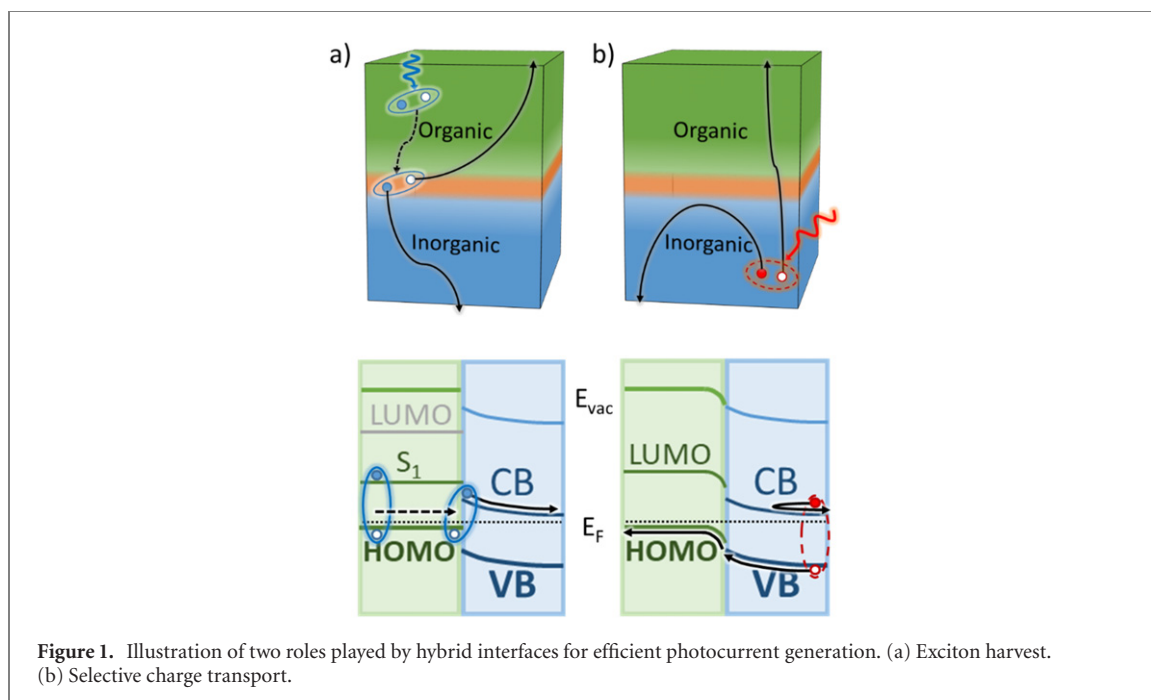
Figure 1. Illustration of two roles played by hybrid interfaces for efficient photocurrent generation. (a) Exciton harvest. (b) Selective charge transport.

materials. Since organic materials are comprised largely of carbon and hydrogen, replacing their inorganic counterparts in solar cells can address some issues of material scarcity. Furthermore, introducing innovative materials that are cheaper or require lower processing temperatures harbors the potential to reduce the costs and energy requirements for fabrication and recycling. Such advances can further improve the ecological and economic benefit of solar cells and accelerate the transition to a sustainable way of life.

1.2. Photophysics

π-conjugated organic molecules and polymers can exhibit very strong electronic absorption bands. While the bandwidth of these absorption features in a single chromophore is typically not comparable to the continuum absorption of a bulk crystalline semiconductor, the many sources of broadening that act upon these electronic bands, particularly in the solid state, as well as the increasing density of allowed electronic transitions above the optical gap can lead to what is effectively a quasi-continuous absorption band. Therefore, the thickness of a π-conjugated organic film can be a fraction of that of inorganic absorbers while still achieving a comparable absorbance. Since thinner solar cell absorber layers favor a higher device voltage due to a reduction in bulk defect-mediated recombination, thinning the inorganic absorber layer by the incorporation of a light-harvesting organic chromophore layer may be a useful device strategy [3].

OSCs are excitonic, and thus can exhibit the spectral conversion processes singlet fission and triplet fusion. When used in conjunction with an already-mature high-efficiency ISC, these processes offer a promising path toward surpassing the Shockley–Queisser limit [4], which describes the efficiency of an ideal single-junction solar cell, wherein the only loss mechanism is that of radiative recombination, under one-sun excitation [5, 6]. Pushing the efficiency of mainstream solar cells beyond this limit is important, because continuously falling solar cell prices imply that the balance of systems costs (the costs of the utilities and services required for electricity production from solar cells) account for an increasing fraction of the total system costs. In the limit of the cost of the solar cell itself being negligible and fixed balance-of-systems costs, improving the solar cell efficiency—making more electricity per module—is the only route to a reduction in the cost per unit of electricity.

1.3. Hybrid composite materials

While the focus of this review is on interfaces between disparate material domains, it is noteworthy that intermixing of organic and inorganic components on a finer scale can yield important new materials. Hybrid organo-lead halide perovskites and quantum dots with organic ligands are examples of hybrid and nanocomposite structures. In both cases, the essential function of the organic counterpart is initially structural in nature, but the organic component can additionally contribute electronic functionality, for example due to surface trap passivation, or when organic chromophores are integrated into the organic component.

Many more niche factors may induce an interest in the development of hybrid solar cells. Expanding the material range can benefit applications with specific boundary conditions like mechanical flexibility [7, 8], aesthetics [9, 10], or radiation hardness [11].

Given the complexity of hybrid inorganic–organic systems, it is no surprise that their comprehensive treatment is still in its infancy. In this review, we aim to identify concepts to describe interfaces of hybrid solar cells both in the ground and excited states. We first define hybrid interfaces and discuss their formation. This is followed by an introduction to the electronic structure of the individual components and their impact on the overall electronic landscape after combining into a hybrid material. We later explore the impact of hybrid interfaces on various photophysical processes that occur in photovoltaics. Finally, we discuss methods for hybrid interface modification that enable tuning of the excited state dynamics, such as doping, the application of interlayers, and morphological control. To keep this review focused, the details of solar cell structure outside of the hybrid interface are considered only insofar as they provide the necessary background for discussing the interface. Other aspects are covered by other hybrid solar cell reviews [12–21], as well as recent reviews on organic [22–24] and inorganic [25–28] solar cells. For a technology analysis we refer the reader to reference 29.
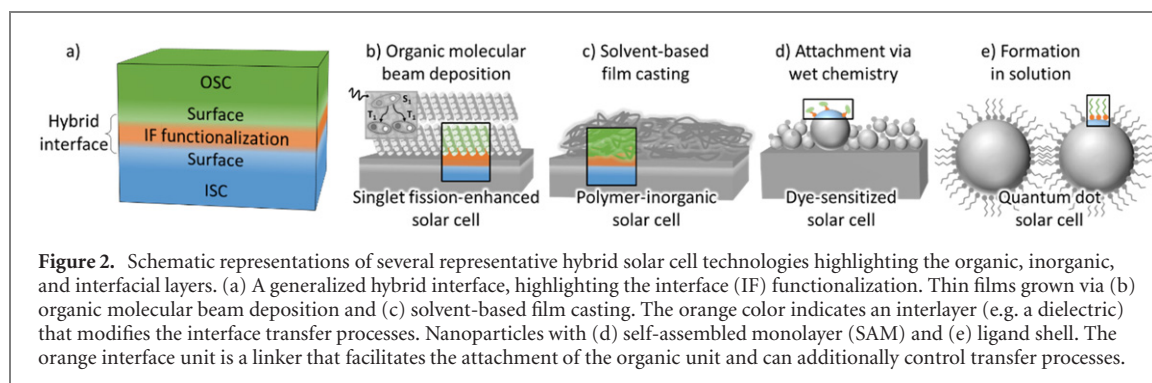
2. The hybrid interface

Inorganic–organic composites rely on the synergistic effects of combining two materials classes that have typically been treated separately according to their physical properties. This is done in order to improve different aspects of performance, often in ways that deviate from commonly employed theories, such as mean field theory or effective medium approximations. The rule of mixtures is a foundational concept in materials science that defines upper and lower boundaries for the properties that composites can express. It states that composite properties can be estimated as the volume weighted average of the properties of the included phases. This rule most frequently applies when considering macroscale composites. The IUPAC defines a hybrid material as a 'material composed of an intimate mixture of inorganic components, organic components, or both types of components' for which 'the components usually interpenetrate on scales of less than 1 μm' [30]. As the dimensions decrease, strong deviations from the properties of the individual materials can often be observed. For instance, an electrical conductivity has been reported for nanoparticle/polymer hybrid materials that cannot be described as a combination of the individual components, and instead is dependent on an unusually high conductivity at the hybrid interface [31, 32]. Important properties can arise depending on whether the inorganic and organic materials share orbital overlap or interact via van der Waals forces. While many properties of hybrid materials are accessible by just relying on intimate contact, certain exotic properties necessitate orbital overlap. This intermixing can result in profound changes in the optoelectronic properties as a result of the inherent differences in the properties of the individual constituent materials, such as their exciton degeneracy, increased absorption coefficients for hybrid excitons, dipole strength, or the lifetime of charge carriers [33]. One example is the formation of hybrid excitons at hybrid interfaces that are predicted to give rise to a greatly enhanced optical non-linearity [34]. As a result, inorganic–organic hybrid materials have been identified as key technologies for the further development of optoelectronic devices.

Hybrid solar cells consist of ISCs [35] and OSCs [36]. ICSs and OSCs express significantly different properties that are ultimately derived from their different bonding characteristics. Where inorganic materials are typically comprised of atoms bonding predominantly via covalent or ionic mechanisms, organic semiconducting materials are more likely to be comprised of a series of alternating π bonds with molecules interacting via weaker van der Waals bonding. These differences in bond energies have a profound effect on the optoelectronic properties (as discussed in sections 3 and 4) and morphologies. ISCs will readily form hard crystalline structures (although their amorphous counterparts are also technologically important) with open shell structures that have highly reactive surfaces that require passivation in order to control the desired properties. The morphology of interfaces between ISCs and organic materials (not necessarily semiconductors) is discussed in the remaining part of this section. While organic materials encompass a wide variety of form and function, we discuss only those of particular importance for optoelectronic applications, namely ligand shells, π-conjugated polymers, and small molecules.

2.1. Interface chemistry: ligands and SAMs
To control the termination of an inorganic material, organic molecules can be attached to their surface via coordination or covalent bonds. Understanding ligation effects is of central importance for detailing the consequent evolution of the optoelectronic properties in hybrid materials and interfaces. The functional headgroup can have varying iono-covalent or weak binding characteristics with the inorganic surface. M L H Green presented a formalism for understanding this interaction at the molecular level via the covalent bond classification (CBC) theory, which was later expanded to inorganic nanoparticle systems [37–39]. According to CBC theory, ligands can be classified into three different categories according to the number of electrons they contribute to the interfacial bond. L-type ligands are neutral donors that rely on lone pairs for coordination with inorganic surfaces, resulting in relatively weak, dative bonds, and contributing two electrons to the inorganic constituent.

Figure 2. Schematic representations of several representative hybrid solar cell technologies highlighting the organic, inorganic, and interfacial layers. (a) A generalized hybrid interface, highlighting the interface (IF) functionalization. Thin films grown via (b) organic molecular beam deposition and (c) solvent-based film casting. The orange color indicates an interlayer (e.g. a dielectric) that modifies the interface transfer processes. Nanoparticles with (d) self-assembled monolayer (SAM) and (e) ligand shell. The orange interface unit is a linker that facilitates the attachment of the organic unit and can additionally control transfer processes.

X-type ligands tend to have an odd number of valence electrons and rely on iono-covalent interactions with the inorganic surface, thereby contributing one electron. Z-type ligands interact with surfaces as pure acceptors, relying on the back-donation of two electrons from the inorganic surface, and in this case contributing zero electrons.

Ligands are critical components during solution-based inorganic nanoparticle synthesis that enable modulation of the nucleation and growth processes, but can have detrimental effects when they remain on the surface after synthesis due to their insulating and sometimes poorly surface passivating properties. The ligands used during synthesis are typically comprised of a functional coordinating head group, a predominately saturated ligand core that provides solubility characteristics (and also results in electronically insulating behavior), and terminal groups that can contain functional components (see figures 2(d) and (e)). In large part, tailoring the functional component is usually done during a post-synthetic ligand exchange process [40–42], although there are also reports of direct target ligand functionalization during synthesis [43–46]. The concepts of ligand exchange on nanoparticles can also be applied to more macroscale inorganic systems in terms of chemical attachment.
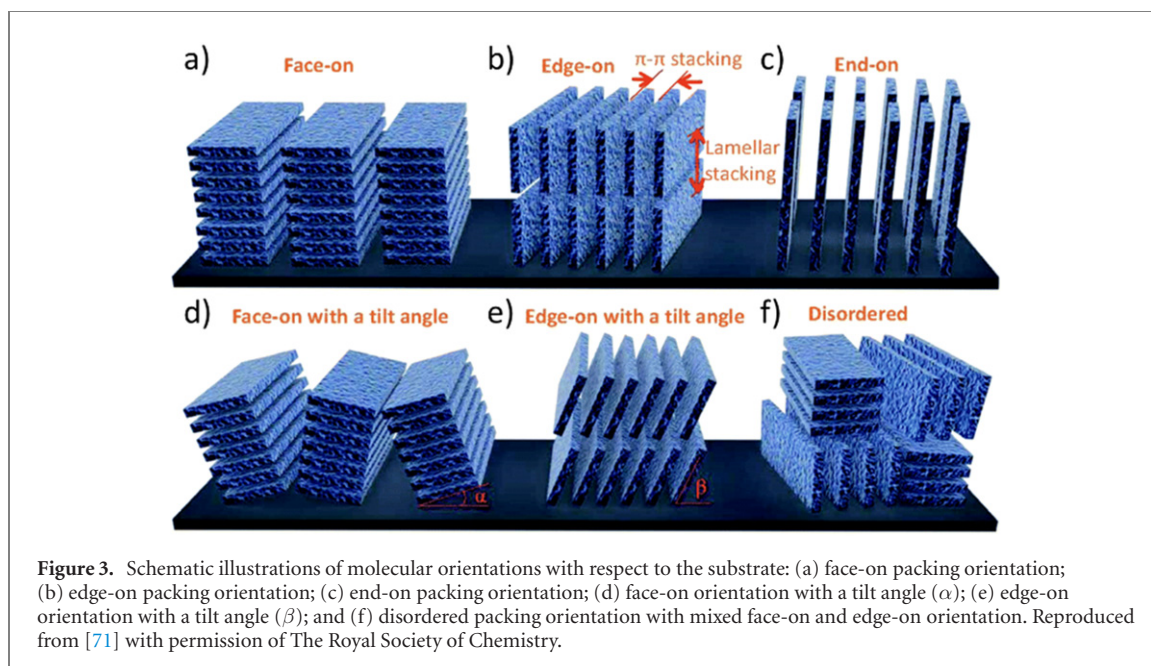
The ligand exchange process or the attachment of an organic layer to an ISC without ligands typically occurs by submerging the inorganic material in a solution that contains the target organic molecules or their precursors. The likelihood of the subsequent exchange reaction is driven by a combination of thermodynamic parameters, including the electroneutrality principle, hard-soft acid–base theory, chelation, and steric effects [47]. The resulting organic film is sometimes referred to as a self-assembled monolayer (SAM). The specifics of the organic monolayer (degree of order, molecular orientation, etc) can often be traced to details of the molecule–substrate bond (chemical elements of the bonding partners and denticity) and the chemical structure of the molecule [48–53] and can be influenced by post-deposition heat treatment [54]. Precursor molecules for attachment to metal oxide surfaces can feature a range of different functional groups [55–57], including hydroxyl, phosphonic acid, and carboxylic acid groups. Attachment is facilitated by coordination bonds to metal atoms in the oxide surfaces. Chalcogenol ligands can additionally be used to link organic molecules to, e.g. transition metal-chalcogenide surfaces [58].

In the case of covalent functionalization of the elemental semiconductors Si and Ge, the ISC usually begins the reaction with a hydrogen-terminated surface, a metastable state that results from chemical etching of the native oxide surface. In this case, the organic linker group has to either replace the hydrogen or insert itself in between the ISC and the hydrogen (hydrometalation reactions). These processes require initiating the surface chemistry via heat, electrochemistry, photochemistry, and/or the formation of an organic radical. Covalent modification of Si and Ge has been successfully realized through a range of different synthetic routes [59–62] and optimized toward minimized oxide formation, maximized surface coverage, and excellent and stable surface passivation [63–67].

Of particular relevance for hybrid solar cells is the case that the attached organic molecules contain a chromophore unit that can act as donor or acceptor for energy transfer from or to the inorganic. Most prominently, dye-sensitized solar cells (DSSCs) combine the large oscillator strength of organic molecules with highly conductive ISCs. Silicon [68], PbS [69], and all-inorganic perovskite [70] nanocrystals have also been functionalized with organic chromophores.

2.2. Interface morphology

When considering organic small molecules or polymers, it is important to keep in mind that these are three-dimensional systems whose properties are anisotropic. The orientation of these molecules relative to inorganic surfaces is critical to the resulting properties, and can be classified as edge-on, face-on, end-on, or disordered/amorphous depending on how the organic materials are arranged (see figure 3). All ordered classifications can also have an associated tilt angle that arises due to structural and energetic factors, such as the

Figure 3. Schematic illustrations of molecular orientations with respect to the substrate: (a) face-on packing orientation; (b) edge-on packing orientation; (c) end-on packing orientation; (d) face-on orientation with a tilt angle (α); (e) edge-on orientation with a tilt angle (β); and (f) disordered packing orientation with mixed face-on and edge-on orientation. Reproduced from [71] with permission of The Royal Society of Chemistry.
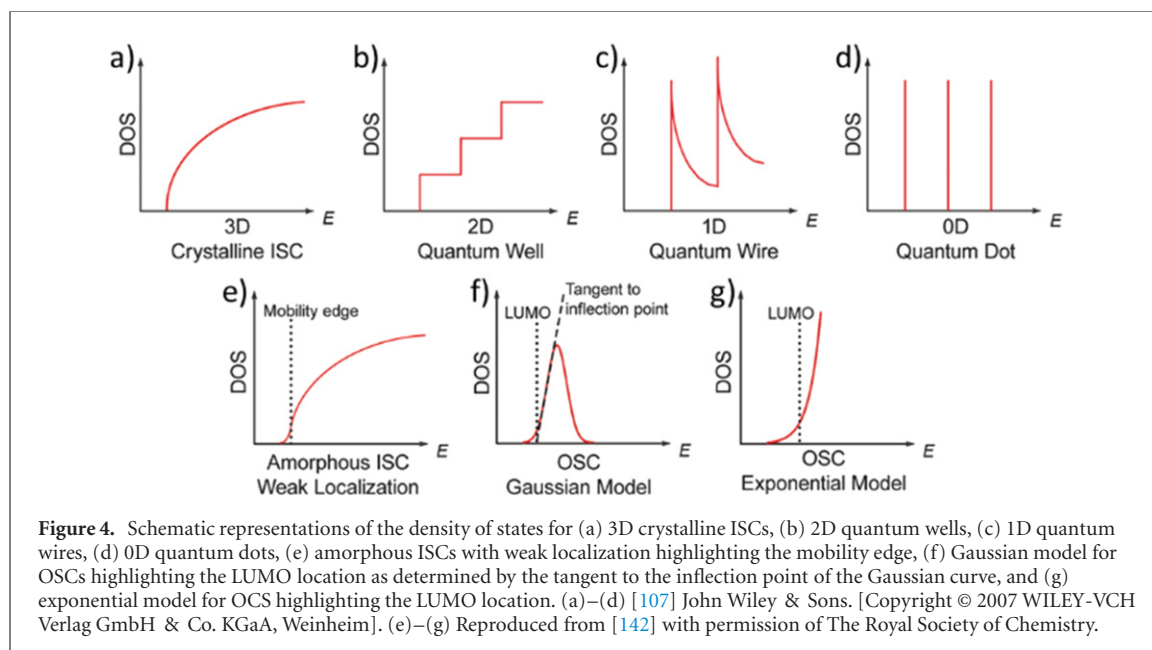
planarity of the molecule, the structure of the side chains, the presence or absence of a coordinating head group, and the orientation of the crystal facet that the organic material is coming into contact with. The morphology of the molecules at the inorganic–organic interface does not necessarily represent that of the bulk of the OSC. In many π-conjugated systems, and in particular for π-conjugated polymers, the ordering is described in terms of $\pi-\pi$ stacking or lamellar stacking, which corresponds to packing in the direction of the π-orbitals or the side chains, respectively. Charge transport in π-conjugated materials can occur along the π-conjugated backbone (where it is fastest) or in the $\pi-\pi$ stacking direction (where the reliance on interchain hopping results in slower transport), and is frequently impeded in the lamellar stacking direction due to the insulating aliphatic chains making interchain hopping in this direction unfavorable [72]. There has been a strong drive to develop methods for controlling the orientation and stacking motifs of these π-conjugated systems in order to improve aggregation behavior and achieve desired molecular orientations for improved performance.

When fabricating monolithic solar cells, layers of organic small molecules are often grown by organic molecular beam deposition or physical vapor deposition onto the inorganic counterpart that acts as substrate. In this case, the geometric structure of the first organic layer(s) and the growth mode strongly depend on the interfacial interaction. Organic film growth both on atomically clean as well as passivated Si have been actively studied for more than thirty years [73–79] and will be used here as pertinent example. In the chemisorption limit, the epitaxial registry and orientation of the first molecular layer is dominated by specific organic–inorganic interactions [80–83]. In contrast, in the physisorption limit the intermolecular interaction dominates the molecular assembly. However, the interface can induce the formation of so-called *thin film* phases [84, 85]. The resulting film morphologies sensitively depend on the deposition rate, as well as the reactivity, crystallinity, and temperature of the ISC surface [86, 87]. For weak organic–inorganic interactions, Volmer–Weber growth, dewetting, and desorption is often observed at temperatures around room temperature [88–92], especially under vacuum conditions. This can be a severe problem when attempting to probe interface properties, since a large fraction of the OSC is not, in fact, in contact with the ISC even for low film thicknesses. Sometimes a small decrease of the substrate temperature is enough to prevent the dewetting and desorption [85, 90]. As another instructive example we mention *p*-sexiphenyl (6P) on ZnO, for which it was shown that the 6P molecular orientation can be switched by using different ZnO crystal faces of a given ISC [93] and that the growth mode can be controlled by partial fluorination of 6P [94]. Quite generally, partial fluorination is a potent strategy for subtly tuning organic film morphologies [95, 96].

The reverse deposition sequence (inorganic on organic) has also been successfully demonstrated [97, 98], but is usually avoided due to the high risk of damaging the organic material. Low-temperature deposition schemes exist for a number of ISCs that can help reduce detrimental effects on the OSC.

Due to their high molecular weight, the thermal evaporation of polymers is difficult. Deposition of polymers and large and/or sensitive molecules under vacuum conditions is possible via electrospray deposition [99–102]. More typically though, polymers are deposited from solution processing methods, such as spin-coating, blade coating, or printing, among others, which results in edge-on or face-on stacking. When an end-on morphology is desired, polymers can also be chemically attached via either 'grafting to' or 'grafting

Figure 4. Schematic representations of the density of states for (a) 3D crystalline ISCs, (b) 2D quantum wells, (c) 1D quantum wires, (d) 0D quantum dots, (e) amorphous ISCs with weak localization highlighting the mobility edge, (f) Gaussian model for OSCs highlighting the LUMO location as determined by the tangent to the inflection point of the Gaussian curve, and (g) exponential model for OCS highlighting the LUMO location. (a)–(d) [107] John Wiley & Sons. [Copyright © 2007 WILEY-VCH Verlag GmbH & Co. KGaA, Weinheim]. (e)–(g) Reproduced from [142] with permission of The Royal Society of Chemistry.

from' approaches [103, 104]. The 'grafting to' approach utilizes pre-formed polymers that associate to the inorganic surface via chemical attachment, but can result in poor coverage due to steric effects. The 'grafting from' technique takes advantage of a surface-bound initiator from which the polymer is grown via chain growth polymerization. End-on orientation can also be achieved by use of a fluorinated surface-segregated layer and/or suitable SAMs [105, 106].
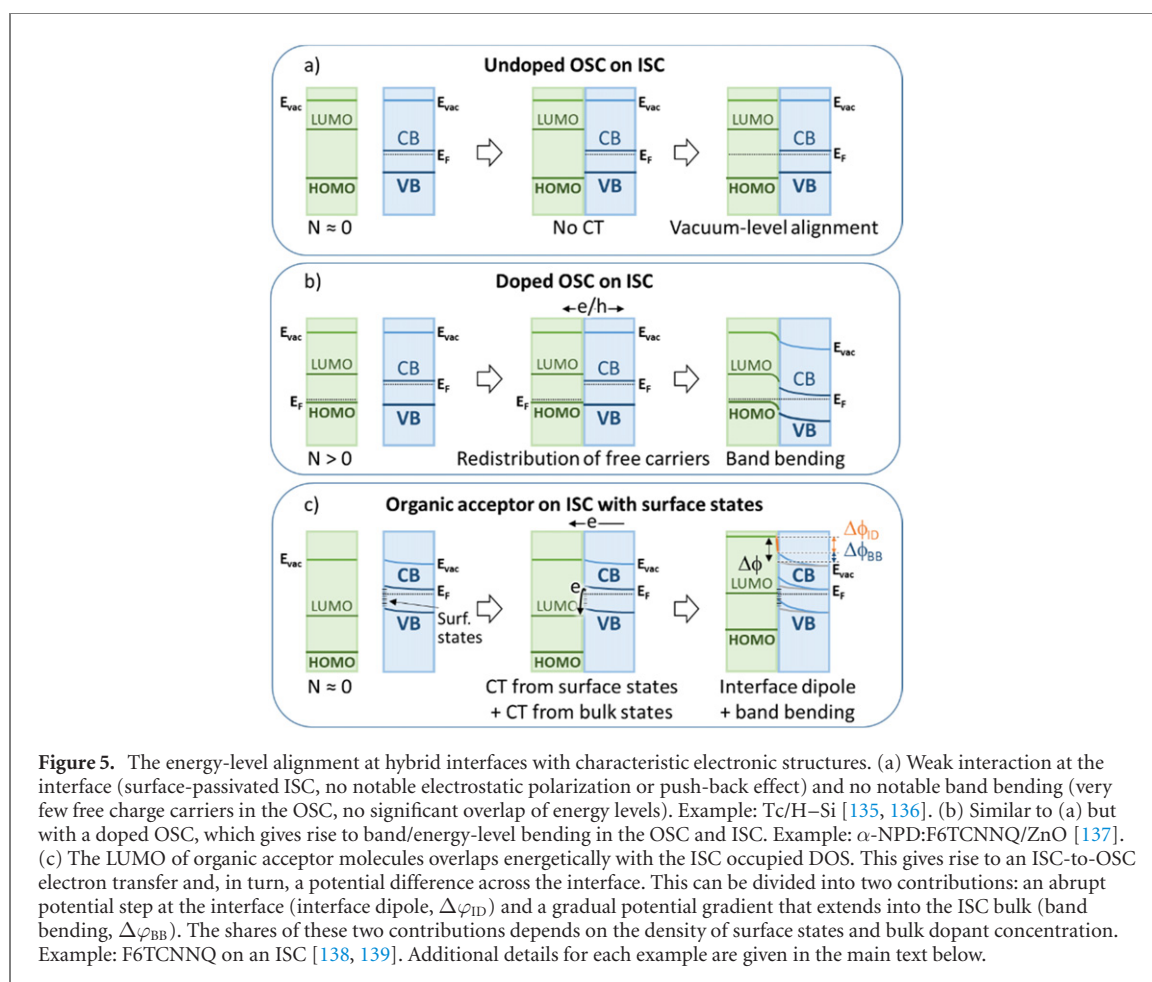
3. Electronic structure

We now turn to a discussion of the optoelectronic properties of hybrid interfaces, starting with the ground state electronic structure, which controls the fate of photo-generated charge carriers.

3.1. Intrinsic energy levels of ISCs and OSCs

The relevant energy levels for optoelectronic devices are those that derive from the valence shell of the atomic constituents. Intermixing of atomic orbitals gives rise to occupied and unoccupied molecular orbitals. In ISCs the atoms of the whole lattice overlap, which leads to formation of a continuum of energy levels known as energy bands. The highest occupied band and the lowest unoccupied band are the valence band (VB) and conduction band (CB), respectively. When the dimensions of inorganic materials are reduced from the bulk to lower than the Bohr radius of the exciton, they can eventually experience quantum confinement in one [108–110] or more [111–114] dimensions. As particle size is reduced, there are fewer available electronic states in the CB and VB, and eventually this results in the widening of the bandgap and development of discreet states near the band edges. Depending on the number of quantum confined dimensions, there can be profound effects on the density of states (DOS), as shown schematically in figure 4, and this can therefore significantly influence the optoelectronic properties, especially at heterointerfaces. Within the strong confinement regime, the dielectric constant will also be impacted by particle size, and in core–shell type structures, the dielectric constant of the matrix material will significantly impact the properties of the quantum confined material. This has the result of modulating the absorption coefficient, donor energy levels, and electric field concentration within the dots, among other effects [115–117], which in turn will determine the electronic properties at heterointerfaces.

In contrast, π-conjugated organic molecules in the condensed state feature large orbital intermixing only within the molecular building blocks, whereas intermolecular hybridization is typically weak. This gives rise to comparably smaller intermolecular band dispersion [118, 119]. Accordingly, the electronic energy levels are primarily determined by the occupancy of the highest occupied molecular orbital (HOMO) and the lowest unoccupied molecular orbital (LUMO). π-conjugated polymers feature bands that derive from the hybridization along the extended polymer chain. State energies additionally depend on the local electrostatic potential, which is influenced, e.g. by molecular sliding [120] and disorder [121].

The surface disrupts the periodic structure of a solid. The resulting asymmetric potential gives rise to additional electronic states (Tamm/Shockley states) [122]. In addition, the different number of bonding partners at the surface compared to the bulk can result in dangling bonds, surface reconstructions, and the formation

Figure 5. The energy-level alignment at hybrid interfaces with characteristic electronic structures. (a) Weak interaction at the interface (surface-passivated ISC, no notable electrostatic polarization or push-back effect) and no notable band bending (very few free charge carriers in the OSC, no significant overlap of energy levels). Example: Tc/H–Si [135, 136]. (b) Similar to (a) but with a doped OSC, which gives rise to band/energy-level bending in the OSC and ISC. Example: α-NPD:F6TCNNQ/ZnO [137]. (c) The LUMO of organic acceptor molecules overlaps energetically with the ISC occupied DOS. This gives rise to an ISC-to-OSC electron transfer and, in turn, a potential difference across the interface. This can be divided into two contributions: an abrupt potential step at the interface (interface dipole, $\Delta\varphi_{ID}$) and a gradual potential gradient that extends into the ISC bulk (band bending, $\Delta\varphi_{BB}$). The shares of these two contributions depends on the density of surface states and bulk dopant concentration. Example: F6TCNNQ on an ISC [138, 139]. Additional details for each example are given in the main text below.

of distinct surface crystal phases, as well as a structural relaxation of the surface layers. A different molecular orientation can be present at the surface than expected from the bulk structure [123]. Native defects in the near-surface region can sensitively influence the surface potential of ISCs, as observed, e.g. for ZnO [124–126]. Due to these effects, the surface electronic structure differs from that of the bulk, which can manifest itself as increased energetic broadening of the DOS or the formation of additional distinct states, leading to shallow and deep traps for charge carriers. The surface structures of many atomically clean and passivated ISC surfaces have been established in the last decades. However, this is not true in all cases. One example is the ZnO(0001) surface (i.e. the Zn-terminated facet of ZnO), for which it is still not fully clear whether and how the observed periodic structures [127] and oxygen species [128, 129] at the surface derive from surface reconstructions [130], adsorbates like hydroxyl groups [131], sub-surface hydrogen [132], or a combination thereof [133, 134].

Figure 5 presents one-particle energy-level diagrams for three characteristic hybrid interface configurations. Such diagrams are frequently used to depict the energy-level alignment (ELA) at interfaces. To that end, the energies of occupied (unoccupied) orbitals/bands are determined by measuring their ionization energies (electron affinities), which correspond to the energy difference between the neutral ground state and the final state with one extra hole (electron) in the orbital/band, respectively. These are also the energies which are most relevant for charge transport.

Upon the removal of an electron, the polarization of the environment screens the bare charge. This dielectric stabilization of the hole reduces the ionization energy (IE). Conversely, the addition of an electron generates a distortion in the local electronic and atomic structure that stabilizes the electron affinity (EA) [140, 141]. The charge and the response of the environment is jointly referred to as a polaron. Polaronic effects have a large influence on the charge transport in OSCs [72, 142–148] and quantum dots [149, 150].

ISCs typically have relatively large dielectric constants, which results in effective screening of the charge carriers [151]. This leads to the working principle that bulk 3D ISCs are populated exclusively by free charge carriers at room temperature. Polaronic effects can in most cases duly be ignored for this category of materials, at least at room temperature and above.

Energy levels are typically given either with respect to the Fermi level or the vacuum level. Note that in the context of interfaces, the vacuum level refers to a location just on top of the surface of the materials and

not at infinity [152–154]. For this reason, energy levels with respect to the vacuum level are sensitive to the surface potential that the electron traverses when leaving the material. This also applies to the work function, which is defined as the energy difference between the Fermi level and vacuum level. Changes in the surface potential directly translate to a corresponding change in the work function and the energy levels referenced to the vacuum level. These energies thus depend, e.g. on the facet of the ISC crystal or the molecular orientation in the organic layer [155–157]. This effect is particularly pronounced in organics, since they feature a very anisotropic charge distribution, with the π-orbitals giving rise to a negative partial charge above and below the π-conjugated plane [158]. This effect can be exploited to tune the energy levels via the implementation of an extra surface potential. This can be achieved, e.g. via a polar surface termination in the case of ISCs [136, 159, 160] and intra-molecular polar bonds in the case of OSCs [156, 158, 161, 162].

3.2. Interface formation

It is often instructive to arrive at the final ELA of a particular interface by first aligning the energy-levels of the individual components assuming vacuum-level alignment, and second incorporating effects induced by the formation of the interface (see figure 5). In the following we initially assume that the intrinsic electronic structures of either constituent also hold for their surfaces and that no new states form upon interface formation.
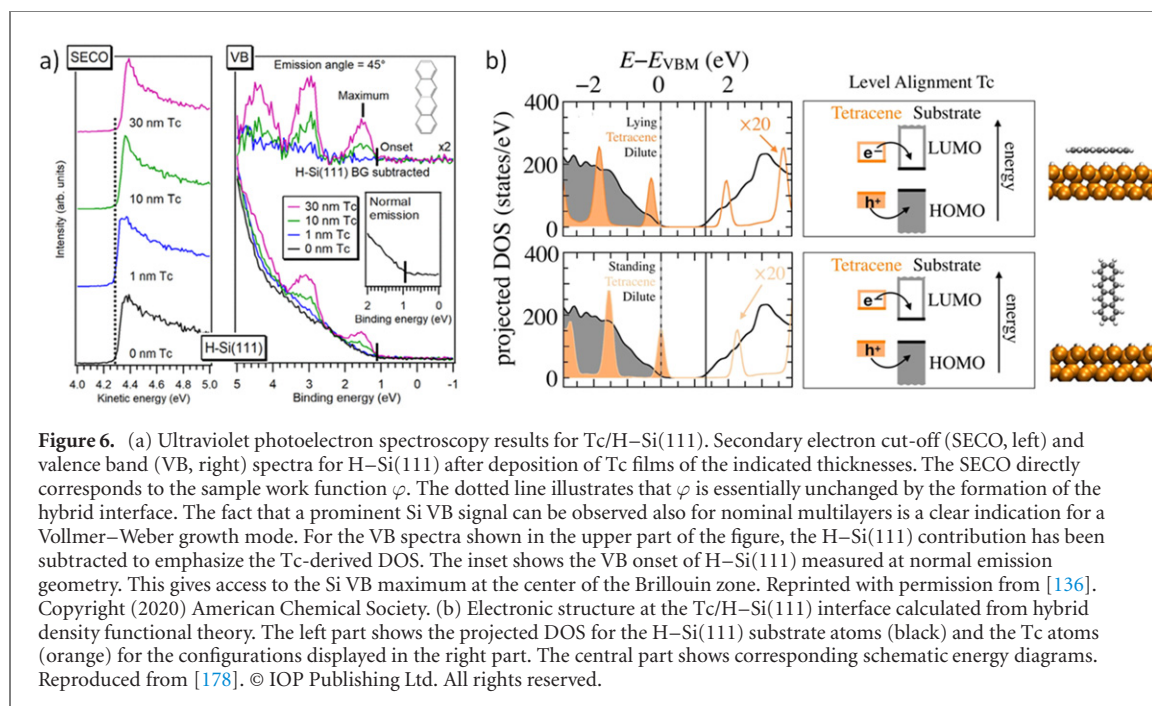
One effect that has to be considered is a possible difference in screening efficiency at the interface compared to the ISC and OSC bulk. It was found that the electronic screening for small molecules is more efficient when they are on a metal surface than when surrounded by other molecules, which gives rise to a decreased electronic gap at the metal–molecule interface compared to the bulk [163–173]. Since ISCs, polymers, and small molecules can have very different dielectric constants, a similar effect can be expected at hybrid interfaces [174, 175].

Next, we consider the ELA in the absence of any significant electronic interaction at the intimate interface. This means we first ignore the possibility of the formation of an interface dipole. In this case, vacuum-level alignment persists also after interface formation and controls the ELA directly at the interface. In contrast, the ELA far away from the interfaces is controlled by the Fermi-levels of the two materials. A possible misalignment of the Fermi levels for assumed vacuum-level alignment gives rise to a charge-carrier redistribution across the interface and within the materials to guarantee electronic equilibrium. This leads to a gradual potential drop that facilitates the alignment of the two Fermi-levels. This potential drop is referred to as band bending. In cases where no bands form, the term energy-level bending is appropriate. Importantly, sufficient free charge carriers are required for full alignment of the Fermi-levels, which is not guaranteed for OSCs, as discussed in the following.

Undoped OSC on passivated ISC (figure 5(a)): small molecule OSCs often have gaps >2 eV [36, 176] and, thus, very small intrinsic charge carrier densities. In these cases and the absence of (intentional or unintentional) doping, vacuum-level alignment persists well into the bulk and no significant band bending occurs for organic layer thicknesses relevant for most opto-electronic devices [152, 177]. In this case, the Schottky–Mott rule applies according to which the hole-injection barrier (HIB, the energy difference between the HOMO of the OSC and the Fermi-level of the ISC) is equal to the difference of the IE of the OSC and the work function of the ISC (φ), HIB = IE − φ.

As a prototypical example, we discuss tetracene (Tc) on crystalline silicon (c-Si) with hydrogen termination (H−Si). The ELA of this interface was experimentally derived via ultraviolet photoelectron spectroscopy (UPS), as shown in figure 6(a) [135, 136]. Indeed, no significant work function change was observed upon interface formation, evidencing vacuum-level alignment at the Tc/H−Si interface. Notably, the experimentally derived ELA deviates from theoretical calculations shown in panel (b) of the same figure [178]. While the latter predicts the Tc HOMO to be lower in energy than the Si VB, the inverse configuration is observed experimentally. Possible reasons for the discrepancy are differences in Si doping (n-type in the experiments vs intrinsic in the calculations) and defects. In addition, the calculations were performed for the intimate interface and include the full screening of the Si surface. In contrast, due to the pronounced Vollmer–Weber growth mode of Tc on H−Si [90], the UPS experiments mostly probe Tc in multilayers, for which the screening is only by other Tc molecules. Lastly, the Tc orientation that was considered in the calculation is more upright than the one that was recently derived for ultrathin Tc on H−Si [90]. Due to the electrostatic effects discussed above, IEs for Tc films with the molecules in an inclined configuration should be higher than for those with more upright molecules, as has been observed for related molecules [179, 180].

Greiner *et al* systematically investigated a number of OSC/metal oxide interfaces [183] where φ covered a large energy range. They found characteristic regimes for the relationship between the HIB on the one hand and IE and φ on the other hand. The behavior is essentially the same as what had been reported previously for N,N′-di(1-naphthyl)-N,N′-diphenyl-(1,1′-biphenyl)-4,4′-diamine (NPB, another name is α-NPD, which is used below) on a variety of organic and inorganic substrates [184] and is shown in figure 7. Below a

Figure 6. (a) Ultraviolet photoelectron spectroscopy results for Tc/H−Si(111). Secondary electron cut-off (SECO, left) and valence band (VB, right) spectra for H−Si(111) after deposition of Tc films of the indicated thicknesses. The SECO directly corresponds to the sample work function φ. The dotted line illustrates that φ is essentially unchanged by the formation of the hybrid interface. The fact that a prominent Si VB signal can be observed also for nominal multilayers is a clear indication for a Vollmer–Weber growth mode. For the VB spectra shown in the upper part of the figure, the H−Si(111) contribution has been subtracted to emphasize the Tc-derived DOS. The inset shows the VB onset of H−Si(111) measured at normal emission geometry. This gives access to the Si VB maximum at the center of the Brillouin zone. Reprinted with permission from [136]. Copyright (2020) American Chemical Society. (b) Electronic structure at the Tc/H−Si(111) interface calculated from hybrid density functional theory. The left part shows the projected DOS for the H−Si(111) substrate atoms (black) and the Tc atoms (orange) for the configurations displayed in the right part. The central part shows corresponding schematic energy diagrams. Reproduced from [178]. © IOP Publishing Ltd. All rights reserved.

critical φ value, the Schottky–Mott rule applies. Note, however, that in contrast to the case of Tc/H−Si discussed above, additional interface dipoles can occur that do not depend on the ELA. Two examples that are discussed in more detail in the corresponding subsection below are the electrostatic polarization due to the interaction of the molecular quadrupole moment and the ISC surface as well as the 'push-back' effect that is caused by Pauli repulsion. We define an effective work function φ_{eff} that accounts for these effects. Above the critical φ_{eff}, Fermi-level pinning sets in. This behavior can be explained with electrostatic considerations alone [182, 185, 186], by assuming that the charge equilibrium between the electronic systems of the organic molecules and the underlying substrate is expressed by the Fermi–Dirac distribution function. As illustrated in figure 8, once the OSC HOMO DOS and the ISC Fermi-level start overlapping substantially ($\varphi \approx$ IE), electronic equilibrium requires charge redistribution across the interface to guarantee overall charge neutrality. The two regimes are characterized by slope parameters $S = \mathrm{d}(\Delta E_{\text{H}})/\mathrm{d}\varphi_{\text{eff}}$ of $S = 0$ and $S = 1$. As illustrated in figure 9, an abrupt transition between the two extreme S values is only observed for sufficiently thick films and narrow HOMO DOS. The less abrupt transition observed for realistic interfaces is sometimes referred to as 'soft' Fermi-level pinning [187, 188]. Compared to the bulk, interface layers can have significantly higher degrees of disorder [18, 189], giving rise to a broadened DOS. This affects the interfacial ELA [190] and makes the Fermi-level pinning softer [187]. Molecules at the interface can feature a different molecular-orientation distribution than those in the bulk [191, 192], and are subject to a different electronic screening [167, 193, 194]. As explained above, both effects influence IE and EA and, thereby, the pinning behavior at the interface. For example, it is the combination of more pronounced screening at the hybrid interface (estimated to be 0.3 eV) and the adoption of a flat-lying molecular orientation that is thought to drive the 6P/ZnO(0001) interface into the pinning regime, which is different than what is expected from the ELA between multilayer 6P films and ZnO(0001) [195].

Zahn *et al* investigated the ELA of a number of interfaces between OSCs and H−Si, Se−GaAs, and S−GaAs that, assuming vacuum-level alignment, have a large energetic distance between the Fermi level of the ISC and the molecular orbitals of the OSC, but were found to not obey the Schottky–Mott rule [196, 197]. Defects in the ISC [198] and a molecular rearrangement as a function of coverage [196] were discussed as possible reasons for the observed behavior. Later, one of these molecules, perylene-3,4,9,10-tetracarboxylic dianhydride (PTCDA), was investigated for additional substrates that span a large φ range. After formation of the PTCDA film, all samples exhibited essentially the same work function and ΔE_{H}, independent of the initial φ and reactivity of the substrate (see figure 7). This was attributed to a high density of interface states for this OSC [199]. The additional DOS can be accounted for via a Lorentzian broadening and gives rise to intermediate values of S, as shown in figure 9 and further detailed in [182, 199–201]. Alternatively, a new DOS in the gap of the OSC can also describe the observed behavior. The effect is that the gap of the OSC essentially becomes much narrower, and so does the φ range without pinning. The identical substrate-independent pinning was also observed for 1,4,5,8,9,12-hexaazatriphenylene-2,3,6,7,10,11-hexacarbonitrile (HATCN) [181] and is included in figure 7. However, for HATCN the intra-gap DOS was also observed beyond the interface region. For this reason, a chemical defect rather than interface states was inferred in this case.
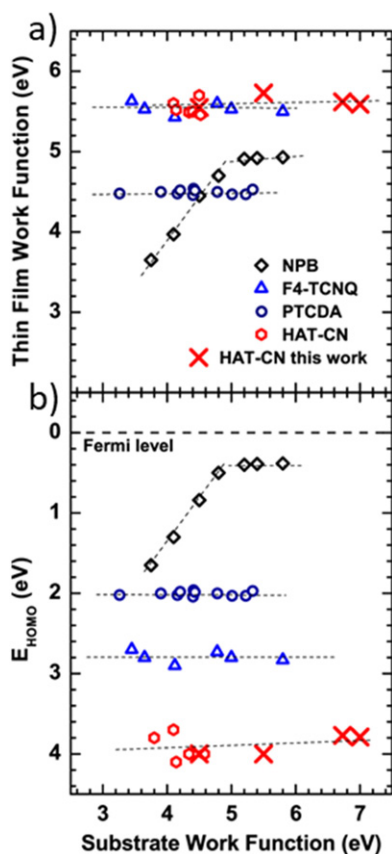
Figure 7. (a) and (b) Work functions and HIBs (E_{HOMO}), respectively, for thin films of the indicated OSCs on different substrates that cover a large substrate work function range. The plots for NPB exhibit two regimes with $S = 1$ and $S = 0$ while the other OSCs exhibit substrate-independent pinning, i.e. no substrate work function regime with $S = 1$. Reprinted with permission from [181]. Copyright (2020) American Chemical Society.
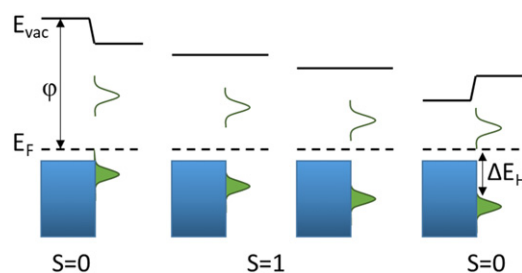

Figure 8. Illustration of the φ regimes with characteristic slope parameters S. Note that a possible push-back effect and effects of a finite layer thickness are not included in this simple sketch.

This occurrence of Fermi-level pinning is related to the observation that the Schottky barrier height at metal/ISC interfaces cannot be readily tuned via the metal work function, which has puzzled scientists and plagued device specialists for the better part of the second half of the twentieth century. Also in this case, the resulting interface chemistry is often (but usually not adequately [202]) accounted for via a Lorentzian broadening of the DOS.

In cases where the OSC is Fermi-level pinned, its intrinsically low free charge carrier density is significantly increased due to contact doping from the ISC. The additional carriers give rise to a drastically increased energy-level bending in the OSC [203, 204]. A complex distribution of the charge carriers can result for OSC bilayers. In these cases, the Fermi level of the conductive substrate controls the energy levels of the whole organic layer stack [205–209] (NB: also under illumination [210, 211]). This situation can give rise to energy-level shifts upon formation of the organic hetero-interface that can be mistaken for interface dipoles at that interface. However, these are not due to the interaction at the interface at all, but rather a charge carrier redistribution that guarantees electronic equilibrium throughout the whole layer stack [203, 212].
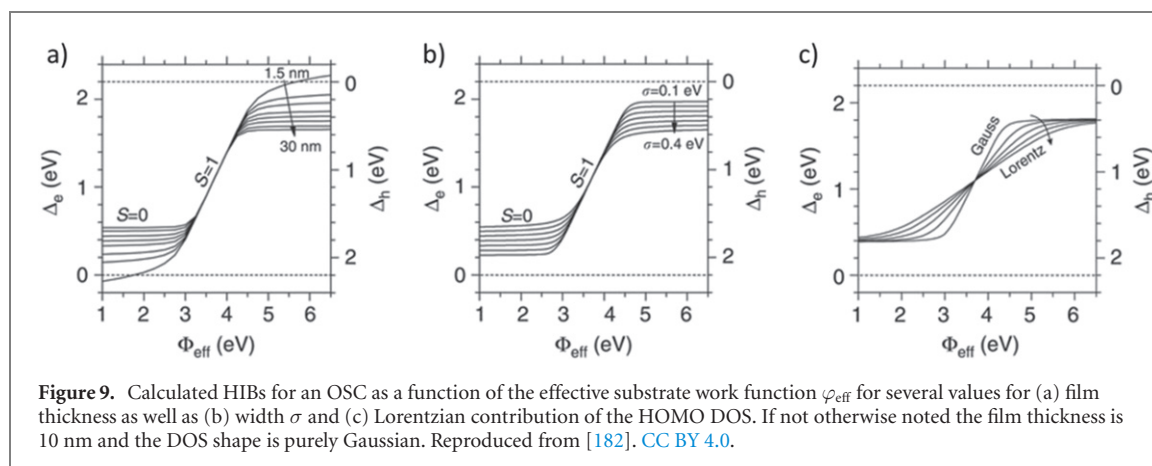
Figure 9. Calculated HIBs for an OSC as a function of the effective substrate work function φ_{eff} for several values for (a) film thickness as well as (b) width σ and (c) Lorentzian contribution of the HOMO DOS. If not otherwise noted the film thickness is 10 nm and the DOS shape is purely Gaussian. Reproduced from [182]. CC BY 4.0.
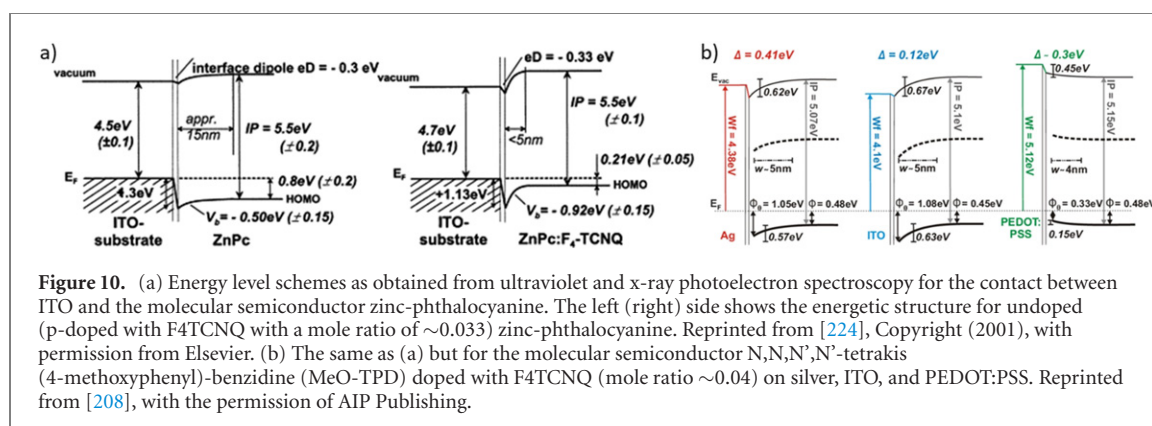

Figure 10. (a) Energy level schemes as obtained from ultraviolet and x-ray photoelectron spectroscopy for the contact between ITO and the molecular semiconductor zinc-phthalocyanine. The left (right) side shows the energetic structure for undoped (p-doped with F4TCNQ with a mole ratio of ~0.033) zinc-phthalocyanine. Reprinted from [224], Copyright (2001), with permission from Elsevier. (b) The same as in (a) but for the molecular semiconductor N,N,N',N'-tetrakis (4-methoxyphenyl)-benzidine (MeO-TPD) doped with F4TCNQ (mole ratio ~0.04) on silver, ITO, and PEDOT:PSS. Reprinted from [208], with the permission of AIP Publishing.
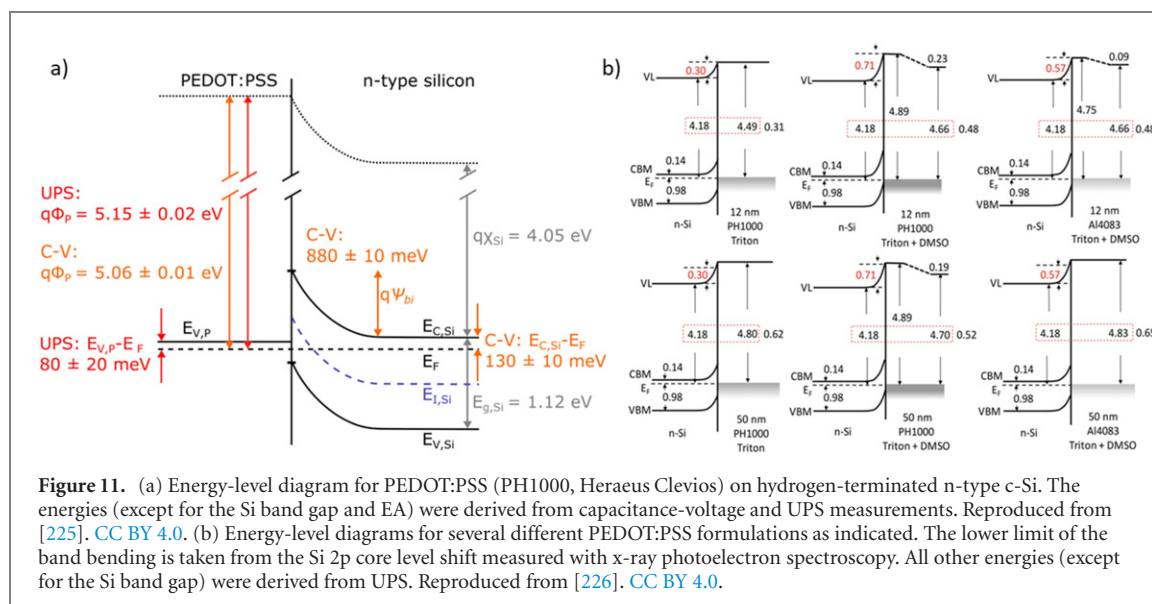
Doped OSC (figure 5(b)): additional charge carriers in organic layers can be induced via doping of the organic films [213–217]. While it was initially believed that molecular doping proceeds via integer charge transfer, there is strong evidence that a charge-transfer complex formation occurs instead in cases where the dopant and matrix consist of small molecules in intimate contact [218, 219]. It is still being debated under which conditions integer charge transfer or charge transfer complex formation prevails. As a note of caution, we would like to point out that diffusion of dopant molecules to the interface has been observed [220–223]. In these cases, the interaction between dopant molecules and the ISC can mimic doping-related effects.

For doped OSCs, significant band/energy-level bending occurs also in thin films. As can be seen in figure 10(a), doping significantly decreases the width of the space charge layer in the OSC and gives rise to a different ELA between multilayer films of the OSC and ITO [224]. Figure 10(b) shows band bending in the OSC for substrates with different work functions [208]. Here, band bending in the OSC achieves a common ELA between the HOMO and E_F within a few nm.

In the above example, the inorganic ITO is degenerately doped while the OSC is not. The opposite configuration is observed for poly(ethylenedioxythiophene):poly(styrenesulfonate) (PEDOT:PSS) on n-type H−Si. PEDOT:PSS is a highly doped organic polymer that is used as a high-performance charge-selective transport material, and depending on the formulation, can be prepared from several solvents, including water [227]. Formation of the PEDOT:PSS/H−Si interface leads to strong band bending in Si and the formation of an inversion layer at its surface [225], as shown in figure 11(a). Notably, the height of the Schottky barrier is directly related to the PEDOT:PSS work function. This is very different from the case of metal/Si contacts, where Schottky barriers significantly deviate from what is expected from the metal work functions [202, 228, 229]. This strongly indicates that interface states are much less important for H−Si contacts to PEDOT:PSS than to metals. Figure 11(b) shows a series of PEDOT:PSS/H-Si interfaces with different PEDOT:PSS formulations [226]. While no indication for band bending in PEDOT:PSS was observed, it was found that potential variations in the PEDOT:PSS layer do occur. These were attributed to a dipole layer either at the PEDOT:PSS/H−Si interface or at the PEDOT:PSS surface.

A case where band-bending was observed both in the inorganic and OSCs is discussed in reference [137] and shown in figure 12. Here, n-type ZnO and p-doped α-NPD form a hybrid pn-junction.

We note that molecular doping can also be used to passivate charge carrier traps in OSCs, and thereby improve the carrier mobility by orders of magnitude [230–232].

Figure 11. (a) Energy-level diagram for PEDOT:PSS (PH1000, Heraeus Clevios) on hydrogen-terminated n-type c-Si. The energies (except for the Si band gap and EA) were derived from capacitance-voltage and UPS measurements. Reproduced from [225]. CC BY 4.0. (b) Energy-level diagrams for several different PEDOT:PSS formulations as indicated. The lower limit of the band bending is taken from the Si 2p core level shift measured with x-ray photoelectron spectroscopy. All other energies (except for the Si band gap) were derived from UPS. Reproduced from [226]. CC BY 4.0.

Interface dipoles: interface dipoles arise in cases of a preferential vertical charge distribution at the interface [155, 233]. If matter replaces the vacuum on top of surfaces of inorganic materials, Pauli repulsion gives rise to the 'push-back' or 'pillow' effect, which is well-known for organic/metal interfaces [173, 234, 235]. The name refers to the fact that the adsorbate displaces the electron-density that spills out of clean metal surfaces. The electron density redistribution gives rise to an interface dipole. The identical phenomenon was reported to occur at metal oxide/organic interfaces. Here, an interface dipole of approximately 0.3 eV was consistently observed for a number of different interfaces [137, 183, 224, 236] and attributed to the push-back effect.

In some cases, interface formation was found to induce an intramolecular charge density rearrangement. At the interface between 6P and the non-polar $(10\bar{1}0)$ facet of the ionic semiconductor ZnO, Della Sala *et al* reported an electrostatic coupling of the molecule with the periodic dipolar electric field generated by the Zn–O surface dimers that gives rise to an induced vertical dipole moment [237]. Additional evidence for the importance of the molecular quadrupole moment comes from organic heterojunctions. Calculations predict that at the C_{60}/pentacene interface, the non-zero multipole moments of pentacene gives rise to electrostatic polarization of C_{60} [238]. A particularly strong lateral quadrupolar interaction was measured for a blend formed by a single-monolayer of flat-lying perfluoropentacene and pentacene molecules [162]. DFT calculations for the OSC/SAM/gold interface indicate that intramolecular polarization also occurs at the OSC/SAM interface [239].

Different to such *induced* dipoles, polar molecules have a *permanent* dipole moment. If polar molecules exhibit a preferential alignment at the interface, they give rise to an interface dipole [240, 241], as will be further discussed in the context of organic interlayers below.

An interface dipole can also be caused by substrate-to-adsorbate ground state charge transfer at the interface. On the one hand, states of OSCs and ISCs can hybridize, which leads to fractional ground state charge transfer at the intimate interface. On the other hand, interfacial charge transfer can be also due to integer charge transfer between localized states in the ISC (e.g. defects) and molecular orbitals localized in the OSC. In many cases, a detailed understanding of the quantum-mechanical nature of the ground state charge transfer is still not established. This is due to mainly two reasons:

(a) A theoretical description is challenging. For example, the ELA and, thus, the amount of interfacial electron transfer (IET) depends on the employed theoretical method [242]. The sensitivity to the employed method also extends to describing fractional and integer charge transfer [243]. Recent calculations found that both transfer mechanisms can be present at hybrid interfaces simultaneously [244].

(b) The real interface structure is often unclear. However, the structure of the inorganic surface (defects, reconstructions, terminating atom type, presence of adsorbates) and the adsorption geometry of the organic molecules (adsorption site, molecular orientation, adsorption-induced changes in the molecular conformation) control the electronic structure at the interface and which part of the inorganic and organic materials interact most intimately.

Experiments that probed the electronic (and in some cases also the geometric) structures of a number of different moderate molecular acceptors on transition metal oxides identified a prominent role of ISC near-surface defects for the observed interfacial ground state charge transfer [124, 126, 134, 245–248]. The charge transfer is due to the misalignment between OSC EA and ISC Fermi-level (cf figure 8) and larger EAs give
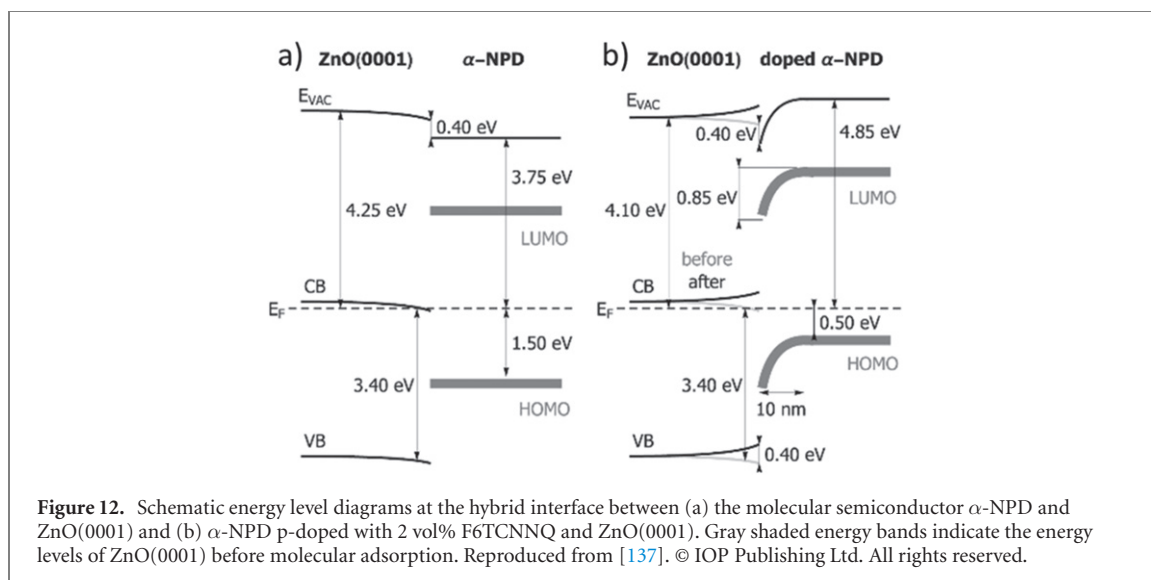
Figure 12. Schematic energy level diagrams at the hybrid interface between (a) the molecular semiconductor α-NPD and ZnO(0001) and (b) α-NPD p-doped with 2 vol% F6TCNNQ and ZnO(0001). Gray shaded energy bands indicate the energy levels of ZnO(0001) before molecular adsorption. Reproduced from [137]. © IOP Publishing Ltd. All rights reserved.
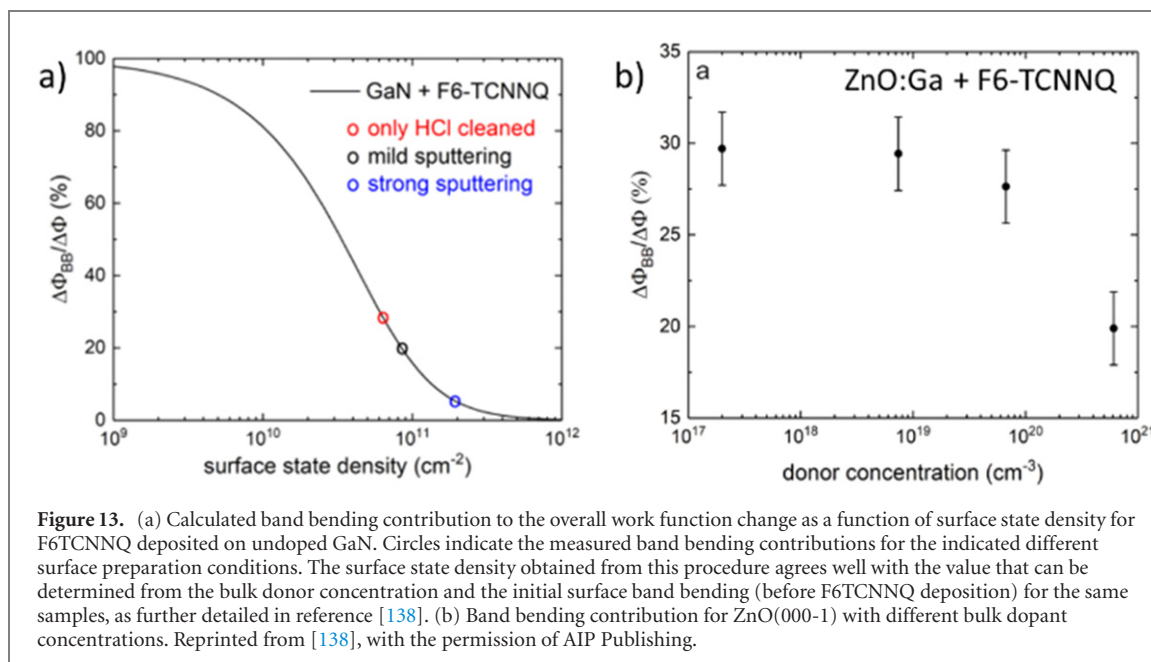

Figure 13. (a) Calculated band bending contribution to the overall work function change as a function of surface state density for F6TCNNQ deposited on undoped GaN. Circles indicate the measured band bending contributions for the indicated different surface preparation conditions. The surface state density obtained from this procedure agrees well with the value that can be determined from the bulk donor concentration and the initial surface band bending (before F6TCNNQ deposition) for the same samples, as further detailed in reference [138]. (b) Band bending contribution for ZnO(000-1) with different bulk dopant concentrations. Reprinted from [138], with the permission of AIP Publishing.

rise to a more pronounced effect. Therefore, strong acceptor molecules offer a means of quantifying the ISC bulk and surface DOS [138, 139, 188, 249, 250]. To that end, the fraction of charges originating from the ISC surface is compared to the fraction stemming from its bulk. As illustrated in figure 5(c)), electron transfer from the bulk and the surface both give rise to a potential drop across the hybrid interface, but only the latter also registers as band bending. The potential drop (bend bending) directly corresponds to the work function change (ISC energy level shifts) upon interface formation, both of which can be probed with photoelectron spectroscopy. This procedure was used to systematically investigate how surface treatments and the bulk dopant concentration affect the ISC surface DOS [138]. As can be seen in figure 13, a strong effect of the surface state density is observed in all investigated cases. Notably, a pronounced influence of the bulk doping is observed only at very high dopant concentrations.

Note that while the described procedure allows quantifying the influence of the surface states on the charge redistribution across the interfaces, it does not allow a resolution of the nature of the interaction at the hybrid interface. The two very strong acceptors, 2,3,5,6-tetrafluoro-7,7,8,8-tetracyanoquinodimethane (F4TCNNQ) and 2,2-(perfluoronaphthalene-2,6-diylidene)dimalononitrile (F6TCNNQ) are an interesting case. While a pronounced chemical shift in the nitrogen atoms of molecules at the interface (indicative for charge transfer) are observed for H–Si [251], this is not the case for ZnO [249, 252]. Therefore, despite further insightful investigations with other techniques [253, 254], the exact nature of the interfacial interaction at these organic/ZnO interfaces is not yet completely resolved.

The introduction of insulating interlayers induces the transition from fractional to integer charge transfer [255]. The thickness of the interlayer controls the number of transferred charges [205, 207, 209, 256], which shows that an interface dipole is formed between substrate and overlayer, whereas the insulating interlayer is neutral. The opposite trend in interface chemistry strength can be induced by covalently binding the organic and inorganic materials at the hybrid interface. The ELA at these interfaces has been studied as well and we list examples for Si [63, 257] and TiO$_2$ [258, 259].

We conclude this section by noting that organic and hybrid materials are often prone to chemical changes and structural rearrangements. The rate of these aging processes can be significantly increased by exposure to vacuum and irradiation. References [260, 261] give a good overview about how these effects should be considered when determining the relevant energy levels for organo-halide perovskites, which is a particularly dynamic material class.

4. Photoinduced excited state dynamics

The purpose of a solar cell is to convert incident light into electricity via the photovoltaic effect. In broad terms, this is achieved by delivering electrons and holes that have been generated by photoexcitation of a semiconductor to separate electrical contacts, where an attached electrical load can be driven. A well-optimized solar cell operated at the maximum power point maintains a chemical potential difference between the electron and hole populations that is close to the band gap energy of the semiconductor. Charge carrier recombination within the solar cell beyond the amount necessary to satisfy thermodynamic constraints is a loss process, which reduces the chemical potential difference between electrons and holes, expressed as a reduction in the quasi-Fermi level splitting, and hence the achievable voltage of the solar cell.

The exact process by which a solar cell converts light into usable electricity depends on the details of the cell design, and this must be disambiguated in order to give a concise account of the relevant excited state processes. Our scope in this work is restricted to the different variations of hybrid inorganic–organic solar cells, and the hybrid interfaces of these devices in particular. We first make an important distinction regarding the nature of the semiconductor light absorber. For an OSC absorber layer, photoexcitation leads to exciton formation, and the mechanics of charge separation are chiefly concerned with driving efficient exciton separation at heterojunctions while providing a device structure that supports electron and hole diffusion away from the heterojunction. An OSC absorber also allows for spectral conversion processes, such as singlet fission, to be implemented. In the case of the semiconductor light absorber having a negligibly low exciton binding energy (this corresponds with all classical bulk ISCs, but also with the bulk hybrid lead halide perovskite family), free electron–hole pairs are generated directly upon photoexcitation.
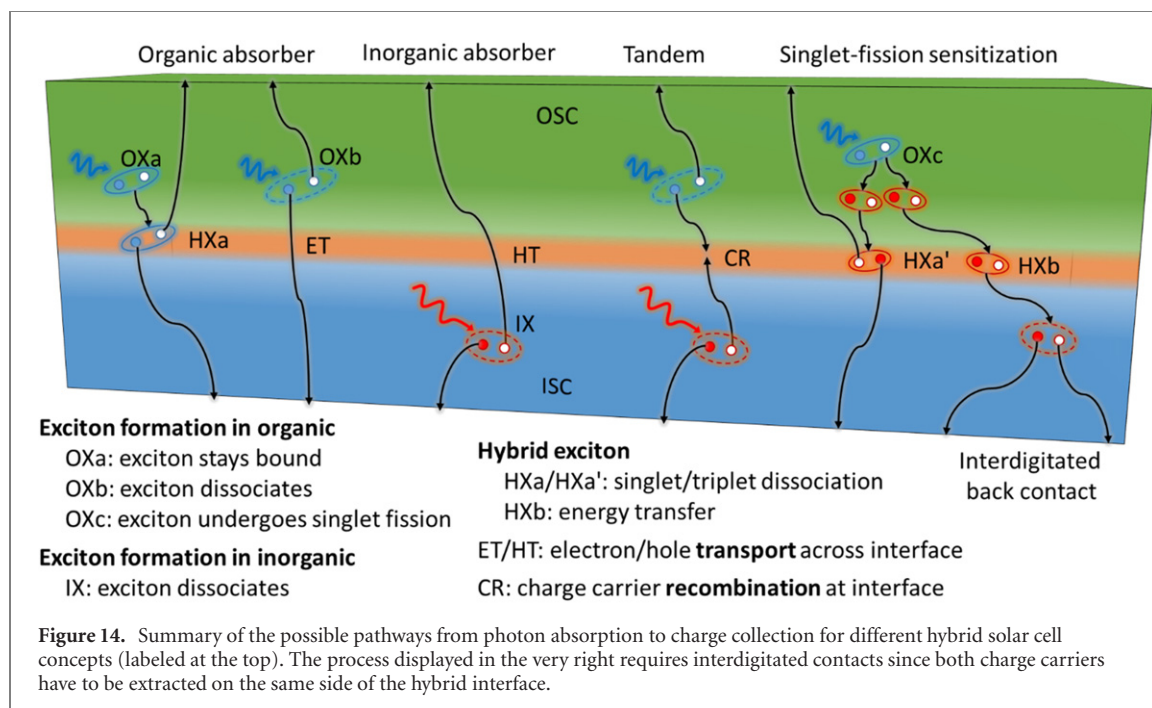
In the following, we briefly discuss exciton formation and transfer mechanisms, and then collect the different possible exciton evolution pathways available in hybrid solar cells (see sketch in figure 14). We then separately discuss the role of the hybrid interface in the two different cases described above, namely that (i) excitons or (ii) free charge carriers arrive at a hybrid interface.

4.1. Exciton formation within OSC and ISC layers

If a photon reaches an absorber of the solar cell, it may get absorbed by inducing an electronic transition for which the energy difference between initial and final state corresponds to the photon energy. The immediate effect of the electronic transition can be described as the filling of one formerly unoccupied higher-lying electron level and the simultaneous creation of a hole in the lower-lying level. In response to the electronic transition, the electronic and atomic structure of the local environment adapts to the new charge configuration and stabilizes it. This is referred to as electronic and lattice relaxation, respectively, and the former is much faster than the latter. An exciton is a quasi-particle that consists of the electron-hole pair as well as the environmental response. The exciton binding energy is the energy difference between the bound electron–hole pair and the situation where the electron and hole are sufficiently separated for their Coulomb interaction to be negligible. The exciton immediately after the transition is 'hot', since it typically contains excess vibrational and/or electronic energy compared to the lowest excited state of the same multiplicity. Accordingly, the exciton is considered 'cold' once it has thermalized by shedding this excess energy.

As mentioned previously, the relatively large dielectric constants of bulk crystalline ISCs reduces the Coulomb attraction between geminate electron–hole pairs as a result of dielectric screening. These materials are often referred to as non-excitonic since the exciton binding energy is small, on the order of a few meV [262], which is less than the thermal energy available at room temperature. The electron–hole pairs produced by photoexcitation rapidly dissociate into free charge carriers, and excitonic effects can be largely ignored. Despite different initial expectations, hybrid lead halide perovskites also appear to be non-excitonic by this definition [263, 264].

This is in contrast to what occurs in the case of a typical π-conjugated organic material [265, 266] and low-dimensional ISCs [114, 267–272]. Here, two factors combine to produce distinctive excitonic effects. A low

Figure 14. Summary of the possible pathways from photon absorption to charge collection for different hybrid solar cell concepts (labeled at the top). The process displayed in the very right requires interdigitated contacts since both charge carriers have to be extracted on the same side of the hybrid interface.

dielectric constant for organic and organic-dominated hybrid materials results in weak dielectric screening and hence a strong Coulomb interaction between electrons and holes. In addition, a high degree of spatial confinement in one or more dimensions occurs, resulting in localizing and hence increasing the Coulomb attraction of electrons and holes [273]. This leads to the formation of strongly bound and localized (Frenkel) excitons upon photoexcitation. These necessitate dissociation in order to generate photocurrent in a solar cell.

Frenkel excitons exhibit significant correlation effects, meaning the total electron spin of the exciton sensitively affects the state energy (equivalently, the exciton binding energy). Neglecting for simplicity the various spectroscopic selection rules that come into play, the allowed optical transitions for such a system will be between the electronic ground state and exciton states with the same total electron spin, while optical transitions between unlike spin states are forbidden. According to Hund's rule for maximum multiplicity, triplet excited states (corresponding to a total electron spin of 1) will always be lower in energy than singlet excited states (total electron spin of zero) for a given principle quantum number.

The substantial energy difference between singlet and triplet excited states in some OSCs can be exploited for useful functions. Singlet fission is a process by which a singlet exciton splits into two triplet excitons of approximately half the energy, located on adjacent chromophores [274, 275]. The inverse process is named triplet fusion or triplet–triplet annihilation. Both processes have the potential to support solar cell efficiency beyond the Shockley–Queisser limit in hybrid solar cells, with singlet fission serving as an exciton multiplication scheme that can reduce thermalization losses [4, 135], while triplet fusion can be used in concert with a triplet sensitizing light absorber to generate additional photocurrent from light that is sub-resonant with the optical gap of a solar cell [276, 277]. Several species of quantum dots, especially those from the metal chalcogenide family, have been employed to similar effect in exciton multiplication and triplet fusion schemes [278–280].

Experiments that probe excitons usually measure energy differences (e.g. optical transitions) that do not directly correspond to energy-level differences of the two non-interacting single particles. For example, the difference between the HOMO IE and the LUMO EA (the transport gap) deviates significantly from the energy of the first optical excitation (the optical gap). This is because even in their simplest representation, excitons have to be described as two bound particles (electron and hole) that interact with themselves in addition to their environment. Therefore, one has to be particularly careful when discussing excited states of organic molecules in a one-particle energy-level diagram, as detailed in reference [281].

4.2. Free charge carrier collection

Some hybrid solar cell working principles rely on free charge carriers arriving at hybrid interfaces. This is the case when only non-excitonic absorber materials are used (case IX). However, it also applies to cases where the organic layer itself contains a heterojunction which facilitates exciton dissociation (case OXb). Hybrid interfaces in these devices are formed between the absorber layer and an electrode or transport layer. Examples are an ISC absorber in contact with an organic charge selective contact, or an OSC heterojunction in contact

with metal oxides. In a tandem cell architecture, both the organic and inorganic layers produce free charge carriers. In this case, the hybrid interface between these two absorber layers serves as a recombination layer [282–287].

Free charge carriers are generated at heterojunctions in excitonic systems, or directly upon photoexcitation of a non-excitonic semiconductor. In the former case, electrons and holes diffuse through separate material domains to their respective electrodes. In the latter, electrons and holes have to be separated by steering their respective currents toward separate electrodes. The current densities for electrons and holes are controlled by their conductivities and the gradients of their electrochemical potentials, which, in turn, is equal to their quasi Fermi levels [288]. Maximizing the carrier current to the appropriate contact thus requires a negative gradient of the respective quasi Fermi level and a sufficiently high conductivity, while minimizing the current in the reverse direction requires the opposite. To achieve this anisotropy, at least two distinct regions of the device are required.

A Si pn homojunction is a frequent realization of this requirement. Here the doping level across a monolithic silicon slab is deliberately varied in order to implement the required spatial variation in carrier conductivity. Another strategy for charge carrier separation is the implementation of heterojunctions, where the semiconductor absorber is interfaced with unlike materials, which impart the functions of carrier selectivity [288]. In perhaps the simplest example of this concept, high/low work function metals can be used to create charge-selective heterojunctions on silicon. However, the high density of gap states at the interfaces gives rise to non-ohmic contacts [202, 228, 229] and leads to substantial surface recombination losses [289]. A more successful approach is found in silicon heterojunction cells employing thin amorphous silicon heterojunctions [290]. Dopant-free hetero-contacts are another approach [291–293]. A number of hybrid heterojunctions consisting of organic materials on crystalline silicon have been reported [294–297]. In this role, the strength of organics are their weak interface chemistries, which may reduce the detrimental effects of Fermi-level pinning (compared to metals) and give rise to better passivation of the ISC (compared to inorganic dopant-free hetero contacts). PEDOT:PSS has shown great promise as a hole-selective contact on silicon [298–301]. In section 3 we discussed the ELA at the PEDOT:PSS/H–Si interface. Here, we discuss the charge transport properties. Two different models could apply: in a heterojunction between a p-type semiconductor (PEDOT:PSS) and n-type semiconductor (c-Si), the transport processes are dominated by the diffusion of minority carriers. In contrast, a contact between a metal-like semiconductor (PEDOT:PSS) and a high-mobility semiconductor (c-Si) should behave as a Schottky diode, where thermionic emission over the Schottky barrier controls the charge transport. Jäckle *et al* found that the PEDOT:PSS/H–Si interface behaves like an abrupt pn heterojunction rather than a Schottky diode [225].

The ELA at the hybrid interface controls a possible contact doping into the interface-near region of the absorber layer, which selectively influences the local conductivity for electrons and holes [288, 302–305], but also leads to non-radiative recombination for materials with low mobility, like OSCs [204, 306]. For sufficiently low bimolecular recombination rates, the large increase in mobility already for ultralow doping [232], together with a positive effect on the built-in field, outbalances the increased recombination and warrants employing electrode materials with work functions that force the contacts beyond the onset of ohmic transition [187].

The current density–voltage (J–V) characteristics and open circuit voltage V_{OC} at a hybrid heterojunction between an organic p-type semiconductor (i.e. the Fermi level of the contact material is closer to the OSC HOMO than to its LUMO) and an inorganic n-type semiconductor was semiclassically calculated by Renshaw and Forrest [151]:

$$J = J_s \left[\exp\left(\frac{qV}{n_O k_B T} \right) - \chi(V) \right] - J_{ph}, J_s \propto \exp\left(-\frac{\Delta E_{OI}}{k_B T} \right) \tag{1a}$$

$$q V_{OC} = \Delta E_{OI} - n_O k_B T \ln\left(\frac{k_r}{k_r + k_d} \frac{q\langle a \rangle N_{HOMO} N_c k_{rec}}{J_{ph}} \right). \tag{1b}$$

Here, n_O is the ideality factor that depends on the trap density. J_{ph} is the total photocurrent, which is the sum of the exciton current generated in the OSC times the exciton dissociation efficiency at the interface and the direct carrier generation current in the ISC. $\chi(V)$ is the bias-dependent reverse-bias factor with $\chi(0) \to 1$. The interface energy gap ΔE_{OI} is the energy difference between IE of the OSC and the EA of the ISC. k_r (k_d) are the hybrid CT state recombination (dissociation) rate. The field dependence k_d can be described by the Onsager–Braun model [307, 308]. $\langle a \rangle$ is the characteristic width of the hybrid CT state at the organic–inorganic interface. N_{HOMO} (N_c) is the OSC HOMO (ISC VB) effective DOS. k_{rec} is the bimolecular recombination rate. Further details and formulas for OSC/ISC interfaces with other type configurations can be found in reference [151].

Charge transport through SAMs on ISCs in a metal/organic/ISC configuration was studied for a number of inorganic–organic combinations and modeled as thermionic emission over a Schottky barrier attenuated

by tunneling through a 'molecular insulator' [63, 257, 309], akin to the transport through a metal-oxide-semiconductor junction [310]. Recently, a SAM of methyl-substituted carbazole on ITO has been utilized as the hole-selective layer of a lead halide perovskite absorber used within a silicon/perovskite tandem solar cell [311]. The SAM made a key contribution to the record-setting device performance and high photostability through fast hole extraction and minimized nonradiative recombination at the hole-selective interface. The compositional flexibility and self-limiting monolayer growth of the carbazole derivative, the attributes of which belong to organic molecules in particular, appear instrumental in this function, and make this a good example of the potential boon of hybrid approaches to solar cell interfaces.

4.3. Exciton diffusion and harvest at hybrid interfaces

While single electrons and holes carry a net charge and therefore respond to a gradual electrostatic potential, like band bending, or to a gradient in the quasi-Fermi level, this is not the case for excitons, which are electrically neutral. The Coulombically bound pair of charges that constitute an exciton cannot spontaneously drift apart from one another, at least when the exciton binding energy exceeds kT. An abrupt change in some electronic property—for instance, the EA—is required to drive exciton dissociation, as is typically implemented at heterojunctions. Here we discuss the case that excitons must travel to a hybrid interface prior to their conversion into free charge carriers (cases OXa and OXc) through dissociation at the hybrid interface (cases HXa and HXa'), or exciton transfer across the hybrid interface followed by spontaneous dissociation in a low-exciton binding energy SC (case HXb).

Excitons are typically required to migrate throughout the absorbing medium before encountering a suitable interface. Exciton transfer, migration, or diffusion, as distinct from exciton dissociation, refers to the concerted, resonant relaxation and excitation of electronic transitions in nearby absorbers giving rise to the appearance of an exciton moving throughout a system. Many such transfers may take place before an exciton ultimately expires via recombination or dissociation. The mechanism by which excitons undergo transfer depends on the nature of the electronic transitions involved in the donor (the initially-excited excitonic center) and the acceptor (which may be excitonic or non-excitonic).

In the case of both donor and acceptor transitions being electric dipole allowed, the dominating exciton transfer process is usually Förster resonance energy tranfer (FRET), wherein the transition dipoles of the exciton donor and acceptor couple through the Coulomb interaction, analogous to classical dipole–dipole coupling, and electronic energy is exchanged through a virtual photon. The effective range of FRET is expressed as a critical radius, R_0, defined as the donor–acceptor separation at which the FRET quantum yield reaches 0.5; R_0 values of around 5 nm are typical in molecular solids [312]. While FRET was first formulated in terms of distinct molecular or atomic entities as donor and acceptor, FRET at hybrid interfaces is an important topic in the research of hybrid optoelectronic devices [34, 44, 313]. It has been invoked to describe the transfer of electronic energy to bulk crystalline silicon from metal chalcogenide nanocrystals [314, 315] as well as from fluorescent organic molecules [316].

In the case that the exciton donor and acceptor lack an electronic dipole allowed transition at the relevant frequency, Dexter energy transfer may become significant. The Dexter transfer mechanism is based on the exchange interaction between adjacent chromophores that bear resonant electronic transitions, and permits a non-negligible rate of resonance energy transfer between molecules in spite of the lack of an electric dipole allowed transition [317–319]. Dexter transfer is the mechanism by which triplet excitons may migrate throughout materials when the radiative relaxation of triplet excitons to a singlet ground state is strictly forbidden. Since this applies exactly to singlet fission materials, both in the exciton diffusion and transfer stage, Dexter transfer is particularly relevant for incorporating singlet fission into solar cells [320].

FRET typically occurs at a much higher rate and at longer range than Dexter energy transfer, hence for materials in which FRET is active, the rate due to Dexter is usually negligible. On the other hand, where radiative relaxation of triplets is strictly forbidden, the triplet lifetime is significantly greater than that of singlet excitons, hence the low energy transfer rate may be counteracted. A key metric is the exciton diffusion length, which depends on both the lifetime and the hopping rate. It has been shown that, given optimal energetics of singlet and triplet excitons, triplet exciton diffusion can occur via a cooperative singlet and triplet exciton transport mechanism [321].

Exciton dissociation relies on IET. For relevant cases it is often assumed that IET can be described in the limit of weak electronic coupling between donor and acceptor, and, thus, non-adiabatically [318, 322–326]. In the framework of Marcus theory, this yields for the IET rate at a hybrid interface:

$$K_{\mathrm{IET}} = \frac{2\pi}{h} \int \mathrm{d}E \rho(E) |H(E)|^2 \frac{1}{\sqrt{4\pi\lambda k_\mathrm{B} T}} \exp\left[-\frac{(\lambda + \Delta G - E)^2}{4\lambda k_\mathrm{B} T} \right]. \tag{2}$$

Here ΔG is the free energy difference between electron acceptor and donor and relates to the ELA. $\rho(E)$ is the ISC DOS at energy E, $H(E)$ is the electronic coupling matrix element between donor and acceptor at energy E, and λ is the reorganization energy [327–329] that is related to polaronic effects.

Equation (2) is instructive since it combines several interface parameters that can, at least conceptually, be individually modified. In the following we substantiate the relevance of these parameters.

There is clear evidence that the interfacial ELA sensitively affects exciton harvest. The ELA at the organic/ZnO interface was shown to control the exciton transfer efficiency [330]. For organic heterojunctions, the ELA and the V_{OC} of corresponding solar cells were found to correlate [331] (although with a significant offset of ∼0.5 eV that is thought to be linked to intramolecular vibrations [332, 333]). An optimal driving force has been reported for converting excitons into free carriers in excitonic solar cells [334]. A similar driving force optimum was also found for triplet exciton energy transfer at the interface between pentacene and PbSe nanocrystals [335]. For organic/metal oxide DSSCs, a correlation between the electron injection and the driving force was observed [323].

The electronic coupling, H, was identified as another crucial parameter [336]. The influence of H was systematically studied for DSSCs via the linker type and the incorporation of insulating interlayers [323, 337]. Equation (2) also expresses the fact that the donating OSC state should overlap with a dense manifold of states in the accepting band of the ISC in order to achieve a high IET rate. We note that $\rho(k)$ has to be considered as well, since it was shown that FRET from quantum dots into the indirect ISC Si relies on phonon-assistance [314].

While instructive, equation (2) might not be adequate to describe the most relevant interface processes for exciton harvest.

Firstly, the suitability of Marcus theory in some circumstances has been questioned [338], partially due to the observation of fast transfer times that requires the transfer to be described adiabatically. Such small transfer times were observed for organic/TiO$_2$ [339] and organic/Si [340] interfaces and also for organic heterojunctions [341–343].

Secondly, the relationship between the parameters of equation (2) and the overall exciton dissociation efficiency becomes less simple if the forward process must strongly compete with other parasitic processes, for instance, recombination from a charge transfer state. For example, exciton dissociation at the organic/TiO$_2$ interface can be injection or diffusion limited [344]. A good interface has to facilitate efficient injection, meaning a sufficient rate of electron transfer, but more crucially, a minimal rate of the reverse process. Achieving optimum performance may entail striking a compromise between competing rates.

Lastly, the driving force for exciton dissociation via electron transfer and the rate of subsequent charge separation away from the interface may be related. After the charge transfer over a hybrid interface, electron and hole reside on opposite sides of the interface. Such a state is referred to as CT state ('CT exciton' and 'bound charge pair' are also sometimes used). If injection and subsequent CT state separation occurs coherently, the relevant free energy difference is that for the complete process instead of that for the initial IET. For example, a higher driving force for the initial IET increases the probability for hot CT states, which in turn might increase the probability for successful exciton dissociation. CT states have been observed in the following subset of hybrid interface systems: Zn(Mg)O/organic [345, 346], (In)GaN/organic [109], CdS/organic [347], and transition-metal dichalcogenide/organic [348, 349]. We note in passing that it might be instructive to additionally analyze the CT excitons in van der Waals heterostructures [350], since they allow to study the response of hybrid excitons to a local potential [351], their intra-layer and interfacial interaction [352], the role of momentum conservation [353, 354], and Coulomb engineering of the bandgap and excitons [355]. However, it is still debated whether hot or cold CT states drive exciton dissociation in these materials, and the answer may well be material-dependent. CT states as mediators of recombination was reported for some hybrid systems [356–358]. Non-coherent exciton dissociation via cold CT states has been reported for the poly(3-hexylthiophene-2,5-diyl) (P3HT)/TiO$_2$ interface [359].

While we note that qualitative differences between organic/organic and organic/ZnO interfaces have been reported [359, 362], it is instructive to consider findings from all-organic heterointerfaces, which have been more widely studied. In particular, the body of work on the role of hot CT states in charge separation is significantly larger [326, 363, 364]. Driving force, delocalization, and electron–hole separation were reported to improve the performance for organic heterojunctions and hint at the importance of hot CT states [341, 342, 365–370]. The pathway to separated charges via a hot CT state is illustrated in figure 15. On the other hand, current generation with high efficiency was also observed from relaxed CT states [371–373]. Possible processes that derive from the interface morphology and can assist charge separation from a cold CT state are illustrated in figure 16 [361]. In addition, screening of the charge carriers [364], the mesoscopic structure [374, 375], entropy [376], and different mobilities of electron and holes [377] can assist exciton dissociation. These findings indicate in particular the importance of mesoscopic interface structures that give rise
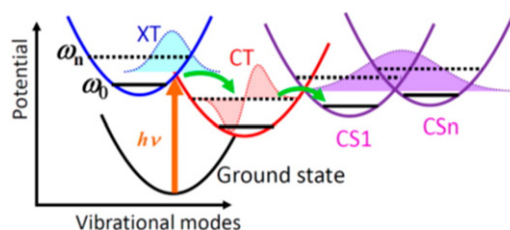
Figure 15. Concept of charge separation mediated by vibronically hot CT states. Potential crossings of exciton (XT), CT, and CS states, together with the vibrational wave functions on the respective states. The solid and dashed black lines illustrate the vibrational ground (ω_0) and excited (ω_n) states, respectively. Reprinted with permission from [360]. Copyright (2013) American Chemical Society.
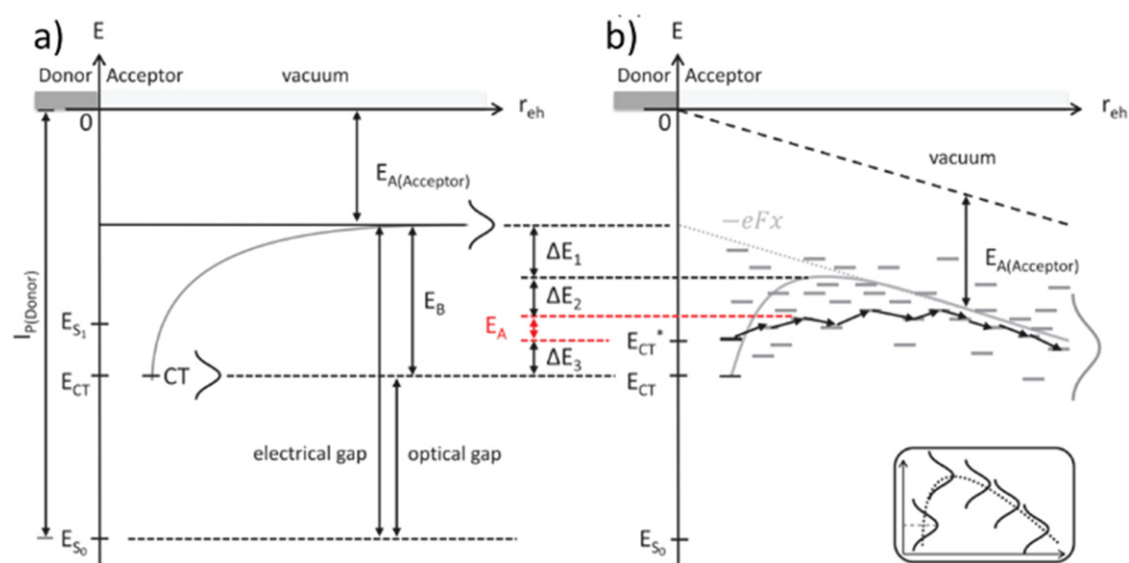

Figure 16. (a) Schematic of the energetics at a donor–acceptor interface in the absence of a field and as a function of electron–hole separation distance r_{eh}. (b) The same as (a) when an electric field is present. The electrical gap and the optical gap are shown. Their difference is due to the Coulomb attraction between electron and hole. The Coulomb energy is indicated by the gray line. The fact that the energies are actually broadened is indicated by the Gaussian line shape that superimposes on the levels. The electrostatic potential gradient reduces the energy barrier by ΔE_1. Energetic disorder further reduces the barrier by ΔE_2. ΔE_3 is a compensation resulting from the zero-point oscillation energy of the electron–hole pair in the Coulomb potential. E_A is the energy that still needs to be overcome to separate charges. [361] John Wiley & Sons. [Copyright © 2019 WILEY-VCH Verlag GmbH & Co. KGaA, Weinheim].

to gradients in crystallinity and intermixed phases that facilitate charge delocalization and favorable energy cascades [378].

5. Modifying hybrid interfaces

The chemical and electronic structure of hybrid interfaces is highly tunable by virtue of the many interoperating components, and many approaches have been undertaken to improve their optoelectronic functions. Figure 17(a) summarizes schematically the three interface modification categories discussed in the following. Example modification materials are given in the figure caption. We discuss the effects of the modification schemes via the expected influence on the parameters in equation (2), namely the driving force ΔG, the electronic coupling H, and the density of acceptor states of the ISC ρ. Echoing a point made previously, enhancing the yield of the desired forward process can also be achieved by reducing the rate of competing loss processes, and interface modifications can also be made to this end.

5.1. Doping
Modifying the ISC by doping allows tuning its electronic interface structure. The electronic structure controls the DOS that are available for accepting charge transfer. This is expressed by ρ in equation (2). Notably, ρ for acceptor states that give rise to bound CT states are to be avoided. As shown in figure 18, Cs doping of ZnO reduces the density of these gap states and the associated effect of electron trapping at the interface [358]. Also N doping of ZnO was shown to facilitate de-trapping of electrons [381].

Figure 17. (a) Interface structure showing schematically a combination of different interface modifiers (orange). Example modifier materials are given in brackets below and discussed in the main text. ISC doping can be used to tune the surface potential (ZnO:Sn), fill gap states (ZnO:Cs, ZnO:N), or passivate the surface (Si:B). The inorganic interlayer (IL) can represent a dielectric layer (SiO$_2$, TiO$_2$, ZrO$_2$, Al$_2$O$_3$, MgO, ZnO, Y$_2$O$_3$, Nb$_2$O$_5$, HfO$_x$N$_y$) or a (highly electronegative) surface-passivating agent (TiCl$_4$, NF$_3$). The π-conjugated core of the SAM can be identical to the molecules that make up the OSC. In this case, conceptually only the linker of the SAM serves as interface modifier. Alternatively, the whole SAM can act as modifier, e.g. by facilitating an interface dipole or energy cascade. The green-red-striped filling accounts for both cases. (b) Illustration of how a linker with suitable chemical structure and an inorganic interlayer with optimized thickness allows for efficient injection and effectively prevents geminate recombination. (c) Illustration of an inorganic interlayer additionally modified with a sub-monolayar of acceptor molecules (F4TCNQ, F6TCNNQ, HATCN) that induce an interface dipole (μ). Dipoles with opposite orientations can also be introduced via donor molecules (19-electron organometallic sandwich compounds [379, 380]).

Figure 18. (a) Cross-section of the inverted bilayer architecture. Light is incident through the glass substrate and the transparent ITO cathode and ZnO:Cs electron acceptor layer. (b) $J-V$ characteristics of representative hybrid ZnO:Cs/P3HT photovoltaic devices with increasing Cs doping level, measured under mismatch-corrected AM 1.5G conditions with 100 mW cm^{-2} light intensity. Comparing the undoped device (open squares) with the optimally doped device (open diamonds) shows the increase in power conversion efficiency upon doping. (c) Simplified model of the processes at the metal oxide/polymer interface after illumination by above-band-gap light, illustrating how a reduction of ZnO gap states by Cs doping leads to a smaller number of bound electron–hole pairs and more free charges. [358] John Wiley & Sons. [Copyright © 2016 WILEY-VCH Verlag GmbH & Co. KGaA, Weinheim].

Extrinsic doping with Sn [382] as well as intrinsic doping from surface defects was shown to control the ELA at oxide/organic interfaces [124, 126, 183]. Changes in the ELA have direct implications for ΔG for forward and backward IET processes as well as for the available ρ [382].

A suitable boron (B) doping profile at Si surfaces gives rise to electron transfer from unsaturated dangling bonds on the Si surface to sub-surface B atoms, thereby passivating the surface Si dangling bond state. This de-activated ISC surface was found to induce a face-on orientation for some organic adsorbates [383–385], indicative of a larger H than in the case of chemically passivated surfaces.

Doping in the alloy regime allows tuning the band gap of the ISC. For example, the combination of ZnMgO and ZnO can be used to form a quantum well structure at the ISC surface and, which enhances FRET to an organic overlayer [313, 386].

5.2. Inorganic interlayers

As shown in figure 19, several insulating oxide interlayers (SiO$_2$, TiO$_2$, ZrO$_2$, Al$_2$O$_3$, [387, 388] MgO [388, 389], ZnO, Y$_2$O$_3$ [388]) were found to improve the efficiency of the exciton dissociation process of DSSCs. Suppressed recombination due to an increased electron–hole separation after injection was suggested as the primary reason for the improvements. Passivation of surface states has also been found to be important [390].

At the P3HT/TiO$_2$ interface, a Nb$_2$O$_5$ interlayer was shown to suppress the formation of CT states [391]. Also in this case, the interlayer was shown to reduce non-geminate recombination both when P3HT and PbSe colloidal quantum dots were used as absorber.

Already in the 1980s, Ng and Card reported an asymmetry in the SiO$_2$ tunneling barriers to electrons (low barrier) and holes (high barrier) [392], showing that interlayers can be used to achieve charge-selective transport. Essentially the same effect was also reported for TiO$_2$ [393, 394].
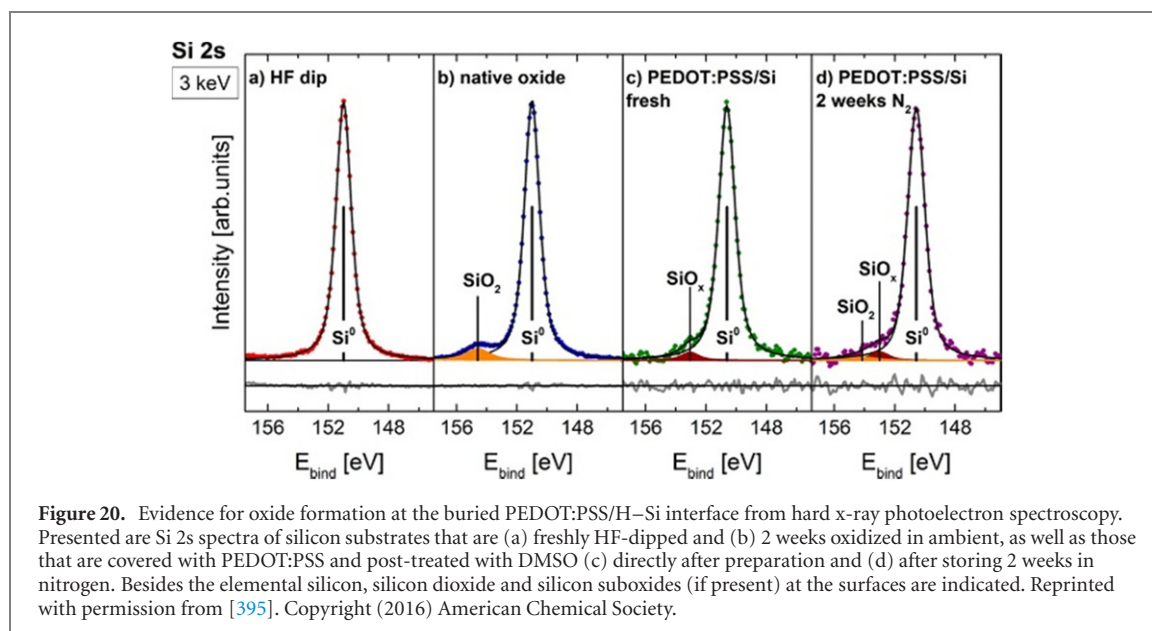
Figure 19. (a) Illustration of the interfacial charge-transfer processes occurring at the nanostructured TiO_2/Al_2O_3 blocking layer/dye/electrolyte interface of DSSCs. (b) Transient absorption data monitoring photoinduced absorption of the dye cation following optical excitation of the dye $RuL_2(NCS)_2$ adsorbed on nanocrystalline TiO_2 films with (a) 0, (b) 1, and (c) 2 Al_2O_3 overlayer coatings. (c) Current/voltage characteristics of typical DSSCs fabricated employing $RuL_2(NCS)_2$ sensitized (a) TiO_2, (b) SiO_2/TiO_2, and (c) Al_2O_3/TiO_2 films. Data are shown for film thicknesses of 8 mm and cell active areas of 0.8 cm². The data shown were obtained under AM1.5 simulated sunlight calibrated to ∼100 mW cm^{-2}. The insert shows the corresponding dark current data. All data were obtained for non-scattering films with transparent counter electrodes. Reprinted with permission from [387]. Copyright (2003) American Chemical Society.

Figure 20. Evidence for oxide formation at the buried PEDOT:PSS/H−Si interface from hard x-ray photoelectron spectroscopy. Presented are Si 2s spectra of silicon substrates that are (a) freshly HF-dipped and (b) 2 weeks oxidized in ambient, as well as those that are covered with PEDOT:PSS and post-treated with DMSO (c) directly after preparation and (d) after storing 2 weeks in nitrogen. Besides the elemental silicon, silicon dioxide and silicon suboxides (if present) at the surfaces are indicated. Reprinted with permission from [395]. Copyright (2016) American Chemical Society.
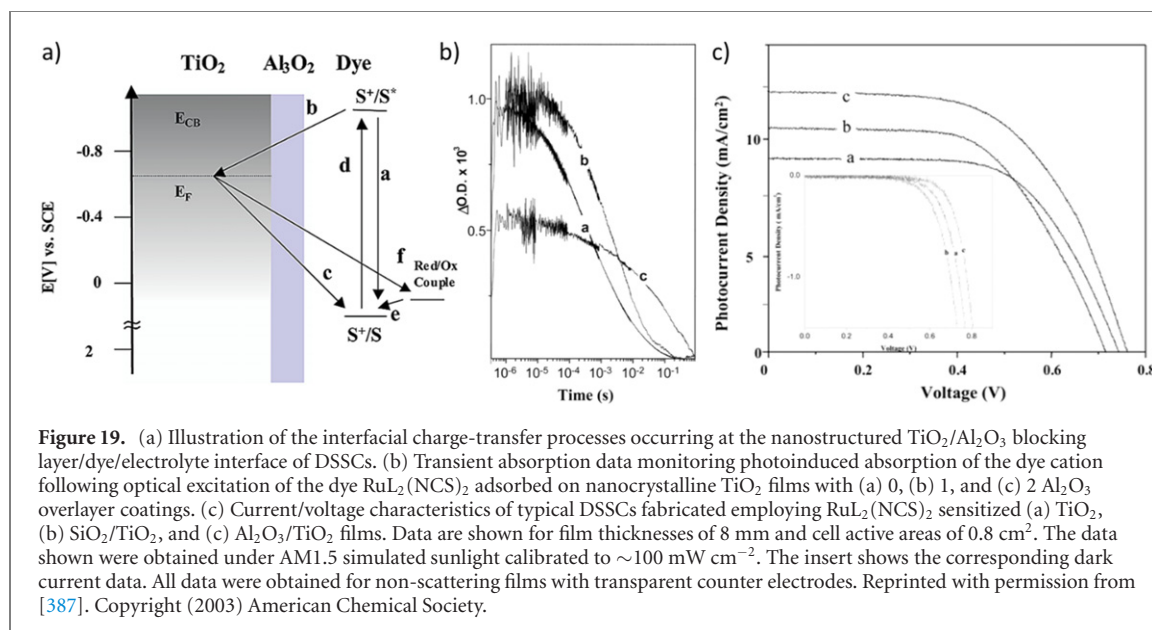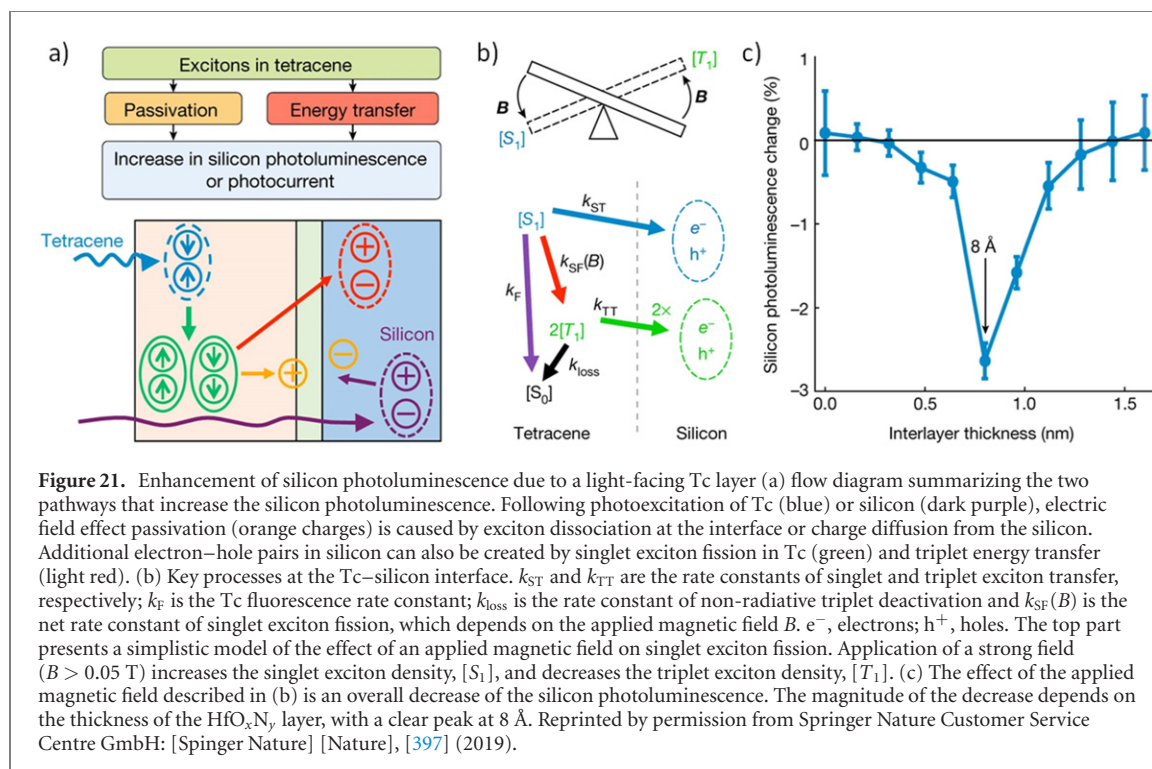
Figure 20 presents an example for an unwanted oxide interlayer. As resolved with hard x-ray photoelectron spectroscopy, the buried Si-PEDOT:PSS interface contains a non-intentional sub-stoichiometric silicon oxide layer immediately after fabrication of the polymer layer [395]. When stored under N_2, the interface continues to oxidize and forms stoichiometric SiO_2. The oxide formation likely derives from residual water in the PEDOT:PSS film and a more stable surface passivation should be chosen, since the uncontrolled silicon oxide growth is expected to deteriorate the interface properties. These results were recently substantiated by a more extensive study [396].

As shown in figure 21, the triplet harvest yield at the Si-organic interface could be enhanced by using a sub-nm hafnium oxynitride (HfO_xN_y) interlayer [397]. By contrast, no improvement was reported when using LiF interlayers at the same interface [398]. However, the thinnest interlayer in the latter study was 5 nm, significantly beyond the narrow thickness range for which a positive effect of the interlayer was reported in reference [397]. The HfO_xN_y interlayer was also found to reduce the surface recombination in Si via field-effect passivation. The passivation effect was most pronounced in the spectral region where Tc absorbs light. This indicates that charges from Tc excitons accumulate at the HfO_xN_y-modified interface, which might also mediate triplet dissociation. Since the interlayer has a larger dielectric constant than the ISC in this case, a more efficient screening of the Coulomb potential of the electron-hole pair might also contribute.

Another kind of interlayer is the terminating surface layer. For example, $TiCl_4$ is a common passivation reagent for TiO_2 that can be used for trap-state engineering [399]. For elemental ISCs like Si, the simplest

Figure 21. Enhancement of silicon photoluminescence due to a light-facing Tc layer (a) flow diagram summarizing the two pathways that increase the silicon photoluminescence. Following photoexcitation of Tc (blue) or silicon (dark purple), electric field effect passivation (orange charges) is caused by exciton dissociation at the interface or charge diffusion from the silicon. Additional electron–hole pairs in silicon can also be created by singlet exciton fission in Tc (green) and triplet energy transfer (light red). (b) Key processes at the Tc–silicon interface. k_{ST} and k_{TT} are the rate constants of singlet and triplet exciton transfer, respectively; k_F is the Tc fluorescence rate constant; k_{loss} is the rate constant of non-radiative triplet deactivation and $k_{SF}(B)$ is the net rate constant of singlet exciton fission, which depends on the applied magnetic field B. e$^-$, electrons; h$^+$, holes. The top part presents a simplistic model of the effect of an applied magnetic field on singlet exciton fission. Application of a strong field ($B > 0.05$ T) increases the singlet exciton density, $[S_1]$, and decreases the triplet exciton density, $[T_1]$. (c) The effect of the applied magnetic field described in (b) is an overall decrease of the silicon photoluminescence. The magnitude of the decrease depends on the thickness of the HfO$_x$N$_y$ layer, with a clear peak at 8 Å. Reprinted by permission from Springer Nature Customer Service Centre GmbH: [Spinger Nature] [Nature], [397] (2019).

termination consists of hydrogen. In comparison, more electronegative groups are expected to give rise to an increase of the work function by up to more than 2 eV [159, 160]. Such a large work function increase has indeed been realized experimentally by exposing H−Si to NF$_3$ [136]. In the same work, it was shown that this polar surface termination allows tuning the ELA at the hybrid interface in much the same way as discussed below for organic interlayers.

    We note that quantum dots can also be used as acceptor interlayers in energy cascades that funnel charges [400] or excitons [315] from an OSC.

5.3. Organic interlayers

Organic interlayers can be used to tune the work function of ISCs within a range of several eV via the introduction of surface dipoles. This can be achieved via induced dipoles generated by donor or acceptor molecules that drive a preferential electron rearrangement between the ISC bulk and its surface [139, 249, 251, 379]. The molecular modifiers are typically prepared via vacuum-deposition, but can also be grown from solution [401]. Alternatively, molecules that bear a permanent dipole moment and are preferentially aligned, e.g. by anchoring to the ISC surface, also give rise to a surface dipole [52, 258, 345, 402, 403].

    The change in work function can be used to tune the ELA at the hybrid interface, as illustrated in figure 17(c), 22, and 23. This was observed, e.g. at organic/ZnO [249, 330, 345, 406] organic/H−Si [136, 380], and organic/TiO$_2$ [258, 407–409] interfaces. A change in ELA can be used to increase (decrease) ΔG as well as the ρ overlap between the OSC and ISC for electron injection (recombination), thereby enhancing exciton dissociation [410]. As can be seen in figure 24, this modification enhances the short circuit current (J_{SC}) but the same change in ELA also reduces the V_{OC} [405, 406]. This follows from the fact that equation (1b) depends on the interface energy gap ΔE_{OI}. In a related case, the opposite approach was employed for a non-solar cell structure. Here, ELA tuning toward smaller ΔG was used to enhance the exciton transfer yield at the ZnO-organic interface and attributed to the fact that the transferred excitons undergo dissociation at the modified hybrid interface with significantly reduced rates [330]. In another study, ELA tuning via molecular acceptors did not notably improve the triplet exciton dissociation at the organic/H−Si interface [136]. C$_{60}$ was one interlayer material examined in this study. In this case, the interface dipole at the ISC/interlayer interface was compensated by a second, unintentional interface dipole at the interlayer/organic interface. This example shows the importance of experimentally confirming an ELA tuning scheme. Co-adsorption of modifier and dye was used in DSSCs to obtain SAM blends [411]. In a recent example, this strategy facilitated an increase of the cell efficiency from 11.1% to 12.9% [412].

    Molecular acceptors not only induce ground state charge transfer from the substrate, but can also accept photogenerated charges from the OSC. This resembles closely the standard operation mode of conventional all-organic solar cells. In hybrid solar cells, this can be exploited to assist exciton harvest via an energy cascade, as further discussed in relation to surface-bonded dyes below. Here we mention that for a zinc phthalocyanine

Figure 22. (a) Effect of interlayers of the electron donor mesitylene pentamethylcyclopentadienyl ruthenium dimer [RuCp*(mes)]₂ and the electron acceptor F6TCNNQ on the energy-levels at the organic/H−Si(111) interface. (Left) SECO and valence spectra for H:Si(111)/[RuCp*(mes)]₂/α-NPD (blue), H:Si(111)/α-NPD (black), and H:Si(111)/F6TCNNQ/α-NPD (red). The α-NPD thickness is ca. 5 nm in all cases. The work function is obtained from the SECO onsets as indicated in the figure. The typical α-NPD valence region spectral shape is clearly observable for all cases. The HOMO onset of α-NPD (indicated by numbers) shifts according to the work function of donor/acceptor-modified H:Si(111), and varies between 0.5 and 2.9 eV. All films were deposited by thermal evaporation in UHV. (Right) Analogous data for films of the polymer semiconductor poly[(9,9-dioctylfluorene-2,7-diyl)-alt-(benzo [2,1,3]thiadiazole-4,7-diyl)] (F8BT, thickness of ca. 4 nm) deposited by solution processing in a glovebox. The F8BT VB onset shifts according to the Si work function change. The structures of the molecules and the polymer are shown next to the spectra, and the schematic heterojunction structures are on the right and left sides. Reproduced from [380]. CC BY 4.0. (b) Electroluminescence (EL) from α-NPD deposited on SAM-modified ZnO. The inset shows a clear correlation between the energy position of the EL maximum and the corresponding energy gap between the CB minimum of ZnO and the HOMO onset of α-NPD derived from UPS. Reprinted with permission from [345]. Copyright (2015) American Chemical Society.

Figure 23. (a) Two-dimensional plot of background-subtracted two-photon photoemission data for 60 nm Tc/H−Si(111). (b) One-dimensional slices of the data in (a) at the indicated times. The S_1 and T_1 positions were determined by visual inspection and comparison with the time series measured for another Tc film reported previously [404]. (c) (Left) One-particle energy-level diagrams for the unmodified Tc/H−Si(111) interface. The energy levels for the Tc HOMO and H−Si(111) VB were derived from the data shown in (b) and figure 6. Unoccupied states do not have an IE and the Tc LUMO is indicated only for completeness. (Center) and (right) Energy-level diagrams with shifted Tc/c-Si ELA due to the introduction of interface dipoles of two different magnitudes. Reprinted with permission from [136]. Copyright (2020) American Chemical Society.

(ZnPc) interlayer, theoretical and experimental results revealed that ZnPc molecules in direct contact with a ZnO surface insert new energy levels due to a strong ZnPc/ZnO coupling, and that electron injection from these new energy levels of ZnPc into ZnO is highly efficient [406]. This possibly contributes to the observed increase in photocurrent and an overall increase in power conversion efficiency.

Similar to inorganic interlayers, organic interlayers can reduce the charge carrier recombination at the hybrid interface via a decreased coupling between organic and ISC [406]. However, an organic interlayer does
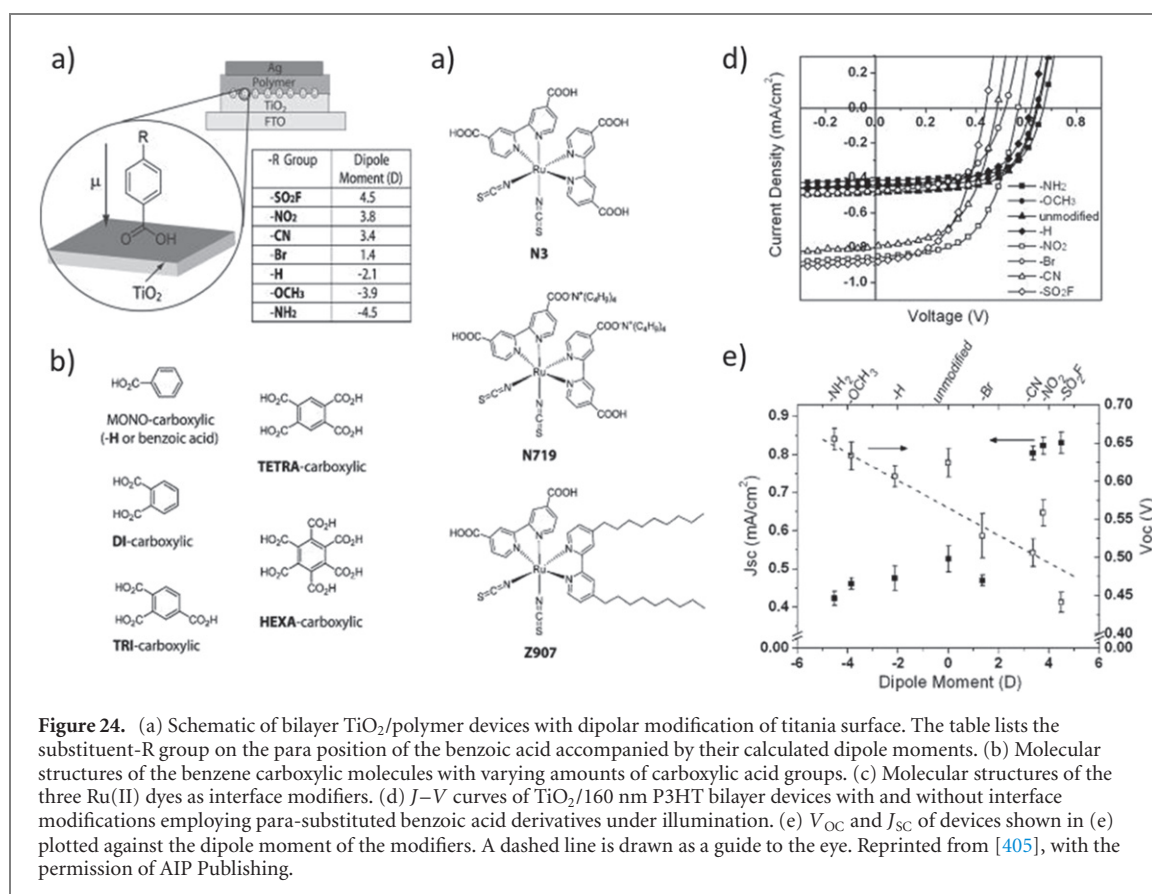
Figure 24. (a) Schematic of bilayer TiO$_2$/polymer devices with dipolar modification of titania surface. The table lists the substituent-R group on the para position of the benzoic acid accompanied by their calculated dipole moments. (b) Molecular structures of the benzene carboxylic molecules with varying amounts of carboxylic acid groups. (c) Molecular structures of the three Ru(II) dyes as interface modifiers. (d) $J-V$ curves of TiO$_2$/160 nm P3HT bilayer devices with and without interface modifications employing para-substituted benzoic acid derivatives under illumination. (e) V_{OC} and J_{SC} of devices shown in (e) plotted against the dipole moment of the modifiers. A dashed line is drawn as a guide to the eye. Reprinted from [405], with the permission of AIP Publishing.

not necessarily prevent the formation of CT states across the hybrid, as evident from CT emission and absorption observed for SAM-modified organic/ZnO interfaces [345]. In this case it was found that the change in ELA induced by the dipole moment of the SAM induces a corresponding change in CT state energy, as shown in figure 22(b).

IET relies on electronically coupling the donor and acceptor. Covalently attaching the organic chromophore to the semiconductor surface allows to systematically control H (as introduced in equation (2)) via the linker. The unoccupied DOS fraction on the linker calculated for the isolated molecule was found to be highly correlated with the initial IET efficiency [344]. It has been shown that increasing the distance between the electron-donating group of the organic and the electron accepting TiO$_2$ by introducing saturated CH$_2$ units in the linker (thereby decreasing H) considerably decreases the rate of electron injection in DSSCs [413]. π-conjugated linkers were found to result in much higher IET rates than when using saturated CH$_2$ units [414, 415]. Given a strong-enough dye-inorganic coupling, light absorption and charge transfer can occur as a coherent process [339].

Notably, different H's for initial IET and interfacial recombination can be achieved by rational design. This is because the initial IET between organic and inorganic constituents proceeds via formerly unoccupied states (the LUMOs of the neutral molecule, LUMO, LUMO+1, ..., and the CB of the ISC) while the final state of the interfacial recombination is the HOMO of the molecular cation or the VB of the ISC. Therefore, it is possible to manipulate the spatial distribution of the electronic states so as to permit the forward IET while shutting off the recombination channel. Figure 25 shows a clear correlation between charge recombination half-time and spatial separation of the dye cation HOMO orbital from the TiO$_2$ surface. From this, an exponential dependence of the electronic transfer rate constant on the separation can be derived [337].

In a similar way, asymmetric substitution of otherwise symmetric molecules can induce directionality of the excited state energy and improve injection into the ISC [416], as shown for zinc tetraphenylporphyrin (ZnTPP) in figure 26. A common structural motif for asymmetric organic sensitizers is a donor-π-bridge-acceptor configuration.

The attachment of dye molecules is also important for quantum dots. If quantum dots act as absorbers, transfer from the quantum dots to the OSC can be used to extract their energy. Triplet exciton transfer to attached organic molecules was observed for quantum dots made, e.g. from PbS [417], Si [68], and perovskites [70, 418, 419]. Exciton dissociation was observed, e.g. for CdSe quantum dots via hole transfer to phenothiazine [420].

Figure 25. Logarithm of the charge recombination half-time determined from transient absorption data as a function of the spatial separation of dye cation HOMO orbital from the TiO$_2$ surface. The influence of the free energy driving force ΔG has been factored into the half-time data to give 'free energy optimized' values. The solid line corresponds to an exponential distance dependence. The chemical and supramolecular structures 1–5 are included in the figure. For the other chemical structures, the reader is referred to [337]. Reproduced from [337] with permission of The Royal Society of Chemistry.

Figure 26. Chemical structures and HOMO/LUMO frontier molecular orbitals of ZnTPP with and without asymmetric substitution. Reproduced from [416] with permission of The Royal Society of Chemistry.

Surface-bound dyes can be used as mediators for exciton harvest from an organic overlayer by acting as electron acceptors [405]. The investigation of a series of acceptor interlayers substantiated that a suitable energy cascade can improve exciton dissociation at organic/TiO$_2$ interfaces [421]. However, the same scheme does not work for ZnO, which the authors ascribe to the more pronounced and unfavorable interface dipole in that case. A different study that employed diethylphosphonate-benzodiathiazole terminated thiophene oligomers of different length highlighted the role of the energetics across the molecularly modified hybrid interface and suggested that both a large energy offset and a suitable energy cascade facilitate exciton dissociation and prevent

Figure 27. (a) Atomic force microscopy (AFM) images for the indicated systems. (b) X-ray diffraction (XRD) data for the same films as in (a). (c) Top (bottom) Devices with C_{60} interlayers of at least (less than) one monolayer and a Tc layer thickness of 60 nm (100 nm) (AMOLF). Reprinted with permission from [136]. Copyright (2020) American Chemical Society.

Figure 28. (a) and (b) AFM images of 20 nm C_{60} thin films on a sapphire substrate without and with pentacene interlayer. (c) and (d) XRD data for the same films as in (a) and (b).[429] with permission of The Royal Society of Chemistry.

recombination [422]. Energy transfer from P3HT to a surface-bonded dye, followed by electron injection from the dye into TiO_2 represents an alternative pathway for exciton harvest [423].

In the electronic structure section we discussed ground-state charge transfer between organic layers and inorganic surface states. This suggests that organic interlayers can passivate ISC surface states. Another passivation mechanism is the chemical attachment of stable moieties that saturate surface radicals and prevent the formation of detrimental chemical species like sub-oxides. While much work has been done on inorganic–inorganic passivation schemes as a result of the growth of the semiconductor industry, inorganic–organic passivation schemes are gaining importance in the optoelectronic fields. Examples for chemisorbed and physisorbed organic interlayers that were found to passivate ZnO defects are mentioned in [424]. Other cases where surface-bonded organic molecules were used for surface passivation comprise perovskite solar cells [311, 425, 426] and Si [427, 428].

5.4. Role of interface morphology changes

The same organic layers in contact with the pristine or modified ISC surface may give rise to very different OSC morphologies (molecular orientation, disorder, growth mode, preferred crystal phases). As shown in figure 27, for Tc on H−Si(111), a 2 nm C_{60} interlayer was found to dramatically increase the roughness and reduce the crystallinity of the Tc films for the same deposition conditions. Accordingly, devices with C_{60} interlayers of

more than one monolayer essentially do not work [136]. Organic interlayers can also improve the crystallinity of the OSC film, as shown in figure 28: C_{60} grows as an amorphous film when deposited directly on sapphire, whereas a pentacene interlayer gives rise to a highly crystalline C_{60} film [429]. Similarly, diindenoperylene-covered SiO_2 gives rise to enhanced C_{60} crystallinity compared to the pristine substrate [430].

These effects are important, because film morphology and polymorphism sensitively influence, e.g. exciton dissociation [148, 189, 374, 375, 431, 432] and singlet fission [191, 433–435]. The molecular orientation at the hybrid interface was shown to influence exciton quenching rates [436] and the lifetime of charge-separated states [437]. The interlayer-induced change of OSC morphology can be exploited in rational ways to better control the interface structure [18, 438, 439].

6. Conclusions & outlook

Progress in the field of hybrid solar cells is a mixed bag. On the one hand, the use of OSCs in combination with ISC absorbers to realize purely electronic functions like charge-selective transport and surface passivation has come a long way, and reaping benefits like reduced production cost and increased stability seems within reach. In particular, using OSCs as dopant free hetero-contacts holds enormous potential to ease fabrication of c-Si solar cells with the potential extra benefit of increased efficiency.

On the other hand, harvesting excitons at hybrid interfaces still remains very inefficient, aside from in DSSCs and quantum dot solar cells. Initially, the higher degree of charge delocalization in ISCs compared to OSCs was one appealing aspect of hybrid solar cells, since the associated more efficient screening seems to promise efficient exciton dissociation at hybrid interfaces based on experimental results [440] and semi-classical modeling [151]. However, experiments [440] and calculations [362, 441–443] also indicate that the ISC surface can act as a trap for charge carriers, and thus hinder exciton dissociation at hybrid interfaces. A similar trapping is not observed, e.g. for the corresponding organic/fullerene interface [362, 440]. More importantly, experiments find that at organic heterojunctions, often no significant driving force is needed to efficiently split thermalized charge transfer states. This means that the interface with an ISC is not, in fact, required for efficient exciton harvest from an OSC.

However, exciton-harvesting hybrid interfaces have other potential advantages. For example, if singlet fission in an excitonic SC can be tapped via exciton harvesting at a hybrid interface, this opens up a non-tandem cell approach to exceeding the Shockley–Queisser single junction limit with silicon, the quintessential solar cell material. Notably in such a device concept, current matching between absorber layers is not required. However, the hybrid interface in such a device has steep requirements, and must support efficient exciton dissociation or injection, excellent passivation of both semiconductor materials, and in the case of a hetero-junction devices, high selectivity charge extraction from silicon. These commingled functions pose a challenge to device designers.

In attempting to review this diverse field, we have discussed prevalent concepts used to describe relevant interfaces in hybrid solar cell technologies. We have presented a comprehensive discussion of mechanisms that govern the electronic structure and excited state dynamics at these interfaces, as well as strategies to control them. However, this is still a far cry from a complete description of the complex property-function relationships in hybrid solar cells. This is due partly to the sheer breadth of the field, which prohibits an all-encompassing review, but also to the inherent complexity of those interfaces that do indeed function successfully [444]. The following is a shortlist of these complexity-compounding phenomena:

- **3D morphologies**, such as bulk heterojunctions, the nanostructured interface of a DSSC, and the surfaces of thin film perovskites, imply complications for investigations, both theoretical and experimental. Theoretical modeling that can account for local quantum effects while capturing the relevant spatial and temporal dimensions is being attempted, but whether the employed structures are representative of the real 3D arrangements still needs to be established. Experiments are often performed on planar interfaces that enable controlled interface preparation and straightforward data interpretation. However, these might miss the role of the surface curvature [441] as well as low-dimensional features like defects that gain in importance for 3D structures, highlighting the necessity of techniques capable of probing buried interfaces.

- Research on organic bulk-heterojunctions indicate that gradients in crystallinity at the interface, as well as phases that feature intermixing, facilitate energy cascades and charge delocalization. Such **mesoscopic structures** are challenging to rationally implement at hybrid interfaces.

- Calculations for organic hetero-interfaces suggest the need to control the electrostatic **potential landscape beyond interface dipoles** [374, 375, 432].

- The triplet exciton harvest at the interface between Tc and HfO_xN_y-covered Si might be assisted by transient interface dipoles that arise from accumulation of photo-generated charges [397]. This suggests that

ISC surface states do not just act as recombination centers and sensitively influence the ELA and surface band bending, but can also give rise to **transient local fields.**

These considerations indicate that controlling both the morphological microstructure as well as the electrostatic potential in space and time is required to realize an efficient exciton harvest. To get a handle on this complexity requires experimental methods capable of probing all of these properties and processes.

A number of methods are available to study solar cells on different spatial and temporal scales [28]. However, different effects might contribute to what can be observed by the different methods [445]. This hampers directly linking derived parameters, like energies from optical and (inverse) photoelectron spectroscopy [194, 345]. Probing both ground state and excited state energies with the same technique should alleviate this issue, as laid out in reference [281].

For resolving the excited state dynamics, our current understanding is largely based on all-optical pump–probe spectroscopy, which can routinely achieve sub-ps resolution. In comparison, time-resolved x-ray spectroscopy is still underdeveloped. However, spectroscopy in the x-ray regime has a number of important advantages over all-optical characterization techniques. It provides elemental, chemical, and surface sensitivity, allowing selective probing of the materials building the hybrid interfaces, rather than the less informative bulk. In addition, the high spatial resolving power of x-ray microcopy (a few 10 nm) allows to selectively probe single grains of the typically multi-crystalline organic films, and can thus help disentangle some of the structural complexity at the interfaces. Laser pump and x-ray probe spectroscopy at storage ring synchrotron sources can readily resolve ns to μs dynamics from interface state charging [446] and surface photovoltage build-up [447]. Recently, pioneering experiments have resolved triplet signatures in the sub-100 ps timescale [448]. By not relying on a pump–probe scheme but instead using the core–hole lifetime as an internal clock, IET can be resolved on a sub-10 fs timescale [449, 450]. Given the advent of next-generation synchrotron sources, free electron lasers, and high harmonic generation, as well as advances in computational methods, the future of excited state dynamics investigations at hybrid interfaces looks promising.

Acknowledgments

Data availability statement

No new data were created or analysed in this study.

ORCID iDs

Jens Niederhausen ⓘ https://orcid.org/0000-0003-1273-4880
Katherine A Mazzio ⓘ https://orcid.org/0000-0001-9565-7301
Rowan W MacQueen ⓘ https://orcid.org/0000-0001-6935-1480

References

[1]   NREL Best research-cell efficiency chart Available from: https://nrel.gov/pv/cell-efficiency.html
[2]   Haegel N M *et al* 2019 Terawatt-scale photovoltaics: transform global energy *Science* **364** 836–8
[3]   Danos L and Markvart T 2010 Excitation energy transfer rate from Langmuir Blodgett (LB) dye monolayers to silicon: effect of aggregate formation *Chem. Phys. Lett.* **490** 194–9
[4]   Rao A and Friend R H 2017 Harnessing singlet exciton fission to break the Shockley–Queisser limit *Nat. Rev. Mater.* **2** 17063
[5]   Guillemoles J-F, Kirchartz T, Cahen D and Rau U 2019 Guide for the perplexed to the Shockley–Queisser model for solar cells *Nat. Photon.* **13** 501–5
[6]   Shockley W and Queisser H J 1961 Detailed balance limit of efficiency of p–n junction solar cells *J. Appl. Phys.* **32** 510–9
[7]   Lin Q, Huang H, Jing Y, Fu H, Chang P, Li D, Yao Y and Fan Z 2014 Flexible photovoltaic technologies *J. Mater. Chem.* C **2** 1233–47
[8]   Popoola I K, Gondal M A and Qahtan T F 2018 Recent progress in flexible perovskite solar cells: materials, mechanical tolerance and stability *Renewable Sustainable Energy Rev.* **82** 3127–51
[9]   Pagliaro M, Ciriminna R and Palmisano G 2010 BIPV: merging the photovoltaic with the construction industry *Prog. Photovolt., Res. Appl.* **18** 61–72

[10] Sánchez-Pantoja N, Vidal R and Pastor M C 2018 Aesthetic impact of solar energy systems *Renewable Sustainable Energy Rev.* **98** 227–38

[11] Lang F *et al* 2016 Radiation hardness and self-healing of perovskite solar cells *Adv. Mater.* **28** 8726–31

[12] Fan X, Zhang M, Wang X, Yang F and Meng X 2013 Recent progress in organic–inorganic hybrid solar cells *J. Mater. Chem.* A **1** 8694–709

[13] Lee J, Mubeen S, Hernandez-Sosa G, Sun Y, Toma F M, Stucky G D and Moskovits M 2013 High-efficiency panchromatic hybrid Schottky solar cells *Adv. Mater.* **25** 256–60

[14] Bouclé J, Ravirajan P and Nelson J 2007 Hybrid polymer-metal oxide thin films for photovoltaic applications *J. Mater. Chem.* **17** 3141–53

[15] Borchert H 2010 Elementary processes and limiting factors in hybrid polymer/nanoparticle solar cells *Energy Environ. Sci.* **3** 1682–94

[16] Coakley K M, Liu Y, Goh C and McGehee M D 2011 Ordered organic–inorganic bulk heterojunction photovoltaic cells *MRS Bull.* **30** 37–40

[17] Milliron D J, Gur I and Alivisatos A P 2011 Hybrid organic-nanocrystal solar cells *MRS Bull.* **30** 41–4

[18] Hsu J W P and Lloyd M T 2010 Organic/inorganic hybrids for solar energy generation *MRS Bull.* **35** 422–8

[19] Wang P, Zhao Y and Wang T 2020 Recent progress and prospects of integrated perovskite/organic solar cells *Appl. Phys. Rev.* **7** 031303

[20] Kim Y, Shin S A, Lee J, Yang K D and Nam K T 2014 Hybrid system of semiconductor and photosynthetic protein *Nanotechnology* **25** 342001

[21] Lloyd M T 2012 Hybrid solar cells *Encyclopedia of Nanotechnology* ed ed B Bhushan (Berlin: Springer) pp 1042–8

[22] Xu Y, Yao H, Ma L, Wang J and Hou J 2020 Efficient charge generation at low energy losses in organic solar cells: a key issues review *Rep. Prog. Phys.* **83** 082601

[23] Sorrentino R, Kozma E, Luzzati S and Po R 2021 Interlayers for non-fullerene based polymer solar cells: distinctive features and challenges *Energy Environ. Sci.* **14** 180–223

[24] Naveed H B, Zhou K and Ma W 2019 Interfacial and bulk nanostructures control loss of charges in organic solar cells *Acc. Chem. Res.* **52** 2904–15

[25] Hermle M, Feldmann F, Bivour M, Goldschmidt J C and Glunz S W 2020 Passivating contacts and tandem concepts: approaches for the highest silicon-based solar cell efficiencies *Appl. Phys. Rev.* **7** 021305

[26] Allen T G, Bullock J, Yang X, Javey A and De Wolf S 2019 Passivating contacts for crystalline silicon solar cells *Nat. Energy* **4** 914–28

[27] Massiot I, Cattoni A and Collin S 2020 Progress and prospects for ultrathin solar cells *Nat. Energy* **5** 959–72

[28] Gurney R S, Lidzey D G and Wang T 2019 A review of non-fullerene polymer solar cells: from device physics to morphology control *Rep. Prog. Phys.* **82** 036601

[29] Nayak P K, Mahesh S, Snaith H J and Cahen D 2019 Photovoltaic solar cell technologies: analysing the state of the art *Nat. Rev. Mater.* **4** 269–85

[30] McNaught A D and Wilkinson A 1997 *IUPAC. Compendium of Chemical Terminology (The 'Gold Book')* 2nd edn (Oxford: Blackwell Scientific Publications)

[31] Coates N E, Yee S K, McCulloch B, See K C, Majumdar A, Segalman R A and Urban J J 2013 Effect of interfacial properties on polymer-nanocrystal thermoelectric transport *Adv. Mater.* **25** 1629–33

[32] Mazzio K A, Kojda D, Rubio-Govea R, Niederhausen J, Ryll B, Raja-Thulasimani M, Habicht K and Raoux S 2020 P-Type-to-N-Type transition in hybrid Ag$_x$Te/PEDOT:PSS thermoelectric materials via stoichiometric control during solution-based synthesis *ACS Appl. Energy Mater.* **3** 10734–43

[33] Steiner A M, Lissel F, Fery A, Lauth J and Scheele M 2021 Prospects of coupled organic–inorganic nanostructures for charge and energy transfer applications *Angew. Chem., Int. Ed.* **60** 1152–75

[34] Agranovich V M, Gartstein Y N and Litinskaya M 2011 Hybrid resonant organic–inorganic nanostructures for optoelectronic applications *Chem. Rev.* **111** 5179–214

[35] Sze S M and Ng K K 2006 *Physics of Semiconductor Devices* (New York: Wiley) pp 5–75

[36] Forrest S R 2020 *Organic Electronics: Foundations to Applications* (Oxford: Oxford University Press) p 1072

[37] Green M L H 1995 A new approach to the formal classification of covalent compounds of the elements *J. Organomet. Chem.* **500** 127–48

[38] Owen J 2015 The coordination chemistry of nanocrystal surfaces *Science* **347** 615–6

[39] Anderson N C, Hendricks M P, Choi J J and Owen J S 2013 Ligand exchange and the stoichiometry of metal chalcogenide nanocrystals: spectroscopic observation of facile metal-carboxylate displacement and binding *J. Am. Chem. Soc.* **135** 18536–48

[40] Lokteva I, Radychev N, Witt F, Borchert H, Parisi J and Kolny-Olesiak J 2010 Surface treatment of CdSe nanoparticles for application in hybrid solar cells: the effect of multiple ligand exchange with pyridine *J. Phys. Chem.* C **114** 12784–91

[41] Kango S, Kalia S, Celli A, Njuguna J, Habibi Y and Kumar R 2013 Surface modification of inorganic nanoparticles for development of organic–inorganic nanocomposites—a review *Prog. Polym. Sci.* **38** 1232–61

[42] Pentzer E B, Bokel F A, Hayward R C and Emrick T 2012 Nanocomposite 'superhighways' by solution assembly of semiconductor nanostructures with ligand-functionalized conjugated polymers *Adv. Mater.* **24** 2254–8

[43] Mazzio K A, Okamoto K, Li Z, Gutmann S, Strein E, Ginger D S, Schlaf R and Luscombe C K 2013 A one pot organic/CdSe nanoparticle hybrid material synthesis with *in situ* π-conjugated ligand functionalization *Chem. Commun.* **49** 1321–3

[44] Mazzio K A, Prasad S K K, Okamoto K, Hodgkiss J M and Luscombe C K 2018 End-functionalized semiconducting polymers as reagents in the synthesis of hybrid II–VI nanoparticles *Langmuir* **34** 9692–700

[45] Xu J, Wang J, Mitchell M, Mukherjee P, Jeffries-EL M, Petrich J W and Lin Z 2007 Organic−inorganic nanocomposites via directly grafting conjugated polymers onto quantum dots *J. Am. Chem. Soc.* **129** 12828–33

[46] Zhao L, Pang X, Adhikary R, Petrich J W, Jeffries-EL M and Lin Z 2011 Organic−inorganic nanocomposites by placing conjugated polymers in intimate contact with quantum rods *Adv. Mater.* **23** 2844–9

[47] Boles M A, Ling D, Hyeon T and Talapin D V 2016 The surface science of nanocrystals *Nat. Mater.* **15** 141–53

[48] Bashir A, Käfer D, Müller J, Wöll C, Terfort A and Witte G 2008 Selenium as a key element for highly ordered aromatic self-assembled monolayers *Angew. Chem., Int. Ed.* **47** 5250–2

[49] Kaefer D, Bashir A and Witte G 2007 Interplay of anchoring and ordering in aromatic self-assembled monolayers *J. Phys. Chem.* C **111** 10546–51

[50] Schreiber F 2000 Structure and growth of self-assembling monolayers *Prog. Surf. Sci.* **65** 151–257

[51] Heimel G, Romaner L, Brédas J-L and Zojer E 2008 Odd–even effects in self-assembled monolayers of ω-(biphenyl-4-yl)alkanethiols: a first-principles study *Langmuir* **24** 474–82

[52] Timpel M *et al* 2014 Surface modification of ZnO(0001)–Zn with phosphonate-based self-assembled monolayers: binding modes, orientation, and work function *Chem. Mater.* **26** 5042–50

[53] Lee H J, Jamison A C and Lee T R 2015 Surface dipoles: a growing body of evidence supports their impact and importance *Acc. Chem. Res.* **48** 3007–15

[54] Käfer D, Witte G, Cyganik P, Terfort A and Wöll C 2006 A comprehensive study of self-assembled monolayers of anthracenethiol on gold: solvent effects, structure, and stability *J. Am. Chem. Soc.* **128** 1723–32

[55] Barteau M A 1996 Organic reactions at well-defined oxide surfaces *Chem. Rev.* **96** 1413–30

[56] Diebold U 2003 The surface science of titanium dioxide *Surf. Sci. Rep.* **48** 53–229

[57] Choi K, Choi H, Min J, Kim T, Kim D, Son S Y, Kim G-W, Choi J and Park T 2020 A short review on interface engineering of perovskite solar cells: a self-assembled monolayer and its roles *Sol. RRL* **4** 1900251

[58] Buckley J J, Couderc E, Greaney M J, Munteanu J, Riche C T, Bradforth S E and Brutchey R L 2014 Chalcogenol ligand toolbox for CdSe nanocrystals and their influence on exciton relaxation pathways *ACS Nano* **8** 2512–21

[59] Buriak J M 2002 Organometallic chemistry on silicon and germanium surfaces *Chem. Rev.* **102** 1271–308

[60] Ciampi S, Harper J B and Gooding J J 2010 Wet chemical routes to the assembly of organic monolayers on silicon surfaces via the formation of Si–C bonds: surface preparation, passivation and functionalization *Chem. Soc. Rev.* **39** 2158–83

[61] Fabre B 2016 Functionalization of oxide-free silicon surfaces with redox-active assemblies *Chem. Rev.* **116** 4808–49

[62] Veerbeek J and Huskens J 2017 Applications of monolayer-functionalized H-terminated silicon surfaces: a review *Small Methods* **1** 1700072

[63] Vilan A and Cahen D 2017 Chemical modification of semiconductor surfaces for molecular electronics *Chem. Rev.* **117** 4624–66

[64] Rappich J, Merson A, Roodenko K, Dittrich T, Gensch M, Hinrichs K and Shapira Y 2006 Electronic properties of Si surfaces and side reactions during electrochemical grafting of phenyl layers *J. Phys. Chem. B* **110** 1332–7

[65] Peng W, Rupich S M, Shafiq N, Gartstein Y N, Malko A V and Chabal Y J 2015 Silicon surface modification and characterization for emergent photovoltaic applications based on energy transfer *Chem. Rev.* **115** 12764–96

[66] Wong K T and Lewis N S 2014 What a difference a bond makes: the structural, chemical, and physical properties of methyl-terminated Si(111) surfaces *Acc. Chem. Res.* **47** 3037–44

[67] Pescara B and Mazzio K A 2020 Morphological and surface-state challenges in Ge nanoparticle applications *Langmuir* **36** 11685–701

[68] Xia P, Raulerson E K, Coleman D, Gerke C S, Mangolini L, Tang M L and Roberts S T 2020 Achieving spin-triplet exciton transfer between silicon and molecular acceptors for photon upconversion *Nat. Chem.* **12** 137–44

[69] Garakyaraghi S, Mongin C, Granger D B, Anthony J E and Castellano F N 2017 Delayed molecular triplet generation from energized lead sulfide quantum dots *J. Phys. Chem. Lett.* **8** 1458–63

[70] Luo X *et al* 2020 Mechanisms of triplet energy transfer across the inorganic nanocrystal/organic molecule interface *Nat. Commun.* **11** 28

[71] Wang L, Guo S, Zhou K and Ma W 2020 Control of the molecular orientation in small molecule-based organic photovoltaics *Sustainable Energy Fuels* **4** 4934–55

[72] Fratini S, Nikolka M, Salleo A, Schweicher G and Sirringhaus H 2020 Charge transport in high-mobility conjugated polymers and molecular semiconductors *Nat. Mater.* **19** 491–502

[73] Schreiber F 2004 Organic molecular beam deposition: growth studies beyond the first monolayer *Phys. Status Solidi a* **201** 1037–54

[74] Tao F, Bernasek S L and Xu G-Q 2009 Electronic and structural factors in modification and functionalization of clean and passivated semiconductor surfaces with aromatic systems *Chem. Rev.* **109** 3991–4024

[75] Zimmermann U, Schnitzler G, Karl N, Umbach E and Dudde R 1989 Epitaxial growth and characterization of organic thin films on silicon *Thin Solid Films* **175** 85–8

[76] Schedel T, Frank K-H, Karlsson U and Koch E E 1990 Orientation of tetracene as a large hydrocarbon on Si(111)-(7 × 7) and oxidized Si(111) *Vacuum* **41** 652–5

[77] Weidkamp K P, Hacker C A, Schwartz M P, Cao X, Tromp R M and Hamers R J 2003 Interfacial chemistry of pentacene on clean and chemically modified silicon (001) surfaces *J. Phys. Chem. B* **107** 11142–8

[78] Han Y, Liu Y, Yuan J, Dong H, Li Y, Ma W, Lee S-T and Sun B 2017 Naphthalene diimide-based n-type polymers: efficient rear interlayers for high-performance silicon-organic heterojunction solar cellss *ACS Nano* **11** 7215–22

[79] Yang Q, Muntwiler M and Zhu X-Y 2009 Charge transfer excitons and image potential states on organic semiconductor surfaces *Phys. Rev. B* **80** 115214

[80] Meyer zu Heringdorf F-J, Reuter M C and Tromp R M 2001 Growth dynamics of pentacene thin films *Nature* **412** 517–20

[81] Choudhary D, Clancy P and Bowler D R 2005 Adsorption of pentacene on a silicon surface *Surf. Sci.* **578** 20–6

[82] Suzuki T, Sorescu D C and Yates J T 2006 The chemisorption of pentacene on Si(001)-2 × 1 *Surf. Sci.* **600** 5092–103

[83] Yong K S, Zhang Y P, Yang S-W, Wu P and Xu G Q 2007 Studies of chemisorbed tetracene on Si(111)-7 × 7 *J. Phys. Chem. A* **111** 12266–74

[84] Dimitrakopoulos C D, Brown A R and Pomp A 1996 Molecular beam deposited thin films of pentacene for organic field effect transistor applications *J. Appl. Phys.* **80** 2501–8

[85] Pithan L *et al* 2018 Molecular structure of the substrate-induced thin-film phase of tetracene *J. Chem. Phys.* **149** 144701

[86] Ruiz R *et al* 2004 Pentacene thin film growth *Chem. Mater.* **16** 4497–508

[87] Nahm R K and Engstrom J R 2017 Who's on first? Tracking in real time the growth of multiple crystalline phases of an organic semiconductor: tetracene on SiO₂ *J. Chem. Phys.* **146** 052815

[88] Kaefer D, Wöll C and Witte G 2009 Thermally activated dewetting of organic thin films: the case of pentacene on SiO₂ and gold *Appl. Phys. A* **95** 273–84

[89] Shi J and Qin X R 2008 Nucleation and growth of tetracene films on silicon oxide *Phys. Rev. B* **78** 115412

[90] Niederhausen J, MacQueen R W, Lips K, Aldahhak H, Schmidt W G and Gerstmann U 2020 Tetracene ultrathin film growth on hydrogen-passivated silicon *Langmuir* **36** 9099–113

[91] Soubatch S, Temirov R, Weinhold M and Tautz F S 2006 The interplay between molecular orientation, film morphology and luminescence properties of tetracene thin films on epitaxial AlO_x/Ni₃Al(111) *Surf. Sci.* **600** 4679–89

[92] Nahm R K and Engstrom J R 2016 Unexpected effects of the rate of deposition on the mode of growth and morphology of thin films of tetracene grown on SiO₂ *J. Phys. Chem. C* **120** 7183

[93]   Blumstengel S, Glowatzki H, Sadofev S, Koch N, Kowarik S, Rabe J P and Henneberger F 2010 Band-offset engineering in organic/inorganic semiconductor hybrid structures *Phys. Chem. Chem. Phys.* **12** 11642−6

[94]   Sparenberg M *et al* 2014 Controlling the growth mode of para-sexiphenyl (6P) on ZnO by partial fluorination *Phys. Chem. Chem. Phys.* **16** 26084−93

[95]   Leclerc N, Chávez P, Ibraikulov O, Heiser T and Lévêque P 2016 Impact of backbone fluorination on π-conjugated polymers in organic photovoltaic devices: a review *Polymers* **8** 11

[96]   Niederhausen J *et al* 2018 Subtle fluorination of conjugated molecules enables stable nanoscale assemblies on metal surfaces *J. Phys. Chem.* C **122** 18902−11

[97]   Blumstengel S, Kirmse H, Sparenberg M, Sadofev S, Polzer F and Henneberger F 2014 Texture and morphology of ZnO grown on nanocrystalline p-sexiphenyl thin films *J. Cryst. Growth* **402** 187−94

[98]   Kirmse H, Sparenberg M, Zykov A, Sadofev S, Kowarik S and Blumstengel S 2016 Structure of p-sexiphenyl nanocrystallites in ZnO revealed by high-resolution transmission electron microscopy *Cryst. Growth Des.* **16** 2789−94

[99]   Temperton R H, O'Shea J N and Scurr D J 2017 On the suitability of high vacuum electrospray deposition for the fabrication of molecular electronic devices *Chem. Phys. Lett.* **682** 15−9

[100] Rinke G, Rauschenbach S, Schrettl S, Hoheisel T N, Blohm J, Gutzler R, Rosei F, Frauenrath H and Kern K 2015 Soft-landing electrospray ion beam deposition of sensitive oligoynes on surfaces in vacuum *Int. J. Mass Spectrom.* **377** 228−34

[101] Saywell A, Sprafke J K, Esdaile L J, Britton A J, Rienzo A, Anderson H L, O'Shea J N and Beton P H 2010 Conformation and packing of porphyrin polymer chains deposited using electrospray on a gold surface *Angew. Chem., Int. Ed.* **49** 9136−9

[102] Förster S and Widdra W 2014 Structure of single polythiophene molecules on Au(001) prepared by *in situ* UHV electrospray deposition *J. Chem. Phys.* **141** 054713

[103] Doubina N, Jenkins J L, Paniagua S A, Mazzio K A, MacDonald G A, Jen A K-Y, Armstrong N R, Marder S R and Luscombe C K 2012 Surface-initiated synthesis of poly(3-methylthiophene) from indium tin oxide and its electrochemical properties *Langmuir* **28** 1900−8

[104] Giussi J M, Cortez M L, Marmisollé W A and Azzaroni O 2019 Practical use of polymer brushes in sustainable energy applications: interfacial nanoarchitectonics for high-efficiency devices *Chem. Soc. Rev.* **48** 814−49

[105] Ma J, Hashimoto K, Koganezawa T and Tajima K 2013 End-on orientation of semiconducting polymers in thin films induced by surface segregation of fluoroalkyl chains *J. Am. Chem. Soc.* **135** 9644−7

[106] Ma J, Hashimoto K, Koganezawa T and Tajima K 2014 Enhanced vertical carrier mobility in poly(3-alkylthiophene) thin films sandwiched between self-assembled monolayers and surface-segregated layers *Chem. Commun.* **50** 3627−30

[107] Dresselhaus M S, Chen G, Tang M Y, Yang R G, Lee H, Wang D Z, Ren Z F, Fleurial J-P and Gogna P 2007 New directions for low-dimensional thermoelectric materials *Adv. Mater.* **19** 1043−53

[108] Schulman D S, Arnold A J and Das S 2018 Contact engineering for 2D materials and devices *Chem. Soc. Rev.* **47** 3037−58

[109] Panda A and Forrest S R 2017 Quantum confinement of hybrid charge transfer excitons in GaN/InGaN/organic semiconductor quantum wells *Nano Lett.* **17** 7853−8

[110] Huang Y, Liang J, Wang C, Yin S, Fu W, Zhu H and Wan C 2020 Hybrid superlattices of two-dimensional materials and organics *Chem. Soc. Rev.* **49** 6866−83

[111] Meunier V, Souza Filho A G, Barros E B and Dresselhaus M S 2016 Physical properties of low-dimensional sp^2-based carbon nanostructures *Rev. Mod. Phys.* **88** 025005

[112] Bryant G W 1988 Excitons in quantum boxes: correlation effects and quantum confinement *Phys. Rev.* B **37** 8763−72

[113] Takagahara T and Takeda K 1992 Theory of the quantum confinement effect on excitons in quantum dots of indirect-gap materials *Phys. Rev.* B **46** 15578−81

[114] Kucur E, Riegler J, Urban G A and Nann T 2003 Determination of quantum confinement in CdSe nanocrystals by cyclic voltammetry *J. Chem. Phys.* **119** 2333−7

[115] Zeiri N, Naifar A, Abdi-Ben Nasrallah S and Said M 2019 Dielectric environment effect on linear and nonlinear optical properties for CdS/ZnS core/shell quantum dots *Results Phys.* **15** 102661

[116] Chafai A, Essaoudi I, Ainane A and Ahuja R 2019 Linear and nonlinear optical properties of donors inside a CdSe/ZnTe core/shell nanodot: role of size modulation *Results Phys.* **14** 102414

[117] Vahdani M R K and Ehsanfard N 2017 Effect of intrinsic optical feedback on the intersubband optical properties of spherical quantum dots *Physica* E **89** 100−4

[118] Koller G, Berkebile S, Oehzelt M, Puschnig P, Ambrosch-Draxl C, Netzer F P and Ramsey M G 2007 Intra- and intermolecular band dispersion in an organic crystal *Science* **317** 351−5

[119] Zhang J L, Ye X, Gu C, Han C, Sun S, Wang L and Chen W 2020 Non-covalent interaction controlled 2D organic semiconductor films: molecular self-assembly, electronic and optical properties, and electronic devices *Surf. Sci. Rep.* **75** 100481

[120] Kang J H, da Silva Filho D, Bredas J-L and Zhu X-Y 2005 Shallow trap states in pentacene thin films from molecular sliding *Appl. Phys. Lett.* **86** 152115

[121] Gemünden P, Poelking C, Kremer K, Daoulas K and Andrienko D 2015 Effect of mesoscale ordering on the density of states of polymeric semiconductors *Macromol. Rapid Commun.* **36** 1047−53

[122] Echenique P M, Berndt R, Chulkov E V, Fauster T, Goldmann A and Höfer U 2004 Decay of electronic excitations at metal surfaces *Surf. Sci. Rep.* **52** 219−317

[123] Morisaki H, Koretsune T, Hotta C, Takeya J, Kimura T and Wakabayashi Y 2014 Large surface relaxation in the organic semiconductor tetracene *Nat. Commun.* **5** 5400

[124] Winget P *et al* 2014 Defect-driven interfacial electronic structures at an organic/metal-oxide semiconductor heterojunction *Adv. Mater.* **26** 4711−6

[125] Li H, Schirra L K, Shim J, Cheun H, Kippelen B, Monti O L A and Bredas J-L 2012 Zinc oxide as a model transparent conducting oxide: a theoretical and experimental study of the impact of hydroxylation, vacancies, interstitials, and extrinsic doping on the electronic properties of the polar ZnO (0002) surface *Chem. Mater.* **24** 3044−55

[126] Schulz P *et al* 2014 Tailoring electron-transfer barriers for zinc oxide/C60 fullerene interfaces *Adv. Funct. Mater.* **24** 7381−9

[127] Valtiner M, Todorova M, Grundmeier G and Neugebauer J 2009 Temperature stabilized surface reconstructions at polar ZnO(0001) *Phys. Rev. Lett.* **103** 065502

[128] Önsten A, Stoltz D, Palmgren P, Yu S, Göthelid M and Karlsson U O 2010 Water adsorption on ZnO(0001): transition from triangular surface structures to a disordered hydroxyl terminated phase *J. Phys. Chem.* C **114** 11157−61

[129] Heinhold R, Williams G T, Cooil S P, Evans D A and Allen M W 2013 Influence of polarity and hydroxyl termination on the band bending at ZnO surfaces *Phys. Rev.* B **88** 235315

[130] Dulub O, Diebold U and Kresse G 2003 Novel stabilization mechanism on polar surfaces: ZnO(0001)-Zn *Phys. Rev. Lett.* **90** 016102

[131] Grånäs E *et al* 2021 Role of hydroxylation for the atomic structure of a non-polar vicinal zinc oxide *Commun. Chem.* **4** 7

[132] Hellström M, Beinik I, Broqvist P, Lauritsen J V and Hermansson K 2016 Subsurface hydrogen bonds at the polar Zn-terminated ZnO(0001) surface *Phys. Rev.* B **94** 245433

[133] Valtiner M, Todorova M and Neugebauer J 2010 Hydrogen adsorption on polar ZnO(0001)-Zn: extending equilibrium surface phase diagrams to kinetically stabilized structures *Phys. Rev.* B **82** 165418

[134] Niederhausen J *et al* 2020 X-ray standing waves reveal lack of OH termination at hydroxylated ZnO(0001) surfaces *Phys. Rev. Mater.* **4** 020602

[135] MacQueen R W *et al* 2018 Crystalline silicon solar cells with tetracene interlayers: the path to silicon-singlet fission heterojunction devices *Mater. Horiz.* **5** 1065–75

[136] Niederhausen J *et al* 2020 Energy-level alignment tuning at tetracene/c-Si interfaces *J. Phys. Chem.* C **124** 27867–81

[137] Futscher M H, Schultz T, Frisch J, Ralaiarisoa M, Metwalli E, Nardi M V, Müller-Buschbaum P and Koch N 2018 Electronic properties of hybrid organic/inorganic semiconductor pn-junctions *J. Phys.: Condens. Matter* **31** 064002

[138] Schultz T, Niederhausen J, Schlesinger R, Sadofev S and Koch N 2018 Impact of surface states and bulk doping level on hybrid inorganic/organic semiconductor interface energy levels *J. Appl. Phys.* **123** 245501

[139] Schultz T *et al* 2016 Tuning the work function of GaN with organic molecular acceptors *Phys. Rev.* B **93** 125309

[140] D'Avino G, Muccioli L, Castet F, Poelking C, Andrienko D, Soos Z G, Cornil J and Beljonne D 2016 Electrostatic phenomena in organic semiconductors: fundamentals and implications for photovoltaics *J. Phys.: Condens. Matter* **28** 433002

[141] Yamada K, Yanagisawa S, Koganezawa T, Mase K, Sato N and Yoshida H 2018 Impact of the molecular quadrupole moment on ionization energy and electron affinity of organic thin films: experimental determination of electrostatic potential and electronic polarization energies *Phys. Rev.* B **97** 245206

[142] Haneef H F, Zeidell A M and Jurchescu O D 2020 Charge carrier traps in organic semiconductors: a review on the underlying physics and impact on electronic devices *J. Mater. Chem.* C **8** 759–87

[143] Marinov O, Deen M J, Jiménez-Tejada J A and Chen C H 2020 Variable-range hopping charge transport in organic thin-film transistors *Phys. Rep.* **844** 1–105

[144] Hsu C-P 2020 Reorganization energies and spectral densities for electron transfer problems in charge transport materials *Phys. Chem. Chem. Phys.* **22** 21630–41

[145] Shuai Z, Li W, Ren J, Jiang Y and Geng H 2020 Applying Marcus theory to describe the carrier transports in organic semiconductors: limitations and beyond *J. Chem. Phys.* **153** 080902

[146] Brédas J-L, Beljonne D, Coropceanu V and Cornil J 2004 Charge-transfer and energy-transfer processes in π-conjugated oligomers and polymers: a molecular picture *Chem. Rev.* **104** 4971–5004

[147] Coropceanu V, Cornil J, da Silva Filho D A, Olivier Y, Silbey R and Brédas J-L 2007 Charge transport in organic semiconductors *Chem. Rev.* **107** 926–52

[148] Nayak P K, Garcia-Belmonte G, Kahn A, Bisquert J and Cahen D 2012 Photovoltaic efficiency limits and material disorder *Energy Environ. Sci.* **5** 6022–39

[149] Prodanović N, Vukmirović N, Ikonić Z, Harrison P and Indjin D 2014 Importance of polaronic effects for charge transport in CdSe quantum dot solids *J. Phys. Chem. Lett.* **5** 1335–40

[150] Scheele M, Brütting W and Schreiber F 2015 Coupled organic–inorganic nanostructures (COIN) *Phys. Chem. Chem. Phys.* **17** 97–111

[151] Renshaw C K and Forrest S R 2014 Excited state and charge dynamics of hybrid organic/inorganic heterojunctions: I. Theory *Phys. Rev.* B **90** 045302

[152] Ishii H, Sugiyama K, Ito E and Seki K 1999 Energy level alignment and interfacial electronic structures at organic/metal and organic/organic interfaces *Adv. Mater.* **11** 605–25

[153] Cahen D and Kahn A 2003 Electron energetics at surfaces and interfaces: concepts and experiments *Adv. Mater.* **15** 271–7

[154] Koch N 2008 Energy levels at interfaces between metals and conjugated organic molecules *J. Phys.: Condens. Matter* **20** 184008

[155] Zojer E, Taucher T C and Hofmann O T 2019 The impact of dipolar layers on the electronic properties of organic/inorganic hybrid interfaces *Adv. Mater. Interfaces* **6** 1900581

[156] Chen W, Huang H, Chen S, Huang Y L, Gao X Y and Wee A T S 2008 Molecular orientation-dependent ionization potential of organic thin films *Chem. Mater.* **20** 7017–21

[157] Duhm S, Heimel G, Salzmann I, Glowatzki H, Johnson R L, Vollmer A, Rabe J P and Koch N 2008 Orientation-dependent ionization energies and interface dipoles in ordered molecular assemblies *Nat. Mater.* **7** 326–32

[158] Heimel G, Salzmann I, Duhm S and Koch N 2011 Design of organic semiconductors from molecular electrostatics *Chem. Mater.* **23** 359–77

[159] Bertocchi M, Amato M, Marri I and Ossicini S 2017 Tuning the work function of Si(100) surface by halogen absorption: a DFT study *Phys. Status Solidi c* **14** 1700193

[160] Arefi H H and Fagas G 2014 Chemical trends in the work function of modified Si(111) surfaces: a DFT study *J. Phys. Chem.* C **118** 14346–54

[161] Salzmann I, Duhm S, Heimel G, Oehzelt M, Kniprath R, Johnson R L, Rabe J P and Koch N 2008 Tuning the ionization energy of organic semiconductor films: the role of intramolecular polar bonds *J. Am. Chem. Soc.* **130** 12870–1

[162] D'Avino G, Duhm S, Valle R D G, Heimel G, Oehzelt M, Kera S, Ueno N, Beljonne D and Salzmann I 2020 Electrostatic interactions shape molecular organization and electronic structure of organic semiconductor blends *Chem. Mater.* **32** 1261–71

[163] Hill I G, Mäkinen A J and Kafafi Z H 2000 Initial stages of metal/organic semiconductor interface formation *J. Appl. Phys.* **88** 889–95

[164] Hesper R, Tjeng L H and Sawatzky G A 1997 Strongly reduced band gap in a correlated insulator in close proximity to a metal *Europhys. Lett.* **40** 177–82

[165] Fernández Torrente I, Franke K J and Ignacio Pascual J 2008 Spectroscopy of C_{60} single molecules: the role of screening on energy level alignment *J. Phys.: Condens. Matter* **20** 184001

[166] Helander M G, Greiner M T, Wang Z B and Lu Z H 2010 Effect of electrostatic screening on apparent shifts in photoemission spectra near metal/organic interfaces *Phys. Rev.* B **81** 153308

[167] Tsiper E V *et al* 2002 Electronic polarization at surfaces and thin films of organic molecular crystals: PTCDA *Chem. Phys. Lett.* **360** 47–52

[168] Knupfer M and Peisert H 2004 Electronic properties of interfaces between model organic semiconductors and metals *Phys. Status Solidi a* **201** 1055−74

[169] Cahen D, Kahn A and Umbach E 2005 Energetics of molecular interfaces *Mater. Today* **8** 32−41

[170] Flores F, Ortega J and Vázquez H 2009 Modelling energy level alignment at organic interfaces and density functional theory *Phys. Chem. Chem. Phys.* **11** 8658−75

[171] Tan A and Zhang P 2019 Tailoring the growth and electronic structures of organic molecular thin films *J. Phys.: Condens. Matter* **31** 503001

[172] Gao Y 2010 Surface analytical studies of interfaces in organic semiconductor devices *Mater. Sci. Eng. R Rep.* **68** 39−87

[173] Franco-Cañellas A, Duhm S, Gerlach A and Schreiber F 2020 Binding and electronic level alignment of π-conjugated systems on metals *Rep. Prog. Phys.* **83** 066501

[174] Friend R H, Phillips M, Rao A, Wilson M W B, Li Z and McNeill C R 2012 Excitons and charges at organic semiconductor heterojunctions *Faraday Discuss.* **155** 339−48

[175] Forrest S R 2015 Excitons and the lifetime of organic semiconductor devices *Phil. Trans. R. Soc. A.* **373** 20140320

[176] Kahn A, Koch N and Gao W 2003 Electronic structure and electrical properties of interfaces between metals and π-conjugated molecular films *J. Polym. Sci.* B **41** 2529−48

[177] Ishii H, Hayashi N, Ito E, Washizu Y, Sugi K, Kimura Y, Niwano M, Ouchi Y and Seki K 2004 Kelvin probe study of band bending at organic semiconductor/metal interfaces: examination of Fermi level alignment *Phys. Status Solidi a* **201** 1075−94

[178] Janke S M, Janke S M, Rossi M, Levchenko S V, Kokott S and Blum V 2020 Pentacene and tetracene molecules and films on H/Si(111): level alignment from hybrid density functional theory *Electron. Struct.* **2** 035002

[179] Bussolotti F, Han S W, Honda Y and Friedlein R 2009 Phase-dependent electronic properties of monolayer and multilayer anthracene films on graphite [0001] surfaces *Phys. Rev.* B **79** 245410

[180] Niederhausen J *et al* 2014 Seleno groups control the energy-level alignment between conjugated organic molecules and metals *J. Chem. Phys.* **140** 014705

[181] Zhai T, Wang R, Katase T, Quigley F, Ohta H, Amsalem P, Koch N and Duhm S 2020 Substrate-independent energy-level pinning of an organic semiconductor providing versatile hole-injection electrodes *ACS Appl. Electron. Mater.* **2** 3994−4001

[182] Oehzelt M, Koch N and Heimel G 2014 Organic semiconductor density of states controls the energy level alignment at electrode interfaces *Nat. Commun.* **5** 4174

[183] Greiner M T, Helander M G, Tang W-M, Wang Z-B, Qiu J and Lu Z-H 2012 Universal energy-level alignment of molecules on metal oxides *Nat. Mater.* **11** 76−81

[184] Braun S, Osikowicz W, Wang Y and Salaneck W R 2007 Energy level alignment regimes at hybrid organic−organic and inorganic−organic interfaces *Org. Electron.* **8** 14−20

[185] Ley L, Smets Y, Pakes C I and Ristein J 2012 Calculating the universal energy-level alignment of organic molecules on metal oxides *Adv. Funct. Mater.* **23** 794−805

[186] Yang J-P, Bussolotti F, Kera S and Ueno N 2017 Origin and role of gap states in organic semiconductor studied by UPS: as the nature of organic molecular crystals *J. Phys. D: Appl. Phys.* **50** 423002

[187] Zhao C, Tang C G, Seah Z-L, Koh Q-M, Chua L-L, Png R-Q and Ho P K H 2021 Improving organic photovoltaic cells by forcing electrode work function well beyond onset of Ohmic transition *Nat. Commun.* **12** 2250

[188] Schlesinger R, Bussolotti F, Yang J, Sadofev S, Vollmer A, Blumstengel S, Kera S, Ueno N and Koch N 2019 Gap states induce soft Fermi level pinning upon charge transfer at ZnO/molecular acceptor interfaces *Phys. Rev. Mater.* **3** 074601

[189] Kandada A R S, Guarnera S, Tassone F, Lanzani G and Petrozza A 2014 Charge generation at polymer/metal oxide interface: from molecular scale dynamics to mesoscopic effects *Adv. Funct. Mater.* **24** 3094−9

[190] Bussolotti F, Yang J, Hinderhofer A, Huang Y, Chen W, Kera S, Wee A T S and Ueno N 2014 Origin of the energy level alignment at organic/organic interfaces: the role of structural defects *Phys. Rev.* B **89** 115319

[191] Strong S E and Eaves J D 2015 Tetracene aggregation on polar and nonpolar surfaces: implications for singlet fission *J. Phys. Chem. Lett.* **6** 1209−15

[192] Opitz A *et al* 2016 Organic heterojunctions: contact-induced molecular reorientation, interface states and charge re-distribution *Sci. Rep.* **6** 21291

[193] Zhao L-H, Png R-Q, Chiam C C H, Guo H, Zhuo J-M, Chua L-L, Wee A T S and Ho P K H 2012 Polarization effects on energy-level alignment at the interfaces of polymer organic semiconductor films *Appl. Phys. Lett.* **101** 053304

[194] Kirchhuebel T *et al* 2020 Role of initial and final states in molecular spectroscopies: example of tetraphenyldibenzoperiflanthene (DBP) on graphite *J. Phys. Chem.* C **124** 19622−38

[195] Schlesinger R, Winkler S, Brandt M, Blumstengel S, Ovsyannikov R, Vollmer A and Koch N 2019 Energy level alignment at organic/inorganic semiconductor heterojunctions: Fermi level pinning at the molecular interlayer with a reduced energy gap *Phys. Chem. Chem. Phys.* **21** 15072−9

[196] Gorgoi M and Zahn D R T 2005 'Band bending' in copper phthalocyanine on hydrogen-passivated Si(111) *Org. Electron.* **6** 168−74

[197] Zahn D R T, Gavrila G N and Gorgoi M 2006 The transport gap of organic semiconductors studied using the combination of direct and inverse photoemission *Chem. Phys.* **325** 99−112

[198] Kampen T U, Gavrila G, Méndez H, Zahn D R T, Vearey-Roberts A R, Evans D A, Wells J, McGovern I and Braun W 2003 Electronic properties of interfaces between perylene derivatives and GaAs(001) surfaces *J. Phys.: Condens. Matter* **15** 2679S−92

[199] Samadi Khoshkhoo M, Peisert H, Chassé T and Scheele M 2017 The role of the density of interface states in interfacial energy level alignment of PTCDA *Org. Electron.* **49** 249−54

[200] Vázquez H, Flores F and Kahn A 2007 Induced density of states model for weakly-interacting organic semiconductor interfaces *Org. Electron.* **8** 241−8

[201] Vázquez H, Flores F, Oszwaldowski R, Ortega J, Pérez R and Kahn A 2004 Barrier formation at metal-organic interfaces: dipole formation and the charge neutrality level *Appl. Surf. Sci.* **234** 107−12

[202] Tung R T 2014 The physics and chemistry of the Schottky barrier height *Appl. Phys. Rev.* **1** 011304

[203] Oehzelt M, Akaike K, Koch N and Heimel G 2015 Energy-level alignment at organic heterointerfaces *Sci. Adv.* **1** e1501127

[204] Akaike K 2020 Distributions of potential and contact-induced charges in conventional organic photovoltaics *Materials* **13** 2411

[205] Amsalem P, Heimel G, Oehzelt M and Koch N 2015 The interface electronic properties of organic photovoltaic cells *J. Electron Spectrosc. Relat. Phenom.* **204** 177−85

[206] Niederhausen J, Amsalem P, Wilke A, Schlesinger R, Winkler S, Vollmer A, Rabe J P and Koch N 2012 Doping of C$_{60}$ (sub)monolayers by Fermi-level pinning induced electron transfer *Phys. Rev.* B **86** 081411

[207] Amsalem P, Niederhausen J, Wilke A, Heimel G, Schlesinger R, Winkler S, Vollmer A, Rabe J P and Koch N 2013 Role of charge transfer, dipole−dipole interactions, and electrostatics in Fermi-level pinning at a molecular heterojunction on a metal surface *Phys. Rev.* B **87** 035440

[208] Olthof S, Tress W, Meerheim R, Lüssem B and Leo K 2009 Photoelectron spectroscopy study of systematically varied doping concentrations in an organic semiconductor layer using a molecular p-dopant *J. Appl. Phys.* **106** 103711

[209] Wang H, Amsalem P, Heimel G, Salzmann I, Koch N and Oehzelt M 2014 Band-bending in organic semiconductors: the role of alkali-halide interlayers *Adv. Mater.* **26** 925−30

[210] Frisch J, Schubert M, Preis E, Rabe J P, Neher D, Scherf U and Koch N 2012 Full electronic structure across a polymer heterojunction solar cell *J. Mater. Chem.* **22** 4418−24

[211] Hellmann T, Das C, Abzieher T, Schwenzer J A, Wussler M, Dachauer R, Paetzold U W, Jaegermann W and Mayer T 2020 Electronic structure of MAPI-based perovskite solar cells: detailed band diagram determination by photoemission spectroscopy comparing classical and inverted device stacks *Adv. Energy Mater.* **10** 2002129

[212] Akaike K, Koch N and Oehzelt M 2014 Fermi level pinning induced electrostatic fields and band bending at organic heterojunctions *Appl. Phys. Lett.* **105** 223303

[213] Lüssem B, Keum C-M, Kasemann D, Naab B, Bao Z and Leo K 2016 Doped organic transistors *Chem. Rev.* **116** 13714−51

[214] Lüssem B, Riede M and Leo K 2013 Doping of organic semiconductors *Phys. Status Solidi a* **210** 9−43

[215] Skotheim T A 1997 *Handbook of Conducting Polymers* 2nd edn (London: Taylor and Francis)

[216] Jacobs I E and Moulé A J 2017 Controlling molecular doping in organic semiconductors *Adv. Mater.* **29** 1703063

[217] Hiramoto M, Kikuchi M and Izawa S 2019 Parts-per-million-level doping effects in organic semiconductor films and organic single crystals *Adv. Mater.* **31** 1801236

[218] Salzmann I *et al* 2012 Intermolecular hybridization governs molecular electrical doping *Phys. Rev. Lett.* **108** 035502

[219] Salzmann I, Heimel G, Oehzelt M, Winkler S and Koch N 2016 Molecular electrical doping of organic semiconductors: fundamental mechanisms and emerging dopant design rules *Acc. Chem. Res.* **49** 370−8

[220] Duhm S, Salzmann I, Bröker B, Glowatzki H, Johnson R L and Koch N 2009 Interdiffusion of molecular acceptors through organic layers to metal substrates mimics doping-related energy level shifts *Appl. Phys. Lett.* **95** 093305

[221] Amsalem P, Wilke A, Frisch J, Niederhausen J, Vollmer A, Rieger R, Müllen K, Rabe J P and Koch N 2011 Interlayer molecular diffusion and thermodynamic equilibrium in organic heterostructures on a metal electrode *J. Appl. Phys.* **110** 113709

[222] Wang Q *et al* 2021 Pentacene/perfluoropentacene bilayers on Au(111) and Cu(111): impact of organic−metal coupling strength on molecular structure formation *Nanoscale Adv.* **3** 2598−606

[223] Yang J, Wang Q, Wan S, Wu D, Chen M, Kashtanov S and Duhm S 2021 Photoelectron spectroscopy reveals molecular diffusion through physisorbed template layers on Au(111) *Electron. Struct.* **3** 024002

[224] Blochwitz J, Fritz T, Pfeiffer M, Leo K, Alloway D M, Lee P A and Armstrong N R 2001 Interface electronic structure of organic semiconductors with controlled doping levels *Org. Electron.* **2** 97−104

[225] Jäckle S, Mattiza M, Liebhaber M, Brönstrup G, Rommel M, Lips K and Christiansen S 2015 Junction formation and current transport mechanisms in hybrid n-Si/PEDOT:PSS solar cells *Sci. Rep.* **5** 13008

[226] Wang R, Wang Y, Wu C, Zhai T, Yang J, Sun B, Duhm S and Koch N 2020 Direct observation of conductive polymer induced inversion layer in n-Si and correlation to solar cell performance *Adv. Funct. Mater.* **30** 1903440

[227] Gueye M N, Carella A, Faure-Vincent J, Demadrille R and Simonato J-P 2020 Progress in understanding structure and transport properties of PEDOT-based materials: a critical review *Prog. Mater. Sci.* **108** 100616

[228] Cowley A M and Sze S M 1965 Surface states and barrier height of metal-semiconductor systems *J. Appl. Phys.* **36** 3212−20

[229] Tersoff J 1984 Schottky barrier heights and the continuum of gap states *Phys. Rev. Lett.* **52** 465−8

[230] Tietze M L, Burtone L, Riede M, Lüssem B and Leo K 2012 Fermi level shift and doping efficiency in p-doped small molecule organic semiconductors: a photoelectron spectroscopy and theoretical study *Phys. Rev.* B **86** 035320

[231] Tietze M L, Pahner P, Schmidt K, Leo K and Lüssem B 2015 Doped organic semiconductors: trap-filling, impurity saturation, and reserve regimes *Adv. Funct. Mater.* **25** 2701−7

[232] Olthof S, Mehraeen S, Mohapatra S K, Barlow S, Coropceanu V, Brédas J-L, Marder S R and Kahn A 2012 Ultralow doping in organic semiconductors: evidence of trap filling *Phys. Rev. Lett.* **109** 176601

[233] Natan A, Kronik L, Haick H and Tung R T 2007 Electrostatic properties of ideal and non-ideal polar organic monolayers: implications for electronic devices *Adv. Mater.* **19** 4103−17

[234] Witte G, Lukas S, Bagus P S and Wöll C 2005 Vacuum level alignment at organic/metal junctions: 'Cushion' effect and the interface dipole *Appl. Phys. Lett.* **87** 263502

[235] Vázquez H, Dappe Y J, Ortega J and Flores F 2007 Energy level alignment at metal/organic semiconductor interfaces: pillow effect, induced density of interface states, and charge neutrality level *J. Chem. Phys.* **126** 144703

[236] Winkler S, Frisch J, Schlesinger R, Oehzelt M, Rieger R, Räder J, Rabe J P, Müllen K and Koch N 2013 The impact of local work function variations on Fermi level pinning of organic semiconductors *J. Phys. Chem.* C **117** 22285−9

[237] Della Sala F, Blumstengel S and Henneberger F 2011 Electrostatic-field-driven alignment of organic oligomers on ZnO surfaces *Phys. Rev. Lett.* **107** 146401

[238] Verlaak S, Beljonne D, Cheyns D, Rolin C, Linares M, Castet F, Cornil J and Heremans P 2009 Electronic structure and geminate pair energetics at organic/organic interfaces: the case of pentacene/C$_{60}$ heterojunctions *Adv. Funct. Mater.* **19** 3809−14

[239] Rissner F, Rangger G M, Hofmann O T, Track A M, Heimel G and Zojer E 2009 Understanding the electronic structure of metal/SAM/organic-semiconductor heterojunctions *ACS Nano* **3** 3513−20

[240] Fukagawa H, Hosoumi S, Yamane H, Kera S and Ueno N 2011 Dielectric properties of polar-phthalocyanine monolayer systems with repulsive dipole interaction *Phys. Rev.* B **83** 085304

[241] Niederhausen J, Kersell H R, Christodoulou C, Heimel G, Wonneberger H, Müllen K, Rabe J P, Hla S-W and Koch N 2016 Monolayer phases of a dipolar perylene derivative on Au(111) and surface potential build-up in multilayers *Langmuir* **32** 3587−600

[242] Wang X, Esfarjani K and Zebarjadi M 2017 First-principles calculation of charge transfer at the silicon-organic interface *J. Phys. Chem.* C **121** 15529−37

[243] Hofmann O T, Rinke P, Scheffler M and Heimel G 2015 Integer versus fractional charge transfer at metal(/insulator)/organic interfaces: Cu(/NaCl)/TCNE *ACS Nano* **9** 5391−404

[244] Erker S and Hofmann O T 2019 Fractional and integer charge transfer at semiconductor/organic interfaces: the role of hybridization and metallicity *J. Phys. Chem. Lett.* **10** 848−54

[245] Lanzilotto V, Lovat G, Otero G, Sanchez L, López M F, Méndez J, Martín-Gago J A, Bavdek G and Floreano L 2013 Commensurate growth of densely packed PTCDI islands on the rutile $TiO_2(110)$ surface *J. Phys. Chem.* C **117** 12639–47

[246] Lanzilotto V, Lovat G, Fratesi G, Bavdek G, Brivio G P and Floreano L 2015 $TiO_2(110)$ charge donation to an extended π-conjugated molecule *J. Phys. Chem. Lett.* **6** 308–13

[247] Gruenewald M *et al* 2015 Integer charge transfer and hybridization at an organic semiconductor/conductive oxide interface *J. Phys. Chem.* C **119** 4865–73

[248] Kelly L L *et al* 2016 Spectroscopy and control of near-surface defects in conductive thin film ZnO *J. Phys.: Condens. Matter* **28** 094007

[249] Schlesinger R *et al* 2013 Controlling the work function of ZnO and the energy-level alignment at the interface to organic semiconductors with a molecular electron acceptor *Phys. Rev.* B **87** 155311

[250] Xu Y *et al* 2013 Space-charge transfer in hybrid inorganic-organic systems *Phys. Rev. Lett.* **111** 226802

[251] Wang H, Levchenko S V, Schultz T, Koch N, Scheffler M and Rossi M 2019 Modulation of the work function by the atomic structure of strong organic electron acceptors on H−Si(111) *Adv. Electron. Mater.* **5** 1800891

[252] Mawass M-A, Niederhausen J, Hengge M, Raoux S and Kronast F 2019 Sample cartridge with built-in miniature molecule evaporator for *in situ* measurement with a photoemission electron microscope *Ultramicroscopy* **200** 1–5

[253] Meisel T, Sparenberg M, Gawek M, Sadofev S, Kobin B, Grubert L, Hecht S, List-Kratochvil E J and Blumstengel S 2018 Fingerprint of charge redistribution in the optical spectra of hybrid inorganic/organic semiconductor interfaces *J. Phys. Chem.* C **122** 12913–9

[254] Schöttner L, Erker S, Schlesinger R, Koch N, Nefedov A, Hofmann O T and Wöll C 2020 Doping-induced electron transfer at organic/oxide interfaces: direct evidence from infrared spectroscopy *J. Phys. Chem.* C **124** 4511–6

[255] Hollerer M *et al* 2017 Charge transfer and orbital level alignment at inorganic/organic interfaces: the role of dielectric interlayers *ACS Nano* **11** 6252–60

[256] Hurdax P, Hollerer M, Puschnig P, Lüftner D, Egger L, Ramsey M G and Sterrer M 2020 Controlling the charge transfer across thin dielectric interlayers *Adv. Mater. Interfaces* **7** 2000592

[257] Alon H *et al* 2018 Effect of internal heteroatoms on level alignment at metal/molecular monolayer/Si interfaces *J. Phys. Chem.* C **122** 3312–25

[258] Winkler S, Xin Q, Li C, Kera S, Müllen K, Ueno N, Koch N and Duhm S 2018 Modification of TiO_2 (1 1 0)/organic hole transport layer interface energy levels by a dipolar perylene derivative *Electron. Struct.* **1** 015007

[259] Rangan S, Katalinic S, Thorpe R, Bartynski R A, Rochford J and Galoppini E 2010 Energy level alignment of a zinc(II) tetraphenylporphyrin dye adsorbed onto TiO$_2$(110) and ZnO 11$\bar{2}$0 surfaces *J. Phys. Chem.* C **114** 1139–47

[260] Béchu S, Ralaiarisoa M, Etcheberry A and Schulz P 2020 Photoemission spectroscopy characterization of halide perovskites *Adv. Energy Mater.* **10** 1904007

[261] Schulz P, Cahen D and Kahn A 2019 Halide perovskites: is it all about the interfaces? *Chem. Rev.* **119** 3349–417

[262] Koch S W, Kira M, Khitrova G and Gibbs H M 2006 Semiconductor excitons in new light *Nat. Mater.* **5** 523–31

[263] D'Innocenzo V, Grancini G, Alcocer M J P, Kandada A R S, Stranks S D, Lee M M, Lanzani G, Snaith H J and Petrozza A 2014 Excitons versus free charges in organo-lead tri-halide perovskites *Nat. Commun.* **5** 3586

[264] Collavini S, Völker S F and Delgado J L 2015 Understanding the outstanding power conversion efficiency of perovskite-based solar cells *Angew. Chem., Int. Ed.* **54** 9757–9

[265] Thompson B C and Fréchet J M J 2008 Polymer-fullerene composite solar cells *Angew. Chem., Int. Ed.* **47** 58–77

[266] Mazzio K A and Luscombe C K 2015 The future of organic photovoltaics *Chem. Soc. Rev.* **44** 78–90

[267] Querner C, Reiss P, Sadki S, Zagorska M and Pron A 2005 Size and ligand effects on the electrochemical and spectroelectrochemical responses of CdSe nanocrystals *Phys. Chem. Chem. Phys.* **7** 3204–9

[268] Jasieniak J, Califano M and Watkins S E 2011 Size-dependent valence and conduction band-edge energies of semiconductor nanocrystals *ACS Nano* **5** 5888–902

[269] Meulenberg R W, Lee J R I, Wolcott A, Zhang J Z, Terminello L J and van Buuren T 2009 Determination of the exciton binding energy in CdSe quantum dots *ACS Nano* **3** 325–30

[270] Cheiwchanchamnangij T and Lambrecht W R L 2012 Quasiparticle band structure calculation of monolayer, bilayer, and bulk MoS_2 *Phys. Rev.* B **85** 205302

[271] He K, Kumar N, Zhao L, Wang Z, Mak K F, Zhao H and Shan J 2014 Tightly bound excitons in monolayer WSe_2 *Phys. Rev. Lett.* **113** 026803

[272] Hanbicki A T, Currie M, Kioseoglou G, Friedman A L and Jonker B T 2015 Measurement of high exciton binding energy in the monolayer transition-metal dichalcogenides WS_2 and WSe_2 *Solid State Commun.* **203** 16–20

[273] Scholes G D and Rumbles G 2006 Excitons in nanoscale systems *Nat. Mater.* **5** 683–96

[274] Smith M B and Michl J 2010 Singlet fission *Chem. Rev.* **110** 6891–936

[275] Smith M B and Michl J 2013 Recent advances in singlet fission *Annu. Rev. Phys. Chem.* **64** 361–86

[276] Cheng Y Y *et al* 2012 Improving the light-harvesting of amorphous silicon solar cells with photochemical upconversion *Energy Environ. Sci.* **5** 6953–9

[277] Cheng Y Y *et al* 2016 Increased upconversion performance for thin film solar cells: a trimolecular composition *Chem. Sci.* **7** 559–68

[278] Nozik A J 2008 Multiple exciton generation in semiconductor quantum dots *Chem. Phys. Lett.* **457** 3–11

[279] Tahara H, Sakamoto M, Teranishi T and Kanemitsu Y 2018 Quantum coherence of multiple excitons governs absorption cross-sections of PbS/CdS core/shell nanocrystals *Nat. Commun.* **9** 3179

[280] VanOrman Z A, Bieber A S, Wieghold S and Nienhaus L 2020 Green-to-Blue triplet fusion upconversion sensitized by anisotropic CdSe nanoplatelets *Chem. Mater.* **32** 4734–42

[281] Zhu X-Y 2014 How to draw energy level diagrams in excitonic solar cells *J. Phys. Chem. Lett.* **5** 2283–8

[282] Kim T, Jeon J H, Han S, Lee D-K, Kim H, Lee W and Kim K 2011 Organic-inorganic hybrid tandem multijunction photovoltaics with extended spectral response *Appl. Phys. Lett.* **98** 183503

[283] Seo J H *et al* 2012 High efficiency inorganic/organic hybrid tandem solar cells *Adv. Mater.* **24** 4523–7

[284] Kim T *et al* 2013 Reversed organic−inorganic hybrid tandem solar cells for improved interfacial series resistances and balanced photocurrents *Synth. Met.* **175** 103–7

[285] Albrecht S, Grootoonk B, Neubert S, Roland S, Wördenweber J, Meier M, Schlatmann R, Gordijn A and Neher D 2014 Efficient hybrid inorganic/organic tandem solar cells with tailored recombination contacts *Sol. Energy Mater. Sol. Cells* **127** 157–62

[286] Roland S, Neubert S, Albrecht S, Stannowski B, Seger M, Facchetti A, Schlatmann R, Rech B and Neher D 2015 Hybrid organic/inorganic thin-film multijunction solar cells exceeding 11% power conversion efficiency *Adv. Mater.* **27** 1262–7

[287] Park S H, Shin I, Kim K H, Street R, Roy A and Heeger A J 2015 Tandem solar cells made from amorphous silicon and polymer bulk heterojunction sub-cells *Adv. Mater.* **27** 298–302

[288] Würfel U, Cuevas A and Würfel P 2015 Charge carrier separation in solar cells *IEEE J. Photovolt.* **5** 461–9

[289] Allen T G *et al* 2017 Calcium contacts to n-type crystalline silicon solar cells *Prog. Photovolt., Res. Appl.* **25** 636–44

[290] Yoshikawa K *et al* 2017 Silicon heterojunction solar cell with interdigitated back contacts for a photoconversion efficiency over 26% *Nat. Energy* **2** 17032

[291] Bullock J *et al* 2016 Efficient silicon solar cells with dopant-free asymmetric heterocontacts *Nat. Energy* **1** 15031

[292] Bullock J *et al* 2018 Stable dopant-free asymmetric heterocontact silicon solar cells with efficiencies above 20% *ACS Energy Lett.* **3** 508–13

[293] Wan S, Zhang G, Niederhausen J, Wu D, Wang Q, Sun B, Song T and Duhm S 2021 Schottky contact formation by an insulator: lithium fluoride on silicon *Appl. Phys. Lett.* **118** 241601

[294] He J, Wang W, Cai L, Lin H, Wang Z, Karuturi S K and Gao P 2020 Stable electron-selective contacts for crystalline silicon solar cells enabling efficiency over 21.6% *Adv. Funct. Mater.* **30** 2005554

[295] Zellmeier M, Brenner T J K, Janietz S, Nickel N H and Rappich J 2018 Polythiophenes as emitter layers for crystalline silicon solar cells: parasitic absorption, interface passivation, and open circuit voltage *J. Appl. Phys.* **123** 033102

[296] Zellmeier M, Rappich J, Klaus M, Genzel C, Janietz S, Frisch J, Koch N and Nickel N H 2015 Side chain engineering of poly-thiophene and its impact on crystalline silicon based hybrid solar cells *Appl. Phys. Lett.* **107** 203301

[297] Chen J, Wan W, Li H, Yan J, Ma J, Sun B, Li F and Flavel B S 2020 A polymer/carbon-nanotube ink as a boron-dopant/inorganic-passivation free carrier selective contact for silicon solar cells with over 21% efficiency *Adv. Funct. Mater.* **30** 2004476

[298] Khang D-Y 2019 Recent progress in Si-PEDOT:PSS inorganic–organic hybrid solar cells *J. Phys. D: Appl. Phys.* **52** 503002

[299] Sun Z, He Y, Xiong B, Chen S, Li M, Zhou Y, Zheng Y, Sun K and Yang C 2021 Performance-enhancing approaches for PEDOT:PSS-Si hybrid solar cells *Angew. Chem., Int. Ed.* **60** 5036–55

[300] Wang Y, Xia Z, Wu H, Li S, Wang T and Sun B 2019 Unrevealing charge carrier selective layer in silicon heterojunction solar cells via multifunctional atomic force probes *Sol. RRL* **3** 1900312

[301] Srivastava A, Sharma D, Kumari P, Dutta M, Srivastava S K *et al* 2021 Highly efficient PEDOT:PSS/silicon hybrid solar cells via effective surface microengineering of low-cost solar-grade silicon wafers *ACS Appl. Energy Mater.* **4** 4181–98

[302] Minari T, Miyadera T, Tsukagoshi K, Aoyagi Y and Ito H 2007 Charge injection process in organic field-effect transistors *Appl. Phys. Lett.* **91** 053508

[303] Singh S, Mohapatra S K, Sharma A, Fuentes-Hernandez C, Barlow S, Marder S R and Kippelen B 2013 Reduction of contact resistance by selective contact doping in fullerene n-channel organic field-effect transistors *Appl. Phys. Lett.* **102** 153303

[304] Günther A A, Sawatzki M, Formánek P, Kasemann D and Leo K 2016 Contact doping for vertical organic field-effect transistors *Adv. Funct. Mater.* **26** 768–75

[305] Würfel U *et al* 2016 How molecules with dipole moments enhance the selectivity of electrodes in organic solar cells—a combined experimental and theoretical approach *Adv. Energy Mater.* **6** 1600594

[306] Würfel U *et al* 2019 Recombination between photogenerated and electrode-induced charges dominates the fill factor losses in optimized organic solar cells *J. Phys. Chem. Lett.* **10** 3473–80

[307] Braun C L 1984 Electric field assisted dissociation of charge transfer states as a mechanism of photocarrier production *J. Chem. Phys.* **80** 4157–61

[308] Onsager L 1934 Deviations from Ohm's law in weak electrolytes *J. Chem. Phys.* **2** 599–615

[309] Zhao J and Uosaki K 2004 Electron transfer through organic monolayers directly bonded to silicon probed by current sensing atomic force microscopy: effect of chain length and applied force *J. Phys. Chem.* B **108** 17129–35

[310] Card H C and Rhoderick E H 1971 Studies of tunnel MOS diodes: I. Interface effects in silicon Schottky diodes *J. Phys. D: Appl. Phys.* **4** 1589–601

[311] Al-Ashouri A *et al* 2020 Monolithic perovskite/silicon tandem solar cell with >29% efficiency by enhanced hole extraction *Science* **370** 1300–9

[312] Scholes G D 2003 Long-range resonance energy transfer in molecular systems *Annu. Rev. Phys. Chem.* **54** 57–87

[313] Blumstengel S, Sadofev S, Xu C, Puls J and Henneberger F 2006 Converting wannier into Frenkel excitons in an inorganic/organic hybrid semiconductor nanostructure *Phys. Rev. Lett.* **97** 237401

[314] Yeltik A, Guzelturk B, Hernandez-Martinez P L, Govorov A O and Demir H V 2013 Phonon-assisted exciton transfer into silicon using nanoemitters: the role of phonons and temperature effects in Förster resonance energy transfer *ACS Nano* **7** 10492–501

[315] Tabernig S W, Daiber B, Wang T and Ehrler B 2018 Enhancing silicon solar cells with singlet fission: the case for Förster resonant energy transfer using a quantum dot intermediate *J. Photon. Energy* **8** 022008

[316] Danos L, Greef R and Markvart T 2008 Efficient fluorescence quenching near crystalline silicon from Langmuir–Blodgett dye films *Thin Solid Films* **516** 7251–5

[317] Dexter D L 1953 A theory of sensitized luminescence in solids *J. Chem. Phys.* **21** 836–50

[318] Köhler A and Bässler H 2011 What controls triplet exciton transfer in organic semiconductors? *J. Mater. Chem.* **21** 4003–11

[319] Li X and Tang M L 2017 Triplet transport in thin films: fundamentals and applications *Chem. Commun.* **53** 4429–40

[320] Dexter D L 1979 Two ideas on energy transfer phenomena: ion-pair effects involving the OH stretching mode, and sensitization of photovoltaic cells *J. Lumin.* **18–19** 779–84

[321] Wan Y, Guo Z, Zhu T, Yan S, Johnson J and Huang L 2015 Cooperative singlet and triplet exciton transport in tetracene crystals visualized by ultrafast microscopy *Nat. Chem.* **7** 785–92

[322] Marcus R A and Sutin N 1985 Electron transfers in chemistry and biology *Biochim. Biophys. Acta Rev. Bioenerg.* **811** 265–322

[323] Asbury J B, Hao E, Wang Y, Ghosh H N and Lian T 2001 Ultrafast electron transfer dynamics from molecular adsorbates to semiconductor nanocrystalline thin films *J. Phys. Chem.* B **105** 4545–57

[324] Zhu X-Y 2004 Electronic structure and electron dynamics at molecule–metal interfaces: implications for molecule-based electronics *Surf. Sci. Rep.* **56** 1–83

[325] Troisi A 2013 How quasi-free holes and electrons are generated in organic photovoltaic interfaces *Faraday Discuss.* **163** 377–92

[326] Clarke T M and Durrant J R 2010 Charge photogeneration in organic solar cells *Chem. Rev.* **110** 6736–67

[327] Coropceanu V, Malagoli M, da Silva Filho D A, Gruhn N E, Bill T G and Brédas J L 2002 Hole- and electron-vibrational couplings in oligoacene crystals: intramolecular contributions *Phys. Rev. Lett.* **89** 275503

[328] Kera S, Yamane H and Ueno N 2009 First-principles measurements of charge mobility in organic semiconductors: valence hole–vibration coupling in organic ultrathin films *Prog. Surf. Sci.* **84** 135–54

[329] Duhm S, Xin Q, Hosoumi S, Fukagawa H, Sato K, Ueno N and Kera S 2012 Charge reorganization energy and small polaron binding energy of rubrene thin films by ultraviolet photoelectron spectroscopy *Adv. Mater.* **24** 901–5

[330] Schlesinger R *et al* 2015 Efficient light emission from inorganic and organic semiconductor hybrid structures by energy-level tuning *Nat. Commun.* **6** 6754

[331] Wilke A *et al* 2012 Correlation between interface energetics and open circuit voltage in organic photovoltaic cells *Appl. Phys. Lett.* **101** 233301

[332] Chen X K and Brédas J L 2018 Voltage losses in organic solar cells: understanding the contributions of intramolecular vibrations to nonradiative recombinations *Adv. Energy Mater.* **8** 1702227

[333] Benduhn J *et al* 2017 Intrinsic non-radiative voltage losses in fullerene-based organic solar cells *Nat. Energy* **2** 17053

[334] Coffey D C, Larson B W, Hains A W, Whitaker J B, Kopidakis N, Boltalina O V, Strauss S H and Rumbles G 2012 An optimal driving force for converting excitons into free carriers in excitonic solar cells *J. Phys. Chem.* C **116** 8916–23

[335] Tabachnyk M, Ehrler B, Gélinas S, Böhm M L, Walker B J, Musselman K P, Greenham N C, Friend R H and Rao A 2014 Resonant energy transfer of triplet excitons from pentacene to PbSe nanocrystals *Nat. Mater.* **13** 1033–8

[336] Nelson J, Kirkpatrick J and Ravirajan P 2004 Factors limiting the efficiency of molecular photovoltaic devices *Phys. Rev.* B **69** 035337

[337] Durrant J R, Haque S A and Palomares E 2006 Photochemical energy conversion: from molecular dyads to solar cells *Chem. Commun.* **37** 3279–89

[338] Unger T, Wedler S, Kahle F-J, Scherf U, Bässler H and Köhler A 2017 The impact of driving force and temperature on the electron transfer in donor–acceptor blend systems *J. Phys. Chem.* C **121** 22739–52

[339] Duncan W R and Prezhdo O V 2007 Theoretical studies of photoinduced electron transfer in dye-sensitized TiO_2 *Annu. Rev. Phys. Chem.* **58** 143–84

[340] Herrmann D, Niesar S, Scharsich C, Köhler A, Stutzmann M and Riedle E 2011 Role of structural order and excess energy on ultrafast free charge generation in hybrid polythiophene/Si photovoltaics probed in real time by near-infrared broadband transient absorption *J. Am. Chem. Soc.* **133** 18220–33

[341] Grancini G, Maiuri M, Fazzi D, Petrozza A, Egelhaaf H-J, Brida D, Cerullo G and Lanzani G 2013 Hot exciton dissociation in polymer solar cells *Nat. Mater.* **12** 29–33

[342] Bakulin A A, Rao A, Pavelyev V G, van Loosdrecht P H M, Pshenichnikov M S, Niedzialek D, Cornil J, Beljonne D and Friend R H 2012 The role of driving energy and delocalized states for charge separation in organic semiconductors *Science* **335** 1340–4

[343] Jakowetz A C, Böhm M L, Zhang J, Sadhanala A, Huettner S, Bakulin A A, Rao A and Friend R H 2016 What controls the rate of ultrafast charge transfer and charge separation efficiency in organic photovoltaic blends *J. Am. Chem. Soc.* **138** 11672–9

[344] Liu C and Jakubikova E 2017 Two-step model for ultrafast interfacial electron transfer: limitations of Fermi's golden rule revealed by quantum dynamics simulations *Chem. Sci.* **8** 5979–91

[345] Piersimoni F, Schlesinger R, Benduhn J, Spoltore D, Reiter S, Lange I, Koch N, Vandewal K and Neher D 2015 Charge transfer absorption and emission at ZnO/organic interfaces *J. Phys. Chem. Lett.* **6** 500–4

[346] Eyer M, Frisch J, Sadofev S, Koch N, List-Kratochvil E J W and Blumstengel S 2017 Role of hybrid charge transfer states in the charge generation at ZnMgO/P3HT heterojunctions *J. Phys. Chem.* C **121** 21955–61

[347] Bansal N *et al* 2013 Influence of crystallinity and energetics on charge separation in polymer-inorganic nanocomposite films for solar cells *Sci. Rep.* **3** 1531

[348] Liu X, Gu J, Ding K, Fan D, Hu X, Tseng Y-W, Lee Y-H, Menon V and Forrest S R 2017 Photoresponse of an organic semiconductor/two-dimensional transition metal dichalcogenide heterojunction *Nano Lett.* **17** 3176–81

[349] Rijal K, Rudayni F, Kafle T R and Chan W-L 2020 Collective effects of band offset and wave function dimensionality on impeding electron transfer from 2D to organic crystals *J. Phys. Chem. Lett.* **11** 7495–501

[350] Rivera P *et al* 2015 Observation of long-lived interlayer excitons in monolayer $MoSe_2$–WSe_2 heterostructures *Nat. Commun.* **6** 6242

[351] Unuchek D, Ciarrocchi A, Avsar A, Watanabe K, Taniguchi T and Kis A 2018 Room-temperature electrical control of exciton flux in a van der Waals heterostructure *Nature* **560** 340–4

[352] Unuchek D, Ciarrocchi A, Avsar A, Sun Z, Watanabe K, Taniguchi T and Kis A 2019 Valley-polarized exciton currents in a van der Waals heterostructure *Nat. Nanotechnol.* **14** 1104–9

[353] Zhu X, Monahan N R, Gong Z, Zhu H, Williams K W and Nelson C A 2015 Charge transfer excitons at van der Waals interfaces *J. Am. Chem. Soc.* **137** 8313–20

[354] Kunstmann J *et al* 2018 Momentum-space indirect interlayer excitons in transition-metal dichalcogenide van der Waals heterostructures *Nat. Phys.* **14** 801–5

[355] Raja A *et al* 2017 Coulomb engineering of the bandgap and excitons in two-dimensional materials *Nat. Commun.* **8** 15251

[356] Vaynzof Y, Kabra D, Zhao L, Ho P K H, Wee A T-S and Friend R H 2010 Improved photoinduced charge carriers separation in organic-inorganic hybrid photovoltaic devices *Appl. Phys. Lett.* **97** 033309

[357] Vaynzof Y, Bakulin A A, Gélinas S and Friend R H 2012 Direct observation of photoinduced bound charge-pair states at an organic-inorganic semiconductor interface *Phys. Rev. Lett.* **108** 246605

[358] Sevinchan Y, Hopkinson P E, Bakulin A A, Herz J, Motzkus M and Vaynzof Y 2016 Improving charge separation across a hybrid oxide/polymer interface by Cs doping of the metal oxide *Adv. Mater. Interfaces* **3** 1500616

[359] Grupp A, Ehrenreich P, Kalb J, Budweg A, Schmidt-Mende L and Brida D 2017 Incoherent pathways of charge separation in organic and hybrid solar cells *J. Phys. Chem. Lett.* **8** 4858–64

[360] Tamura H and Burghardt I 2013 Ultrafast charge separation in organic photovoltaics enhanced by charge delocalization and vibronically hot exciton dissociation *J. Am. Chem. Soc.* **135** 16364–7

[361] Athanasopoulos S, Schauer F, Nádaždy V, Weiß M, Kahle F J, Scherf U, Bässler H and Köhler A 2019 What is the binding energy of a charge transfer state in an organic solar cell? *Adv. Energy Mater.* **9** 1900814

[362] Wu G, Li Z, Zhang X and Lu G 2014 Charge separation and exciton dynamics at polymer/ZnO interface from first-principles simulations *J. Phys. Chem. Lett.* **5** 2649–56

[363] Brédas J-L, Norton J E, Cornil J and Coropceanu V 2009 Molecular understanding of organic solar cells: the challenges *Acc. Chem. Res.* **42** 1691–9

[364] Bässler H and Köhler A 2015 'Hot or cold': how do charge transfer states at the donor–acceptor interface of an organic solar cell dissociate? *Phys. Chem. Chem. Phys.* **17** 28451–62

[365] Gélinas S *et al* 2011 The binding energy of charge-transfer excitons localized at polymeric semiconductor heterojunctions *J. Phys. Chem.* C **115** 7114–9

[366] Bakulin A A *et al* 2013 Charge-transfer state dynamics following hole and electron transfer in organic photovoltaic devices *J. Phys. Chem. Lett.* **4** 209–15

[367] Gélinas S, Rao A, Kumar A, Smith S L, Chin A W, Clark J, van der Poll T S, Bazan G C and Friend R H 2014 Ultrafast long-range charge separation in organic semiconductor photovoltaic diodes *Science* **343** 512–6

[368] Barker A J, Chen K and Hodgkiss J M 2014 Distance distributions of photogenerated charge pairs in organic photovoltaic cells *J. Am. Chem. Soc.* **136** 12018–26

[369] Jailaubekov A E *et al* 2013 Hot charge-transfer excitons set the time limit for charge separation at donor/acceptor interfaces in organic photovoltaics *Nat. Mater.* **12** 66–73

[370] Gagorik A G, Mohin J W, Kowalewski T and Hutchison G R 2015 Effects of delocalized charge carriers in organic solar cells: predicting nanoscale device performance from morphology *Adv. Funct. Mater.* **25** 1996–2003

[371] Lee J, Vandewal K, Yost S R, Bahlke M E, Goris L, Baldo M A, Manca J V and Van Voorhis T 2010 Charge transfer state versus hot exciton dissociation in polymer-fullerene blended solar cells *J. Am. Chem. Soc.* **132** 11878–80

[372] Vandewal K, Tvingstedt K, Gadisa A, Inganäs O and Manca J V 2009 On the origin of the open-circuit voltage of polymer–fullerene solar cells *Nat. Mater.* **8** 904–9

[373] Bakulin A A, Martyanov D, Paraschuk D Y, van Loosdrecht P H M and Pshenichnikov M S 2009 Charge-transfer complexes of conjugated polymers as intermediates in charge photogeneration for organic photovoltaics *Chem. Phys. Lett.* **482** 99–104

[374] Poelking C and Andrienko D 2015 Design rules for organic donor–acceptor heterojunctions: pathway for charge splitting and detrapping *J. Am. Chem. Soc.* **137** 6320–6

[375] Poelking C *et al* 2015 Impact of mesoscale order on open-circuit voltage in organic solar cells *Nat. Mater.* **14** 434–9

[376] Monahan N R, Williams K W, Kumar B, Nuckolls C and Zhu X-Y 2015 Direct observation of entropy-driven electron–hole pair separation at an organic semiconductor interface *Phys. Rev. Lett.* **114** 247003

[377] Peumans P and Forrest S R 2004 Separation of geminate charge-pairs at donor–acceptor interfaces in disordered solids *Chem. Phys. Lett.* **398** 27–31

[378] Burke T M and McGehee M D 2014 How high local charge carrier mobility and an energy cascade in a three-phase bulk heterojunction enable >90% quantum efficiency *Adv. Mater.* **26** 1923–8

[379] Akaike K *et al* 2016 Effective work function reduction of practical electrodes using an organometallic dimer *Adv. Funct. Mater.* **26** 2493–502

[380] Schultz T, Lungwitz D, Longhi E, Barlow S, Marder S R and Koch N 2021 The interlayer method: a universal tool for energy level alignment tuning at inorganic/organic semiconductor heterojunctions *Adv. Funct. Mater.* **31** 2010174

[381] Musselman K P, Albert-Seifried S, Hoye R L Z, Sadhanala A, Muñoz-Rojas D, MacManus-Driscoll J L and Friend R H 2014 Improved exciton dissociation at semiconducting polymer:ZnO donor:acceptor interfaces via nitrogen doping of ZnO *Adv. Funct. Mater.* **24** 3562–70

[382] Thu C *et al* 2018 Role of the metal-oxide work function on photocurrent generation in hybrid solar cells *Sci. Rep.* **8** 3559

[383] Wagner S R, Huang B, Park C, Feng J, Yoon M and Zhang P 2015 Growth of metal phthalocyanine on deactivated semiconducting surfaces steered by selective orbital coupling *Phys. Rev. Lett.* **115** 096101

[384] Makoudi Y, Jeannoutot J, Palmino F, Chérioux F, Copie G, Krzeminski C, Cleri F and Grandidier B 2017 Supramolecular self-assembly on the B-Si(111)-($\sqrt{3} \times \sqrt{3}$) R30° surface: from single molecules to multicomponent networks *Surf. Sci. Rep.* **72** 316–49

[385] Aldahhak H, Hogan C, Linder S, Appelfeller S, Eisele H, Schmidt W G, Dähne M, Gerstmann U and Franz M 2021 Electronic structure of the Si(111)$\sqrt{3} \times \sqrt{3}$R30°-B surface from theory and photoemission spectroscopy *Phys. Rev.* B **103** 035303

[386] Blumstengel S, Sadofev S and Henneberger F 2008 Electronic coupling of optical excitations in organic/inorganic semiconductor hybrid structures *New J. Phys.* **10** 065010

[387] Palomares E, Clifford J N, Haque S A, Lutz T and Durrant J R 2003 Control of charge recombination dynamics in dye sensitized solar cells by the use of conformally deposited metal oxide blocking layers *J. Am. Chem. Soc.* **125** 475–82

[388] Kay A and Grätzel M 2002 Dye-sensitized core–shell nanocrystals: improved efficiency of mesoporous tin oxide electrodes coated with a thin layer of an insulating oxide *Chem. Mater.* **14** 2930–5

[389] Tennakone K, Bandara J, Konara P, Bandaranayake M, Kumara G R A and Konno A 2001 Enhanced efficiency of a dye-sensitized solar cell made from MgO-coated nanocrystalline SnO$_2$ *Japan. J. Appl. Phys.* **40** 732L–4

[390] Fabregat-Santiago F, García-Cañadas J, Palomares E, Clifford J N, Haque S A, Durrant J R, Garcia-Belmonte G and Bisquert J 2004 The origin of slow electron recombination processes in dye-sensitized solar cells with alumina barrier coatings *J. Appl. Phys.* **96** 6903–7

[391] Armstrong C L *et al* 2015 Influence of an inorganic interlayer on exciton separation in hybrid solar cells *ACS Nano* **9** 11863–71

[392] Ng K K and Card H C 1980 Asymmetry in the SiO$_2$ tunneling barriers to electrons and holes *J. Appl. Phys.* **51** 2153–7

[393] Avasthi S, McClain W E, Man G, Kahn A, Schwartz J and Sturm J C 2013 Hole-blocking titanium-oxide/silicon heterojunction and its application to photovoltaics *Appl. Phys. Lett.* **102** 203901

[394] Nagamatsu K A *et al* 2015 Titanium dioxide/silicon hole-blocking selective contact to enable double-heterojunction crystalline silicon-based solar cell *Appl. Phys. Lett.* **106** 123906

[395] Jäckle S, Liebhaber M, Niederhausen J, Büchele M, Félix R, Wilks R G, Bär M, Lips K and Christiansen S 2016 Unveiling the hybrid n-Si/PEDOT:PSS interface *ACS Appl. Mater. Interfaces* **8** 8841–8

[396] Angel Trujillo D A, Iyer A, Hack J and Opila R L 2021 Role of oxide at interface between organic layer and silicon substrate in hybrid solar cells *J. Mater. Res.* **36** 557–70

[397] Einzinger M *et al* 2019 Sensitization of silicon by singlet exciton fission in tetracene *Nature* **571** 90–4

[398] Piland G B, Burdett J J, Hung T-Y, Chen P-H, Lin C-F, Chiu T-L, Lee J-H and Bardeen C J 2014 Dynamics of molecular excitons near a semiconductor surface studied by fluorescence quenching of polycrystalline tetracene on silicon *Chem. Phys. Lett.* **601** 33–8

[399] Kerr C S, Kryukovskiy A and Chen J I L 2018 Effects of surface passivation on trap states, band bending, and photoinduced charge transfer in P3HT/TiO$_2$ hybrid inverse opals *J. Phys. Chem.* C **122** 17301–8

[400] Pan Z, Rao H, Mora-Seró I, Bisquert J and Zhong X 2018 Quantum dot-sensitized solar cells *Chem. Soc. Rev.* **47** 7659–702

[401] Frisch J, Glowatzki H, Janietz S and Koch N 2009 Solution-based metal electrode modification for improved charge injection in polymer field-effect transistors *Org. Electron.* **10** 1459–65

[402] Hunger R, Jaegermann W, Merson A, Shapira Y, Pettenkofer C and Rappich J 2006 Electronic structure of methoxy-, bromo-, and nitrobenzene grafted onto Si(111) *J. Phys. Chem.* B **110** 15432–41

[403] Toledano T, Biller A, Bendikov T, Cohen H, Vilan A and Cahen D 2012 Controlling space charge of oxide-free Si by *in Situ* modification of dipolar alkyl monolayers *J. Phys. Chem.* C **116** 11434–43

[404] Tritsch J R, Chan W-L, Wu X, Monahan N R and Zhu X-Y 2013 Harvesting singlet fission for solar energy conversion via triplet energy transfer *Nat. Commun.* **4** 2679

[405] Goh C, Scully S R and McGehee M D 2007 Effects of molecular interface modification in hybrid organic–inorganic photovoltaic cells *J. Appl. Phys.* **101** 114503

[406] Mattioli G *et al* 2014 Interfacial engineering of P3HT/ZnO hybrid solar cells using phthalocyanines: a joint theoretical and experimental investigation *Adv. Energy Mater.* **4** 1301694

[407] Johansson E M J, Schölin R, Siegbahn H, Hagfeldt A and Rensmo H 2011 Energy level alignment in TiO₂/dipole-molecule/P3HT interfaces *Chem. Phys. Lett.* **515** 146–50

[408] Sato M, Tohkairin A, Mase K and Kanai K 2015 Role of oxygen vacancies in TiO$_x$ films in electronic structure at interface with an α-NPD layer *Org. Electron.* **27** 247–52

[409] Godlewski S and Szymonski M 2013 Adsorption and self-assembly of large polycyclic molecules on the surfaces of TiO₂ single crystals *Int. J. Mol. Sci.* **14** 2946–66

[410] Li Z, Zhang X and Lu G 2012 Dipole-assisted charge separation in organic–inorganic hybrid photovoltaic heterojunctions: insight from first-principles simulations *J. Phys. Chem.* C **116** 9845–51

[411] Wang M, Grätzel C, Moon S-J, Humphry-Baker R, Rossier-Iten N, Zakeeruddin S M and Grätzel M 2009 Surface design in solid-state dye sensitized solar cells: effects of zwitterionic co-adsorbents on photovoltaic performance *Adv. Funct. Mater.* **19** 2163–72

[412] Anantharaj G and Lakshminarasimhan N 2018 Interfacial modification of Photoanode|electrolyte interface using oleic acid enhancing the efficiency of dye-sensitized solar cells *ACS Omega* **3** 18285–94

[413] Anderson N A, Ai X, Chen D, Mohler D L and Lian T 2003 Bridge-assisted ultrafast interfacial electron transfer to nanocrystalline SnO₂ thin filmss *J. Phys. Chem.* B **107** 14231–9

[414] Gundlach L, Ernstorfer R and Willig F 2007 Ultrafast interfacial electron transfer from the excited state of anchored molecules into a semiconductor *Prog. Surf. Sci.* **82** 355–77

[415] Campbell W M, Burrell A K, Officer D L and Jolley K W 2004 Porphyrins as light harvesters in the dye-sensitised TiO₂ solar cell *Coord. Chem. Rev.* **248** 1363–79

[416] Clifford J N, Martínez-Ferrero E, Viterisi A and Palomares E 2011 Sensitizer molecular structure-device efficiency relationship in dye sensitized solar cells *Chem. Soc. Rev.* **40** 1635–46

[417] Bender J A, Raulerson E K, Li X, Goldzak T, Xia P, Van Voorhis T, Tang M L and Roberts S T 2018 Surface states mediate triplet energy transfer in nanocrystal–acene composite systems *J. Am. Chem. Soc.* **140** 7543–53

[418] He S, Luo X, Liu X, Li Y and Wu K 2019 Visible-to-ultraviolet upconversion efficiency above 10% sensitized by quantum-confined perovskite nanocrystals *J. Phys. Chem. Lett.* **10** 5036–40

[419] Okumura K, Yanai N and Kimizuka N 2019 Visible-to-UV photon upconversion sensitized by lead halide perovskite nanocrystals *Chem. Lett.* **48** 1347–50

[420] Huang J, Huang Z, Jin S and Lian T 2008 Exciton dissociation in CdSe quantum dots by hole transfer to phenothiazine *J. Phys. Chem.* C **112** 19734–8

[421] Berhe S A, Zhou J Y, Haynes K M, Rodriguez M T and Youngblood W J 2012 Electron transport in acceptor-sensitized polymer-oxide solar cells: the importance of surface dipoles and electron cascade effects *ACS Appl. Mater. Interfaces* **4** 2955–63

[422] Ehrenreich P, Groh A, Goodwin H, Huster J, Deschler F, Mecking S and Schmidt-Mende L 2019 Tailored interface energetics for efficient charge separation in metal oxide-polymer solar cells *Sci. Rep.* **9** 74

[423] Ehrenreich P, Pfadler T, Paquin F, Dion-Bertrand L I, Paré-Labrosse O, Silva C, Weickert J and Schmidt-Mende L 2015 Role of charge separation mechanism and local disorder at hybrid solar cell interfaces *Phys. Rev.* B **91** 035304

[424] Hewlett R M and McLachlan M A 2016 Surface structure modification of ZnO and the impact on electronic properties *Adv. Mater.* **28** 3893–921

[425] Magomedov A, Al-Ashouri A, Kasparavičius E, Strazdaite S, Niaura G, Jošt M, Malinauskas T, Albrecht S and Getautis V 2018 Self-assembled hole transporting monolayer for highly efficient perovskite solar cells *Adv. Energy Mater.* **8** 1801892

[426] Deng W, Liang X, Kubiak P S and Cameron P J 2018 Molecular interlayers in hybrid perovskite solar cells *Adv. Energy Mater.* **8** 1701544

[427] Sieval A B, Linke R, Zuilhof H and Sudhölter E J R 2000 High-quality alkyl monolayers on silicon surfaces *Adv. Mater.* **12** 1457–60

[428] Roodenko K, Yang F, Hunger R, Esser N, Hinrichs K and Rappich J 2010 Passivation of Si(111) surfaces with electrochemically grafted thin organic films *Surf. Sci.* **604** 1623–7

[429] Itaka K, Yamashiro M, Yamaguchi J, Haemori M, Yaginuma S, Matsumoto Y, Kondo M and Koinuma H 2006 High-mobility C₆₀ field-effect transistors fabricated on molecular-wetting controlled substrates *Adv. Mater.* **18** 1713–6

[430] Hinderhofer A, Gerlach A, Broch K, Hosokai T, Yonezawa K, Kato K, Kera S, Ueno N and Schreiber F 2013 Geometric and electronic structure of templated C₆₀ on diindenoperylene thin films *J. Phys. Chem.* C **117** 1053–8

[431] Arkhipov V I, Heremans P and Bässler H 2003 Why is exciton dissociation so efficient at the interface between a conjugated polymer and an electron acceptor? *Appl. Phys. Lett.* **82** 4605–7

[432] Schwarze M *et al* 2019 Impact of molecular quadrupole moments on the energy levels at organic heterojunctions *Nat. Commun.* **10** 2466

[433] Piland G B and Bardeen C J 2015 How morphology affects singlet fission in crystalline tetracene *J. Phys. Chem. Lett.* **6** 1841–6

[434] Arias D H, Ryerson J L, Cook J D, Damrauer N H and Johnson J C 2016 Polymorphism influences singlet fission rates in tetracene thin films *Chem. Sci.* **7** 1185–91

[435] Kolata K, Breuer T, Witte G and Chatterjee S 2014 Molecular packing determines singlet exciton fission in organic semiconductors *ACS Nano* **8** 7377–83

[436] Langner A, Su Y and Sokolowski M 2006 Luminescence quenching of tetracene films adsorbed on an ultrathin alumina AlO$_x$ layer on Ni₃Al(111) *Phys. Rev.* B **74** 045428

[437] Padgaonkar S, Amsterdam S H, Bergeron H, Su K, Marks T J, Hersam M C and Weiss E A 2019 Molecular-orientation-dependent interfacial charge transfer in phthalocyanine/MoS₂ mixed-dimensional heterojunctions *J. Phys. Chem.* C **123** 13337–43

[438] Yang J, Yan D and Jones T S 2015 Molecular template growth and its applications in organic electronics and optoelectronics *Chem. Rev.* **115** 5570–603

[439] Breuer T and Witte G 2015 Controlling nanostructures by templated templates: inheriting molecular orientation in binary heterostructures *ACS Appl. Mater. Interfaces* **7** 20485–92

[440] Noone K M, Subramaniyan S, Zhang Q, Cao G, Jenekhe S A and Ginger D S 2011 Photoinduced charge transfer and polaron dynamics in polymer and hybrid photovoltaic thin films: organic vs inorganic acceptors *J. Phys. Chem.* C **115** 24403−10

[441] Sherkar T S and Koster L J A 2015 Dielectric effects at organic/inorganic interfaces in nanostructured devices *ACS Appl. Mater. Interfaces* **7** 11881−9

[442] Plehn T, Ziemann D and May V 2018 Charge separation at an organic/inorganic nano-hybrid interface: atomistic simulations of a para-sexiphenyl ZnO system *Phys. Chem. Chem. Phys.* **20** 26870−84

[443] Plehn T, Ziemann D and May V 2018 Atomistic simulations of charge separation at a nanohybrid interface: relevance of photoinduced initial state preparation *J. Phys. Chem. Lett.* **9** 209−15

[444] Oosterhout S D, Wienk M M, van Bavel S S, Thiedmann R, Jan Anton Koster L, Gilot J, Loos J, Schmidt V and Janssen R A J 2009 The effect of three-dimensional morphology on the efficiency of hybrid polymer solar cells *Nat. Mater.* **8** 818−24

[445] Kirchhuebel T, Monti O L A, Munakata T, Kera S, Forker R and Fritz T 2019 The role of initial and final states in molecular spectroscopies *Phys. Chem. Chem. Phys.* **21** 12730−47

[446] Ozawa K, Yamamoto S, Yukawa R, Akikubo K, Emori M, Sakama H and Matsuda I 2016 Capturing transiently charged states at the $C_{60}/TiO_2(110)$ interface by time-resolved soft x-ray photoelectron spectroscopy *Org. Electron.* **31** 98−103

[447] Glover T E, Ackermann G D, Hussain Z and Padmore H A 2004 Laser pump and x-ray probe surface photovoltage spectroscopy on Si(111) *J. Mod. Opt.* **51** 2805−11

[448] Costantini R, Faber R, Cossaro A, Floreano L, Verdini A, Hattig C, Morgante A, Coriani S and Dell'Angela M 2019 Picosecond timescale tracking of pentacene triplet excitons with chemical sensitivity *Commun. Phys.* **2** 56

[449] Cao L, Gao X-Y, Wee A T S and Qi D-C 2014 Quantitative femtosecond charge transfer dynamics at organic/electrode interfaces studied by core−hole clock spectroscopy *Adv. Mater.* **26** 7880−8

[450] Hamoudi H, Schüpbach B, Neppl S, Kao P, Feulner P, Terfort A, Allara D and Zharnikov M 2011 Orbital-dependent charge transfer dynamics in conjugated self-assembled monolayers *Phys. Rev. Lett.* **107** 027801